Microstructural design via ultrafast heating to improve mechanical properties of a low carbon steel

by

Miguel Ángel Valdés Tabernero

A dissertation submitted by in partial fulfillment of the requirements for the degree of Doctor of Philosophy in

Materials Science and Engineering

Universidad Carlos III de Madrid

Advisor:

Dr. Ilchat Sabirov

Tutor:

Dr. Jon M. Molina-Aldareguia

Abril 2020

A mi familia, por el apoyo que me han dado durante este tiempo.

ACKNOWLEDGEMENTS

Lo que empezó con una beca de verano que se convirtió en un proyecto de máster ha acabado siendo, aunque en otro tema, esta tesis doctoral. Por eso, ahora que se acerca el final de este largo viaje toca una de las partes que me resultan más complicadas: plasmar en unas cuantas palabras toda la gratitud que siento hacia aquellas personas que, de uno u otro modo, han participado en este proyecto.

In first place, I would like to say thank you to my supervisor, Dr. Ilchat Sabirov, for his trust since the very first moment, but also for his unconditional help and support, being always available during this project. I also want to thank him for all the knowledge share with me, and the advices received not only professionally but also in personal aspects. It has been a pleasure to work with you!

También me gustaría agradecer al Dr. Jon Molina-Aldareguia por ser mi tutor académico, pero también por participar en los distintos proyectos a través de su colaboración, consejos y ayuda durante este tiempo.

Me gustaría dar las gracias también al Prof. Javier Llorca y al Prof. Ignacio Romero por la confianza depositada al abrirme las puertas del Instituto. Y agradecer al centro por haberme otorgado el premio "IMDEA Innovation Award" gracias al cual he podido llevar a cabo este proyecto.

I would like to thank Prof. Roumen Petrov for hosting me and being my supervisor during my stay with the Department of Materials Science and Engineering of Ghent University. Thank you so much for the welcome, the advices, the support and all the knowledge shared with me. I really appreciate it. I would also like to say thank you to the rest of the department, specially to Dr. Bliznuk, Dr. Castro-Cerda and F. Vercruysse for the help and support given. I would like to extend my gratitude to my colleagues from the Department of Materials Science and Engineering of TU Delft, Dr. Kumar and Dr. Celada-Casero for your scientific collaboration and help.

Agradecer también a toda la gente que forma el centro de IMDEA Materiales, que trabaja día a día para que proyectos como este sean posibles. En especial a Miguel Monclús, Marcos,

Amalia, Vanesa, José Luis, Miguel de la Cruz, Pepe, Miguel Castillo. ¡Gracias por vuestra inestimable ayuda!

Cómo no, a todos aquellos que han sido mis compañeros de laboratorio, que habéis creado un ambiente tan especial y que habéis conseguido que ir a trabajar sea un poquito menos trabajo. Hugo, Jaime, Marcos, Alex, Ángel, Vero, Anna, Pablo, Xaquín, Gilbert, Akshya, Alfonso, Ceci, Bárbara, Almu, Luis… Gracias por todos los debates durante las comidas, las conversaciones, las cervezas, las noches... Por todos los consejos y apoyo en los buenos, y sobre todo en los malos momentos. Ha sido un verdadero placer compartir todo este tiempo con vosotros.

Dar las gracias también a mis amigos por las risas, las cervezas, las comidas, los disfraces, los viajes y todos los buenos momentos vividos. ¡Espero que nos queden mucho más por delante!

Gracias, en definitiva, a todos aquellos que han sido durante algún momento, de una u otra forma, parte de este viaje.

Por último, a los más importantes. A mi familia. Quiero dedicarles este trabajo a ellos. A mis padres Miguel Ángel y Ana Isabel. Papá, mamá, mil gracias por todo lo que habéis hecho por nosotros, por todo vuestro esfuerzo y sacrificio, por todo lo que nos habéis enseñado, nos habéis dado y seguís haciendo. Como ya dijo mi hermano, nada de esto hubiera sido posible sin vosotros. Me gustaría que os sintierais orgullosos por todo lo que habéis hecho.

Y a mis hermanos Patricia y Alberto. Patri, Nene no os podré agradecer nunca lo suficiente. Gracias porque vosotros habéis sido mi guía, porque vosotros sois quienes mejor me habéis comprendido, porque vuestra experiencia me ha ayudado siempre y sé que lo seguirá haciendo. Gracias por soportarme, por quererme, por ayudarme siempre. Me siento increíblemente afortunado, con vosotros tengo un tesoro. Os quiero.

Este trabajo ha sido posible gracias a todos vosotros. ¡Muchísimas gracias!

PUBLISHED AND SUBMITTED CONTENT

This PhD Thesis is formed by a compendium of four peer-reviewed articles published in highly ranked (Q1) international journals in the area of materials science. The references to the articles are listed below:

- M.A. Valdes-Tabernero, F. Vercruysse, I. Sabirov, R.H. Petrov, M.A. Monclus, J.M. Molina-Aldareguia. "Effect of Ultrafast Heating on the Properties of the Microconstituents in a Low-Carbon Steel", Metallurgical and Materials Transactions A 49 (2018) 3145-3150, https://doi.org/10.1007/s11661-018-4658-4
  My contribution to this manuscript: Investigation, Formal analysis, Visualization, Funding acquisition, Writing - original draft.
  This manuscript is wholly included in the Thesis. The material from this item appears in sections 1, 3 and 4. The material from this source included in this thesis, it is singled out with typographic means and an explicit reference.

- M.A. Valdes-Tabernero, C. Celada-Casero, I. Sabirov, A. Kumar, R.H. Petrov. "The effect of heating rate and soaking time on microstructure of an advanced high strength steel", Materials Characterization 155 (2019) 109822, https://doi.org/10.1016/j.matchar.2019.109822
  My contribution to this manuscript: Investigation, Formal analysis, Visualization, Funding acquisition, Writing - original draft.
  This manuscript is wholly included in the Thesis. The material from this item appears in sections 1, 3 and 4. The material from this source included in this thesis, it is singled out with typographic means and an explicit reference.

- M.A. Valdes-Tabernero, R.H. Petrov, M.A. Monclus, J.M. Molina-Aldareguia, I. Sabirov, "The effect of soaking time after ultrafast heating on the microstructure and mechanical behavior of a low carbon steel", Materials Science and Engineering A 765 (2019) 138276, https://doi.org/10.1016/j.msea.2019.138276
  My contribution to this manuscript: Investigation, Formal analysis, Visualization, Funding acquisition, Writing - original draft.

This manuscript is wholly included in the Thesis. The material from this item appears in sections 1, 3 and 4. The material from this source included in this thesis, it is singled out with typographic means and an explicit reference.

- M.A. Valdes-Tabernero, A. Kumar, R.H. Petrov, M.A. Monclus, J.M. Molina-Aldareguia, I. Sabirov. "The sensitivity of the microstructure and properties to the peak temperature in an ultrafast heat treated low carbon-steel", Materials Science and Engineering A 776 (2020) 138999, https://doi.org/10.1016/j.msea.2020.138999
  My contribution to this manuscript: Investigation, Formal analysis, Visualization, Funding acquisition, Writing - original draft.
  This manuscript is wholly included in the Thesis. The material from this item appears in sections 1, 3 and 4. The material from this source included in this thesis, it is singled out with typographic means and an explicit reference.

All figures reprinted in this document are referenced to the original work.

OTHER RESEARCH MERITS

Moreover, this work has also been presented in form of poster or oral presentations at the relevant International Conferences:

- M.A. Valdes-Tabernero, F. Vercruysse, R.H. Petrov, I. Sabirov, M.A. Monclus, J.M. Molina-Aldareguia. THERMEC 2018. Paris, France (July, 2018).
- M.A. Valdes-Tabernero, F. Vercruysse, M.A. Monclus, J.M. Molina-Aldareguia, R.H. Petrov, I. Sabirov. Materials Science and Technology 2019, Portland, USA (September, 2019)
- External seminar, Universidad Carlos III de Madrid, Madrid, Spain (June, 2019).

Preface

This PhD Thesis is submitted for the degree of Doctor of Philosophy to the "Universidad Carlos III de Madrid". This manuscript contains the work carried out at IMDEA Materials Institute (Madrid, Spain) under the supervision of Dr. Ilchat Sabirov, being Dr. Jon M. Molina-Aldareguia the academic tutor. The outcomes obtained have been achieved due to the strong collaboration with Prof. Roumen Petrov from the Ghent University (Ghent, Belgium) and Delft University of Technology (Delft, The Netherlands).

This doctoral thesis fulfills all the requirements to be awarded with the International Doctorate mention. Part of the microstructural characterization presented in this manuscript was obtained during my 3 months stay with Ghent University under the supervision of Professor Roumen Petrov. The equipment provided as well as the vast expertise in the field greatly contribute to the development of this investigation. In addition, 2 international experts in the field, Dr. Javier Hidalgo García (Delft University of Technology, The Netherlands) and Dr. Andrea García-Junceda (European Commission, The Netherlands), have reviewed the present manuscript.

Resumen

Las políticas actuales llevadas a cabo por las instituciones públicas están centradas en reducir las emisiones de carbono generadas por todos los sectores de la sociedad, dentro de los cuales se encuentra la industria de la automoción. Para reducir las emisiones generadas por los vehículos, los fabricantes están centrados en aligerar el peso de los coches. Una forma de conseguirlo es mejorando las propiedades mecánicas de los aceros avanzados de alta resistencia (AHSS), para así reducir el peso total del coche. Para ello la industria del acero está buscando nuevas formas de procesado que satisfagan las necesidades de los consumidores a la vez que reducen las emisiones de gases de efecto invernadero. Entre los nuevos tratamientos térmicos que se están desarrollandopara la producción de AHSS destaca el conocido en inglés como "Ultrafast heating" (UFH). Este tipo de tratamiento se basa en la utilización de temperaturas de calentamiento muy superiores (> 100 ºC/s) a las convencionales (< 10 ºC/s), seguido de un corto periodo a máxima temperatura y un templado, reduciendo la duración total del tratamiento a unos pocos segundos. El acero resultante es de gran complejidad, donde la ferrita, martensita y austenita retenida formadas otorgan al material la combinación de propiedades mecánicas necesarias para su uso en los diferentes componentes estructurales. A pesar de las investigaciones llevadas a cabo por la comunidad científica en este campo es necesario entender aún mejor el papel que juegan todos los parámetros de procesado en la arquitectura microestructural y propiedades de los AHSS. Por otra parte, no existe todavía ningún trabajo donde se analicen las propiedades mecánicas de los microconstituyentes de manera individual y su efecto en las propiedades mecánicas generales. Por esta razón, el objetivo de la presente Tesis doctoral es entender en profundidad la relación entre los distintos parámetros de procesado con la microestructura y propiedades mecánicas resultantes. Este conocimiento permitirá desarrollar el concepto de diseño microestructural en aceros mediante el tratamiento UFH. En este trabajo se ha demostrado que se puede obtener una combinación óptima de resistencia y ductilidad a través del diseño microestructural, ya que tanto la fracción volumétrica y el tamaño de los diferentes microconstituyentes dependen en gran medida del tiempo de permanencia y máxima temperatura alcanzada durante el tratamiento.

Abstract

The current regulations carried out by the public institutions are focused on reducing the carbon emissions from any sector of society, including the automotive industry. In order to reduce the emissions generated by vehicles, car manufactures are looking for new solutions to lighten car weight. One way to achieve this goal is by increasing the mechanical properties of Advanced high-strength steels (AHSS), widely used in structural components, reducing the total car weight. Steel industry is searching for new processing routes to satisfy customer demands, reducing, at the same time, the greenhouse emissions during manufacturing. Among the new thermal treatments where research is focused on, the Ultrafast heating (UFH) is receiving significant attention. This process is based on using higher heating rates (>> 100 ºC/s) instead of conventional ones (<10 º C/s), followed by a short soaking time at maximum temperature and subsequent quenching, thus reducing the duration of entire treatment to a few seconds. The resultant steel has a hierarchic multiphase microstructure, formed by ferrite, martensite and retained austenite with the desirable combination of mechanical properties required for the structural components. Despite the efforts made by the scientific community to understand the influence of high heating rates on microstructure and properties, the effect of other processing parameters on the microstructural architecture and properties has not been explored. There are no studies about the mechanical properties of the individual microconstituents and their effect on overall mechanical performance of these steels. Therefore, the main goal of this work is to gain fundamental understanding of the effect of soaking time and peak temperature on the microstructure and properties of UFH treated steels at macro- and micro-scales. This knowledge will allow to develop a concept for microstructural design via UFH treatment to achieve enhanced combination of mechanical and functional properties in steels. This work demonstrates that an optimal combination of mechanical strength and tensile ductility can be reached in the UFH treated steels via microstructural design, since volume fraction and size of individual microconstituents strongly depend on peak temperature and soaking time during UFH process.

INDEX

INDEX

ABREVIATIONS AND SYMBOLS

ABREVIATIONS AND SYMBOLS

ABREVIATIONS

AFG	Average ferritic grain (size)	**AFM**	Atomic force microscopy
AHSS	Advanced high-strength steels	**APT**	Atom probe tomography
BCC	Body centered-cubic (lattice)	**CH**	Conventional heating
CI	Confidence index	**CP**	Complex phase
CR	Cold rolled	**DP**	Dual phase
EBSD	Electron backscatter diffraction	**ECD**	Equivalent circle diameter
EDX	Energy-dispersive X-ray	**EU**	European Union
FCC	Face centered-cubic (lattice)	**FFI**	Ferrite/ferrite interface
FMAI	Ferrite/martensite-austenite interface	**GAM**	Grain average misorientation
GND	Geometrically necessary dislocations	**GOS**	Grain orientation spread
HAGB	High-angle grain boundaries	**HR**	Hot rolled
HSLA	High-strength low-alloy	**IF**	Interstitial free

IPF	Inverse pole figure	**IQ**	Image quality (map)
KAM	Kernel average misorientation	**LAGB**	Low-angle grain boundaries
LENP	Local equilibrium with negligible partitioning	**ND**	Normal direction
Non-RX	Non-recrystallized	**ODF**	Orientation distribution function
OIM	Orientation Imaging Microscopy	**PAGB**	Prior austenite grain boundary
PE	Paraequlibirum	**Q&P**	Quenching and Partitioning
RA	Retained austenite	**RD**	Rolling direction
RX	Recrystallized	**SC**	Spheroidized cementite
SEM	Scanning electron microscopy	**SPM**	Scanning probe microscopy
STEM	Scanning transmission electron microscopy	**t-EBSD**	Transmission electron backscatter diffraction
TEM	Transmission electron microscopy	**TKD**	Transmission Kikuchi diffraction
TMCP	Thermomechanical controlled process	**TRIP**	Transformation induced plasticity
TWIP	Twinning induced plasticity	**UE**	Uniform elongation
UFG	Ultrafine grained	**UFH**	Ultrafast heating

ULSAB	Ultra Light Steel Auto Body	**URA**	Ultra-rapid annealing
UTS	Ultimate tensile strength	**WF**	Widmanstätten ferrite
XRD	X-ray diffraction	**YS**	Yield strength

SYMBOLS

$\mathbf{a_\gamma}$	Austenite lattice parameter	$\mathbf{A_{c1}}$	Lowest temperature for austenite formation
$\mathbf{A_{c3}}$	Finish temperature for austenite formation	$\mathbf{f_\alpha}$	Ferrite volume fraction
$\mathbf{f_\gamma}$	Austenite volume fraction	**F + M**	Ferrite plus martensite
F + P	Ferrite plus pearlite	**h**	Nanoindentation penetration depth
$\dot{\mathbf{h}}$	Nanoindentation penetration rate of the indenter	**HV**	Hardness in Vickers
$\mathbf{k_\alpha}$	Thermal expansion coefficient ferrite	$\mathbf{k_\gamma}$	Thermal expansion coefficient austenite
M	Martensite	$\mathbf{M_f}$	Martensite finish temperature
$\mathbf{M_s}$	Martensite start temperature	**n**	Strain-hardening exponent

$T_{0.1}$	Recrystallization starting temperature	$T_{0.9}$	Recrystallization finish temperature
X_{Al}	Aluminum concentration	X_C	Carbon concentration
X_{Mn}	Manganese concentration	α	Ferrite
ε	Engineering strain	ε_f	Elongation to failure
ε_U	Uniform elongation	λ	Wavelength of the X-ray
γ	Austenite	$\dot{\varepsilon}$	Strain rate
σ	Engineering stress	σ_{UTS}	Ultimate tensile strength
σ_Y	Yield stress	$\sigma_{0.2}$	0.2 % proof stress

LIST OF FIGURES AND TABLES

LIST OF FIGURES

LIST OF TABLES

1. INTRODUCTION

1. Introduction

1.1. Advanced high strength steels (AHSS): historical evolution

Steels have been the most widely used materials all over the world and are likely to remain a key material of choice in construction and manufacturing. Its manufacturing process consists of different steps, where the heat treatment of (semi-)final product (in form of sheet, rod, wire, etc.) to a great extent determines its microstructure and, hence, its properties. The current approach for steel heat treatment is based on homogenization of microstructure at elevated temperatures (either at austenitic or intercritical temperatures) and cooling with controlled rate often followed by further treatment to form the required microstructure. This is a standard approach for processing advanced high strength steels (AHSS) [1]. As a result of the well-controlled process, this group of steels typically shows a multiphase microstructure. The AHSS were developed by a consortium of the major sheet-steel producers in 1994, under the project Ultra-Light Steel Auto Body (ULSAB), in order to fulfill the demands of weight saving in automotive components. Depending on the microstructure formed and, hence, their properties, AHSS can be divided into different families. The so-called first generation of AHSS appeared in the late 90s of the last century. They present a good combination of strength and ductility and are characterized by the use of low amount of alloying elements which facilitates their processing, reducing the cost of the product. This first generation typically shows a yield strength (YS) above 300 MPa, an ultimate tensile strength (UTS) higher than 600 MPa and a reasonable high formability. Different families of steels lay into the first generation: dual phase (DP) steel mainly combines the formability of the ferrite and the strengthening effect of the martensite [2]; the transformation induced plasticity (TRIP) steel composed by ferrite, martensite and retained

austenite (RA), which transforms into martensite during deformation, increasing the strain hardening [3], or the complex phase (CP) steel, where martensite is partially substituted by bainite to increase the formability [4]. However, due to the improvement of security standards in vehicles over the years, their mechanical performance was not sufficient for certain applications, becoming their main drawback. To overcome this problem, at the beginning of the XXI century a series of austenitic steels were developed. They are known as the second generation of AHSS. They presented a unique combination of properties, with a UTS in the 800 - 1100 MPa range and a uniform elongation (UE) superior to 50 %. They are the highly Mn alloyed twinning induced plasticity (TWIP) steels. Due to their outstanding mechanical properties, they were very attractive from the engineering point of view. Nevertheless, their development has slowed down because of the high content of alloying elements (> 20 %), which increases the price, and difficulty of their processing, hindering their incorporation into industrial routes [5].

On the other hand, due to the actual situation where global warming has become a real problem, it is fundamental to find solutions in any sphere of society to reduce greenhouse emissions. This also includes industry in general, and the steel and automotive sectors in particular. In the first case, for example, the optimum heat treatments may last for hours, consuming significant amounts of energy. Hence, the steel industry is currently the second highest energy consumer in the world (51.086 ktoe, 18.59 % of total industrial energy consumption only in EU) and one of the biggest industrial emitters of CO_2, accounting for between 4% and 7% of anthropogenic CO_2 emissions worldwide [6].
In the second case, according to the European Commission, transport, which includes aviation, navigation, railways and road transport, is the source of almost 25 % of the emission of greenhouse gases. Nevertheless, road transport is, by far, the major contributor with more than the 70 %. It means that nearly 21 % of the total CO_2 emissions generated in EU come from vehicles [7]. Hence, the steel and automotive industries are nowadays challenged by carbon emission restrictions imposed by regulatory bodies.

In the steel industry, the energy consumption has been constantly reduced by introducing energy-saving equipment in steel manufacturing processes and improving the efficiency of energy conversion facilities, such as power plants. A potential solution to decrease the CO_2, emissions produced by vehicles is reducing the total weight of the car, without compromising the passengers' safety. It is known that a 10 % weight reduction produces a 3%～7% decreasing of fuel consumption, being helpful to decrease the CO_2 emission from

130 g/km in 2013 to 95 g/km, the target established by EU for passenger cars for 2021 [8]. In order to do so, the mechanical properties of the car components should be improved. In the latter case, the steel industry can also play a key role as it is intimately related to the automotive one, as steel is, in weight, the main material used for car components [9]. Therefore, both sectors are working together continuously, to look for new solutions to fulfill the current society demands.

Nowadays, the research community is making efforts in order to develop the new generation of AHSS: the so-called third generation. This family of new materials shows superior mechanical properties to bridge the gap between the first and second generations of steel, being closer to the TWIP steels, but using less amount of alloying elements to facilitate its processing and recycling, reducing at the same time its cost and weight. *Quenching and Paritioning (Q&P)* steels are one of the main examples which belongs to the third generation. They have been intensively studied by the steel community showing promising results [10–14]. Furthermore, in order to reduce the amount of energy required and the greenhouse emissions, the manufacturing of this new generation of AHSS needs to be based on the application of new and more efficient processing methods, such as the rapid treatments.

1.2. Ultrafast heating as an advanced route for processing AHSS

Steels with an excellent combination of strength and ductility can be produced via intelligent microstructural design, modifying either the chemical composition or the different processing parameters to achieve a variable amount of phases. It is known that increase in strength and ductility can be generated by introducing alloying elements, as in the TWIP steels. However, producing highly alloyed steels is not a durable approach, due to the problems associated (price, weight, recyclability…). The other possibility to enhance the mechanical behavior is via grain refinement. Over the last decades, new strategies for grain refinement have been explored, such as thermomechanical controlled process (TMCP) which combines thermomechanical rolling with accelerated cooling, asymmetric rolling combined with inter stand cooling and severe plastic deformation. In the steel field, a new

method for microstructural design has attracted a lot of attention over the last years: the rapid treatments.

The application of high heating rates for steel processing is not a new topic, as it has been contemplated through decades [15–17], although in a sporadic manner, without the existence of a thorough study. In fact, there is not an established criterion in literature to distinguish between conventional and high heating rates. However, the most extended classification among the research community considers heating rates in the range between 1 ºC/s to 20 ºC/s as conventional ones, while high heating rates lie within the range of 20 – 100 ºC/s. Finally, ultrafast heating rates are referred to those above 100 ºC/s. The last group has been examined in the last decades, since Flash® Bainite developed the most promising set up for industrial applications (**Figure 1.1**). With this tool, Lolla *et. al.* [18] proposed to apply ultrafast heat treatment for processing of AHSS with microstructures as heterogeneous as those processed via conventional heat treatments. This treatment was initially referred to as 'flash processing' [18], and other terms such as 'ultrashort annealing' [19] and 'ultrafast heating (UFH)' [20–23] are widely used for this process in the recent literature. Ultrafast heat treatment is based on heating the material with heating rates above 100 ºC/s to an intercritical or fully austenitic temperature, followed by a very short soaking (0.2–10 s) at this temperature and quenching. It attracted the attention of the steel research community due to several advantages. Due to the high heating rates applied, the time required for thermal treatment of steels is dramatically reduced, from hours to seconds. Moreover, as the whole process lasts just a few seconds, it is also characterized by a significant reduction in energy consumption, reducing also the environmental impact due to the a lower carbon emission during steel manufacturing and, giving the possibility to produce leaner alloys [24].

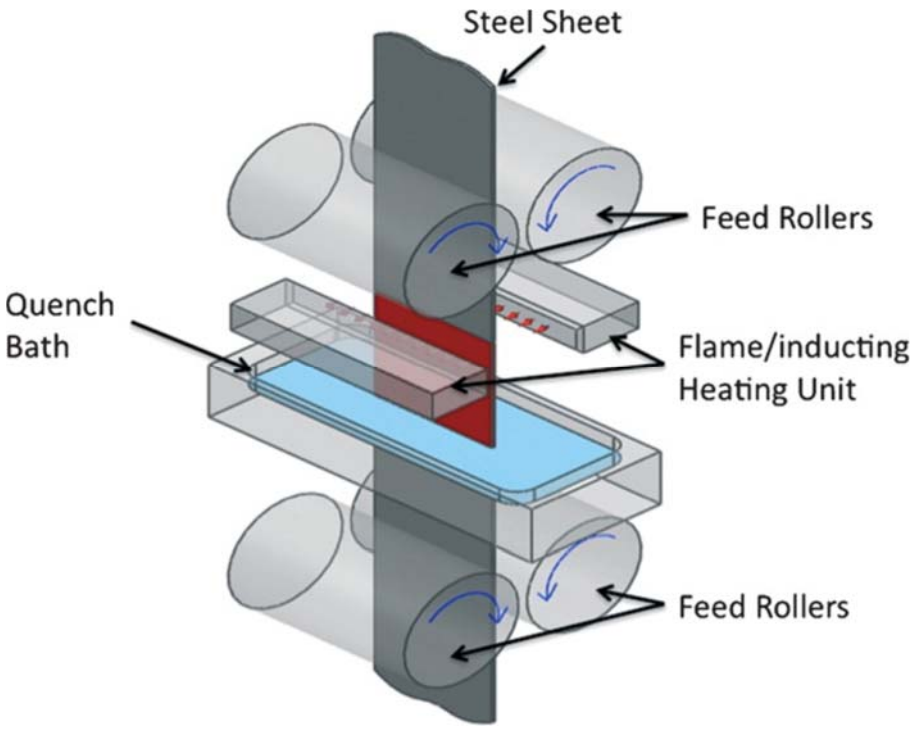

Figure 1.1: Experimental set-up for the UFH processing developed by FlashBainite [24].

1.3. Microstructural design in steels via UFH

1.3.1. Influence of heating rate on microstructure & properties

Next sections provide an overview of UFH and the effect of the heating rate on both microstructure and mechanical properties

1.3.1.1. Phase composition and grain structure

1.3.1.1.1. Role of chemical composition

As in any heat treatment applied in the steel industry, the chemical composition of the steel is one of the elemental aspects to take into account in order to reach the required final microstructure and mechanical properties of the final product. It gains even more importance during ultrafast heating, as the material is far from the equilibrium conditions. Thus, the study of the effect of the main alloying elements is vital to gain fundamental understanding of this process. In [25], Huang *et al.* investigated two steels cold rolled with 50 % reduction ratio having different chemical compositions: one suitable for DP treatment (Fe-C-Mn-Mo)

and the other composition typical for TRIP treatment (Fe-C-Mn-Si). Authors observed that, when 100 ºC/s heating rate was applied to the DP steel, austenite formation started when 90 % of the ferritic matrix was not recrystallized, whereas in the TRIP steel, the onset of austenite formation took place in a fully recrystallized ferritic matrix. This difference in the steel behavior was attributed to the alloying elements, as the presence of Mo retarded the ferrite recrystallization shifting down the A_{C1}, while the presence of Si raised the A_{C1}, affecting the formation of austenite [25]. In their study, they also calculated the heating rate required to have an overlap between recrystallization and austenite formation for the TRIP steel, being above 1000 ºC/s. Moreover, the effect of other micro alloying elements, such as Ti and Nb, was noticed to have a strong influence on the grain size reduction as well. For instance, Lesch *et al.* [26] reported that under similar annealing conditions, ISO composition (C – Mn – Ti) present a coarser grain size compared to HSLA (C – Mn – Nb – Ti), where the main difference between both steels was the amount of both alloying elements. This difference was caused by the interaction of substitutional atoms with recrystallization and transformation during annealing, resulting in a refined microstructure mentioned. Militzer *et al*. [27] studied three different DP steels, where the carbon content was 0.06, 0.12 and 0.17 %, with a varying Mn content between 1.8 – 0.74 %. The materials were subjected to similar treatments, with heating rates between 100 to 300 ºC/s, in order to generate similar microstructures. They reported that mechanical strength of the heat treated steels increased with increasing carbon content, whereas Mn had detrimental effect on their ductility. Particularly, the steel with the lowest % C, and highest Mn content, showed the lowest tensile ductility because of the banded microstructure related to Mn segregation bands [27]. Furthermore, Mn also played an important role in the resultant microconstituents formed after rapid treatments, such as bainite or martensite. Mn delays the kinetics of the austenite to ferrite transformation, which is mainly attributed to the segregation at the grain boundaries producing a strong solute drag effect [28]. As a result, non-equlibrium phases can be generated during cooling [29,30]. Similar results were presented in [31], where the mixture of phases found after heating a steel at 300 ºC/s and quenching were attributed to the gradients in carbon and other substitutional alloying elements. For instance, it was known that the carbon content in martensite formed in steels processed on large-scale (i.e. under industrial conditions) was heterogeneous, and the variations were highest at intercritical annealing temperatures closer to A_{C1} and decreased as A_{C3} was approached [32], [27].

1.3.1.1.2. Effect of heating rate on the recrystallization temperature in matrix

In addition to the chemical composition, it is also important to consider how the application of rapid treatments alter other characteristics of the material, such as the recrystallization temperature. This effect was widely studied by several research groups. In 2001, Ferry [33] and Muljono [34] clearly demonstrated for steels with various chemical compositions and different carbon contents, that an increment on the heating rate shifted both, the recrystallization starting temperature and the temperature for complete recrystallization, to higher values, although the finish temperature seemed to be more affected (**Figure 1.2**). Similar results were reported by Massardier *et al.* in [35], where they observed an increase by 60 ºC in recrystallization temperature, when the heating rate was increased from 20 to 1000 ºC/s. In [36], Bandi and co-workers observed a reduction of the recrystallized ferrite fraction before the onset of austenite formation with increasing heating rate. This effect was seen even when soaking times (1 – 900 s) at maximum temperature were applied. The latter scenario was demonstrated by Xu *et al.* in [37], where a DP steel subjected to two different heating rates (5 and 500 ºC/s) and holding time equal to 80 s at peak temperature, increased its recrystallization temperature from 680 ºC to 740 ºC, thus delaying recovery and recrystallization above the A_{C1} temperature. This effect was rationalized based on much shorter time available for strain-free grains to nucleate and grow at high heating rates. Even slower heating rates (50 ºC/s to 300 ºC/s) were sufficient to alter the microstructure during reheating compared to low heating rates. In [38], Liu *et al*. carried out a dilatometry study on a cold rolled microstructure with various heating rates (0.5, 5, 50 and 300 ºC/s). They noted that for slow heating rates, spheroidization of the pearlite and a recrystallization of ferrite at 690 ºC took place before the austenite formation. The ferrite recrystallized fraction was already reduced at 50 ºC/s, and after heating at 300 ºC/s there were almost no changes in the microstructure compared to the initial one. As a result, the hardness dramatically decreased to nearly the half of the initial value, from ~ 320 HV at 490 ºC to ~ 175 HV at 690 ºC, when 0.5 ºC/s heating was used, while at 300 ºC/s it remained constant. After raising the temperature above the A_{C1}, to 745 ºC, at 5 ºC/s the recrystallized ferrite fraction was around 85 %, whereas at 50 ºC/s it decreased down to 63 %, being only 10 % at 300 ºC/s. The reason claimed by authors to explain this effect was that, the stored energy of the deformed structure was consumed by austenite formation with the increase of heating rate, reducing the driving

force for recrystallization. Hence, the window for recrystallization to be completed becomes larger with heating rate, as reported elsewhere [39].

The first work carried out in this PhD Thesis was to analyze the influence of heating rate on the recrystallization process of the ferritic matrix and its effect on the mechanical response of the individual microconstituents (such as recrystallized and non-recrystallized ferrite). This work is included in section 4.1, corresponding to the paper titled "Effect of ultrafast heating on the properties of the microconstituents in a low-carbon steel" by Valdes-Tabernero *et al.* published in *Metallurgical and Materials Transactions A 49 (2018) 3145-3150*. In this study, a low carbon steel is subjected to a heat treatment with ultrafast heating rates (800 ºC/s) and conventional heating rates (10 ºC/s) without soaking time. The resultant microstructures and mechanical properties of the individual microconstituents formed are analyzed and compared.

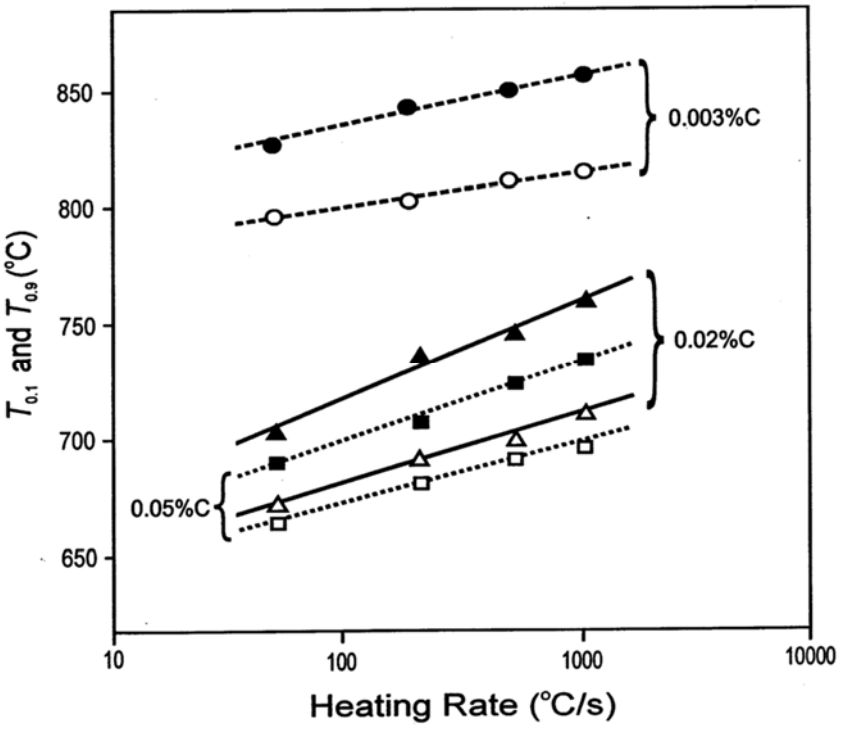

Figure 1.2: Dependence of recrystallization starting temperature ($T_{0.1}$) (open symbols) and finish temperature ($T_{0.9}$) (filled symbols) on heating rate for various chemical compositions [34]

1.3.1.1.3. Influence of UFH on the phase transformation temperatures

Other characteristics that can be modified by the application of high heating rates in steels with the same chemical composition are the phase transformation temperatures: austenite start temperature A_{C1} and finish temperature A_{C3}. In [40], it was reported that the higher the heating rate, the higher the A_{C3} and, in a minor way, the A_{C1}. This effect was rationalized based on the delay of austenite nucleation. Nucleation is a process that requires time to be accomplished, and when the heating rate is accelerated, the onset of austenite formation occurs at higher temperatures [31]. However, if the microstructure is severely deformed prior to heat treatment using high heating rate (*i.e.* cold rolling), non-recrystallized grains, fragmented pearlite and / or spheroidized carbides remain in the structure, being suitable places for austenite nucleation. Hence, the increment of austenite nucleation sites can compensate in some way the increase in A_{C1} temperature caused by the increase in heating rate. Nevertheless, Li *et al.* [39] observed in their work focused on a cold rolled DP steel the increment of both, A_{C1} and A_{C3} with heating rate from 725 ºC to 750 ºC and 865 to 920 ºC, respectively, when heating rates was raised from 5 ºC/s to 500 ºC/s. Furthermore, in [41] authors reported an increase in A_{C1} from 731 ºC to 758 ºC in a Nb - modified steel when heating rate was increased from 0.3 ºC/s to 693 ºC/s. Moreover, Karmakar *et al.* [42] described an increase by 25 ºC – 35 ºC in A_{C1} and 41 ºC – 51 ºC in A_{C3} when heating rate increased from 1 ºC/s to 300 ºC/s for various initial microstructures. Therefore, the effect of heating rate on the transformation temperatures is strongly affected by the chemical composition and the initial structure of the steel.

1.3.1.1.4. Austenite nucleation and grain growth

It is well established in the current literature that, if steel is subjected to intercritical annealing, the amount of austenite (martensite upon quenching) increases with heating rate for a given intercritical temperature [25,38,39,43–45]. This is related with the promotion of austenite nucleation during high heating rates, whereas at slow heating, the austenite growth is the dominant process. Austenite tends to form in high energy regions, carbon enriched areas and at lattice defects, including distorted ferrite grain boundaries (in the non-recrystallized zones) or interface between ferrite and cementite particles. Therefore, if slow heating rates are applied, ferrite has time to recrystallize and grow, reducing the grain

boundary area, thus, decreasing the density of favorable places for austenite to nucleate, as it was shown in [44]. In cold rolled microstructure formed by ferrite and pearlite, slow heating produces spheroidization of the pearlitic colonies, which also reduces the possibility for austenite to form [25,38]. Hence, only a few nuclei will be able to form at the ferrite grain boundaries and ferrite / cementite interface, as austenite nucleation rate can be between 3 to 8 times faster at ferrite grain boundaries than in the grain interior [44], resulting in the growth of the few austenitic grains formed. On the other hand, at high heating rates, ferrite remains in a non-recrystallized state when austenite formation takes places, which, in turn, reduces the ferrite grain size, thus, increasing the grain boundary area. Therefore, austenite nucleation rate is enhanced due to the high amount of the energetically favorable sites. Moreover, in cold rolled steels, austenite forms at the ferrite-pearlite interface, which remains from the initial microstructure, as it was reported by Huang *et al*. [25] and Liu *et al*. [38] for steels heated at 100 ºC/s and 300 ºC/s, respectively. Therefore, austenite nucleation is promoted rather than its growth. This has effect on the spatial distribution of the phases in DP steels, as at low heating rates, the austenite is distributed in a more homogeneous manner, while at high heating rates a banded microstructure is predominant (**Figure 1.3**) [39]. This is caused because austenite grows consuming the elongated colonies in first place, as carbon needs to travel a short distance [25,39,40]. Moreover, fast reheating (300 ºC/s) leads to the formation of carbon gradients in the austenite, as it was described by Li *et al.* [46], where they observed a maximum carbon concentration at the boundary which decreases in the interior of the grain. Authors claimed that this effect could be produced by a two-stage growth of the austenite. In the first stage, austenite nucleates consuming the cementite which has a high carbon concentration. This effect is controlled by the diffusion of carbon into the austenite being a fast process. However, it generates an austenite supersaturated in carbon. Therefore, in the second step, austenite grows into the surrounding ferrite to reach equilibrium. In the interface, the carbon concentration should be in balance, generating the gradient through the austenite grain. In addition to the carbon gradients, the percentage of retained austenite may be greater than at conventional heating rates as a consequence of the finer grain size. This is caused by the high amount of nuclei, which compete to grow, and the lack of time for carbon to diffuse, reducing its travelling distance and, hence avoiding the austenite growth [37]. Moreover, the retained austenite present in the material has different morphologies, being the film-like the predominant one, whereas at slow heating rates, the austenite is mainly of blocky type, which has lower stability because of their lack of ability to rotate, accommodating less plastic deformation [47], thus, transforming into

martensite at the onset of deformation [45,48]. Liu *et al*. mentioned in [45] that, in addition to the difference in morphology, high heating rates lead to the formation of austenite with higher hardenability than the one formed at conventional rates, because of its finer size and its higher carbon content. This increase in hardenability retards, in turn, the bainite transformation during the partitioning process, retaining more martensite/austenite islands, enhancing the ductility of the material.

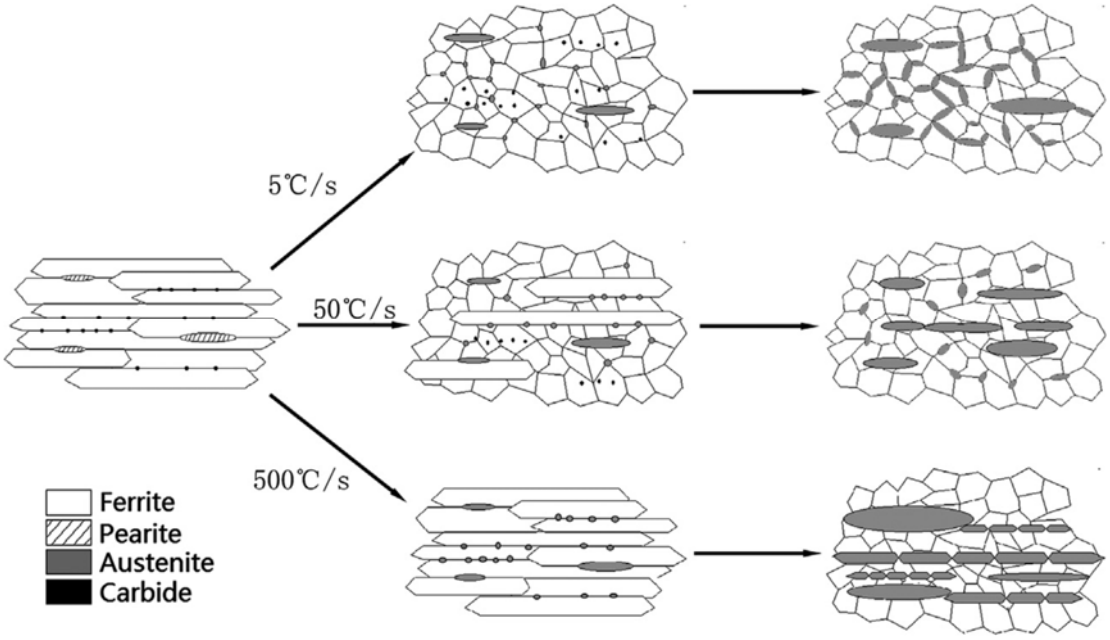

Figure 1.3: Representation of the microstructural evolution in a cold-rolled DP steel for various heating rates [39].

One of the most important benefits of the application of high heating rates in steel processing is the significant grain refinement, which has important effect on the final behavior of the material. Ferry *et al.* [33] clearly demonstrated that increasing the heating rate decreased the mean grain size for steels with different carbon contents, as it is shown in **Figure 1.4**. It can be observed that the grain size decreases constantly, although for the steel with the lower carbon content, the diminution is more pronounced reducing the grain size from 20 μm to 12 μm when heating rate increases from 50 ºC/s to 1000 ºC/s. Massardier *et al.* [35] also reported a grain size reduction from 5.8 to 3.8 μm, when heating rate passed from 20 to 1000 ºC/s. Austenite grain size is also affected by the high heating rates, as it was reported in [49], where authors showed a reduction in grain size for various initial microstructures when heating rate was increased by two orders of magnitude, from 1 ºC/s to 100 ºC/s. Even below

100 ºC/s the grain refinement was observed in a Nb - added steel, when reheating was carried out from 0.5 ºC/s to 50 ºC/s producing a grain size reduction from 5 μm to 1 μm [50]. An interesting idea was proposed by Reis *et al.* in [51]. They reported a grain size reduction from 20 μm to 6 μm when 1000 ºC/s heating rate was applied in a fully recrystallized structure. The difference with the results reported by Ferry [33], where the minimum grain size was 12 μm for 1000 ºC/s, was attributed to the difference in rolling reduction ratio, passing from 75 % in [33] to 95 % in [51] and the variation in chemical composition. Reis [51] studied a material alloyed with Ti (0.044%), whereas in [33] the Ti content was 0.005 %. The reasons behind the significant grain refinement produced by high heating rates are related to the energy of the system. On the one hand, at high heating rates the time available for recovery is reduced, thus the dislocation density is high, increasing the energy for the nucleation process. On the other hand, as it is mentioned above, the recrystallization temperature is shifted to higher values with heating rate. Hence, the higher the temperature, the higher the nucleation rate, as the latter directly depends on the former. Therefore, both effects raise the nucleation rate of the system. And finally, due to the short time of the treatment, the nuclei generated are not able to grow, producing refined microstructure [33,34,52]. Reis also observed that with further increasing heating rate above 1000 ºC/s, the grain size remained stable. This effect can be explained because the grain refining tendency may be compensated by the increased average growth rate of the recrystallization nuclei as the growth stage of recrystallization was delayed to higher temperatures as a result of the rapid annealing cycle [51]. Additionally, authors [51] reported that in the fully austenitic region, for 300 ºC/s heating rate, the grain growth at 20 μm/s, while for heating rates of 10 ºC/s, the grain growth was produced in a slower manner, at 2.7 μm/s. This effect is justified by a heterogeneous nucleation phenomenon. As the α to γ transformation starts in the carbon-rich sites of the parent phase microstructure, it is reasonable to assume that the regions in the vicinity of re-dissolving TiC particles will act as potential nucleation sites.

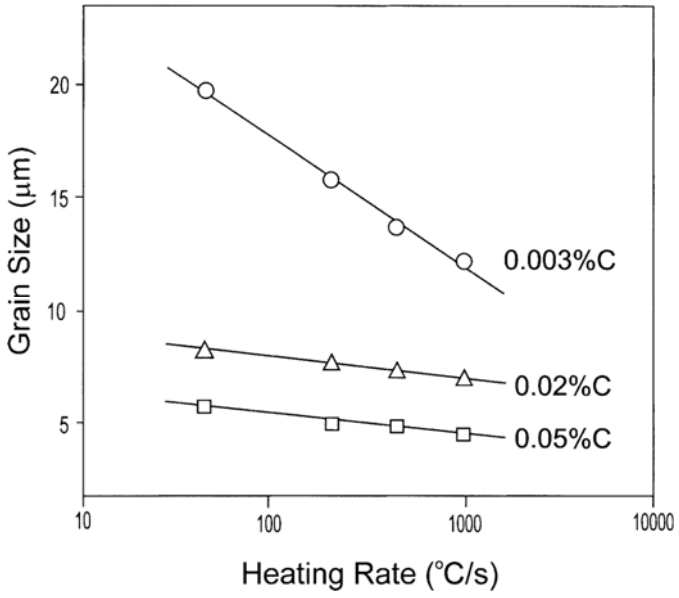

Figure 1.4: Effect of heating rate on grain size for 0.003 %C, 0.02 %C, and 0.05 %C steels [33].

1.3.1.2. Crystallographic texture

The effect of various heating rates on crystallographic texture was extensively recorded for different groups of steels [52–56]. For instance, Kestens *et al.* [52] observed fully recrystallized structures in interstitial free (IF) steels just before the onset of austenite formation, and texture was not affected by heating rate even for short soaking times (0.3 s). The structure developed presented maximum intensity in the ND fiber // {111}‹uvw›, showing a similar behavior as conventionally treated steels. Similar results were shown by Senuma in [56]. Furthermore, when temperature was raised above the onset of austenite formation, the material demonstrated a strong memory effect, due to the increase in the ND fiber intensity, in contrast to the expected randomizing effect of a double phase transformation these textures were even slightly stronger than the recrystallization ones [52]. Moreover, texture analysis were performed in the cold rolled TRIP steels [19,57]. BCC cold rolled structure is characterized by a strong ND – RD fiber with a convex curvature. After slow heating (10 ºC/s and 50 ºC/s), the developed texture showed a typical recrystallized structure with an intense ND fiber but with a concave curvature and weak or even vanished RD fiber [20]. This effect was observed during the application of high heating rates prior Q&P treatment (**Figure 1.5**) [58]. This is caused by the great amount of energy stored by the ND grains compared to the RD ones, presenting more driving force for recrystallization

[59,60]. Thus, at low heating rates, ND grains are the first which nucleate and grow consuming the RD ones, which present less driving force to recrystallize. On the other hand, at high heating rates (3000 ºC/s), the BCC cold rolling texture features are kept. Due to the short time given for recovery and recrystallization, ND components have less time to grow to consume the RD grains. Therefore, alpha components only undergo recovery being present in the structure or even growing in size, which, in turn, increases the RD fiber intensity [21]. This effect was observed at temperatures close to 930 ºC, indicating that microstructure recrystallization was not completed [20]. In addition to the increase in intensity in the ND fiber components, as it happens in ultra-low carbon steels, due to both, recrystallization and memory effect, high heating rates lead to the formation of non-conventional products in TRIP steels [61]. These components appear right after the austenite formation. Authors claimed that the appearance of this texture elements was mainly caused by the dissolution of carbides in preferential orientations, which, in turn, favored the formation of austenite nuclei at carbon rich sites of the microstructure [61].

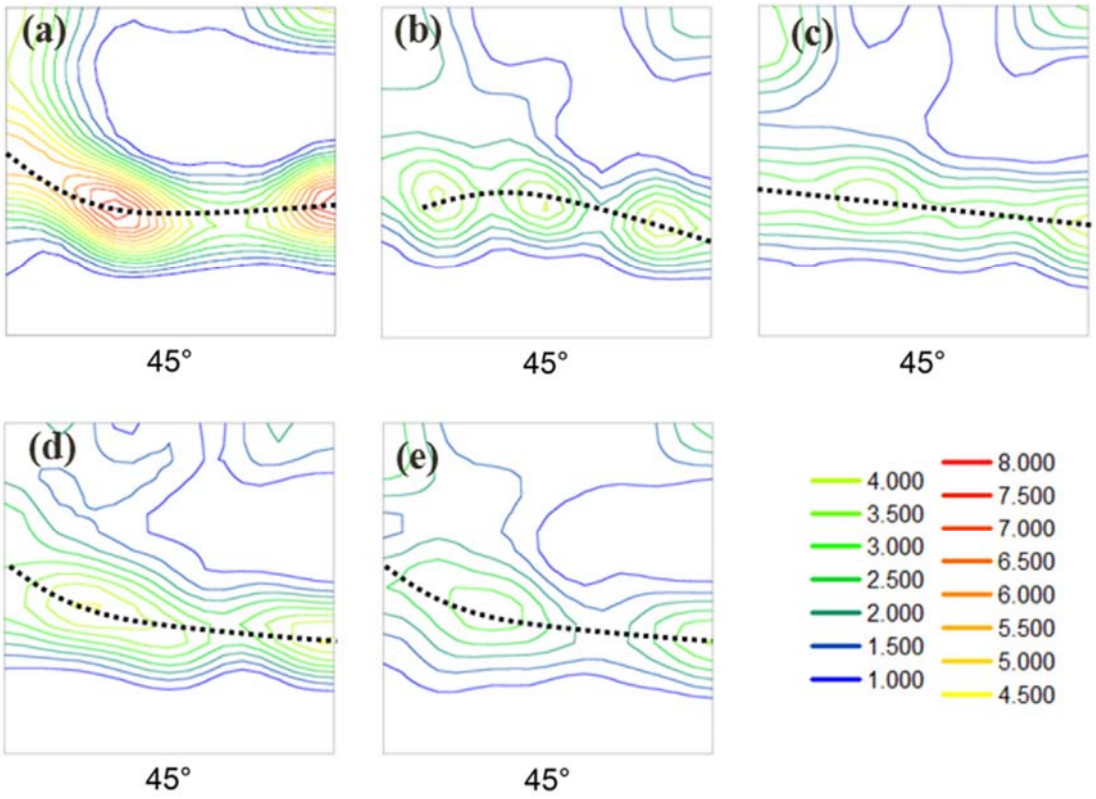

Figure 1.5: Orientation distribution function at a cross-section of $\varphi_2 = 45^o$ of (a) cold rolled and quenched samples after heating at (b) 10 ºC/s with soaking, (c) 10 ºC/s, (d) 500 ºC/s and (e) 1000 ºC/s [58].

1.3.1.3. Properties

1.3.1.3.1. Basic macromechanical properties

One of the main advantages of the application of high heating rates in the steel processing is the improvement of the mechanical properties, being crucial for the automotive sector. Numerous studies reported a better mechanical strength without a significant reduction in ductility in the UFH processed steels compared to the conventionally processed ones [18,21,26,35,46,62,63]. In [64], Meng *et al*. reported an increase of 6.6 % in the tensile strength along with an improvement of 26.6 % in total elongation of a DP590 steel due to the increased heating rate from 5 ºC/s to 500 ºC/s. The high mechanical properties were attributed to the ferrite grain refinement and the change in martensite structure, from a coarser lath-like at low heating rates to a fine fiber-like at 500 ºC/s. This is in a good agreement with the work carried out by Lesch *et al.* in [26], where they achieved a significant

grain refinement in various steel grades (HSLA, C-Mn), leading to remarkable increase in strength by about 130 MPa, with a reduction of ductility around 4 %. In [42], the use of rapid heating (300 ºC/s) drove to a better combination of strength and ductility compared to slow heating rates (1 ºC/s), being the increase in strength between ~200 to 250 MPa and in ductility by ~2 to 6 % for the various microstructures studied. They also attributed this effect to the finest ferritic grain size achieved and the uniform distribution of martensitic islands. Massardier an co-workers [35] studied the effect of the processing parameters on a low carbon steel on the tensile properties at various angles (0 º – 45 º – 90 º) with respect to the rolling direction. During the conventional heat treatment, the material was heated at 20 ºC/s to 720 ºC with a holding time equal to 30 s and a cooling rate of 25 ºC/s, while in the rapid cycle (1000 ºC/s), the peak temperature was 920 ºC, soaking time 1 s and cooling rate 250 ºC/s. These parameters resulted in 80 % of austenite fraction in both cases. High heating rates led to enhanced strength in all conditions studied, mainly attributed to the grain refinement. Moreover, the elongation was also improved because the initial iron carbides were dissolved during heating, precipitating in a finer state during cooling compared to the ones formed during the conventional treatment. In [21], Castro Cerda *et al.* compared the effect of heating rate for a low carbon steel with two different initial microstructures: one was formed by ferrite and pearlite after 50 % cold rolling (50 % F+P) and the other by 50 % of ferrite and martensite (50 % M). For both microstructures, the UTS significantly increased with increasing heating rate from 10 ºC/s to 800 ºC/s (**Figure 1.6** a), being more pronounced in the 50 % M where an increment of ~ 200 MPa was reported. The elongation to failure also showed a marked increment. In the 50 % F + P case, it increased from ~ 12 % to ~ 31 %, while for the 50 % M counterpart, from ~ 6 % to ~ 20 % (**Figure 1.6** b). This increase in strength was associated with a high amount of martensite formed during high heating rates and the reduction of the ferritic grain size, while the enhanced elongation was provoked by the carbon gradients present in the austenite during heating, which led to the formation of martensite-bainite aggregates.

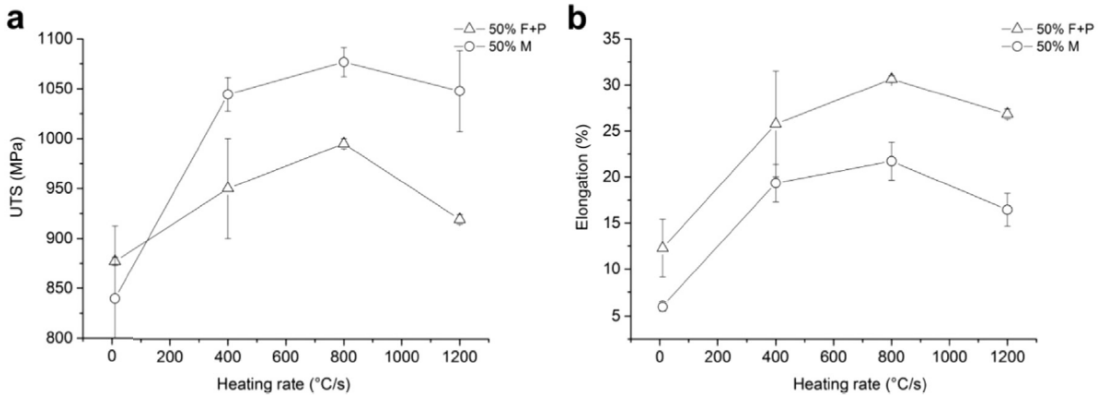

Figure 1.6: a) UTS and b) elongation to fracture values vs heating rate. Peak temperature and soaking time are 860 ºC and 1.5 s, respectively [21].

Some authors also reported an increase in the strain hardening ability at the early stages of deformation associated with the rapid treatments in comparison with the conventional heating rates applied [37,63]. In [63], authors claimed that the main reason for this improvement was the ferrite grain refinement produced by high heating rate (300 ºC/s) compared to conventional heating rate (5 ºC/s). Moreover, the volume expansion, which occurs during austenite to martensite transformation upon cooling, needs to be accommodated by the surrounding ferrite, thus, increasing its dislocation density, hindering its plastic deformation (**Figure 1.7**). At the later stages of deformation, martensite governs the behavior in both cases being the difference negligible.

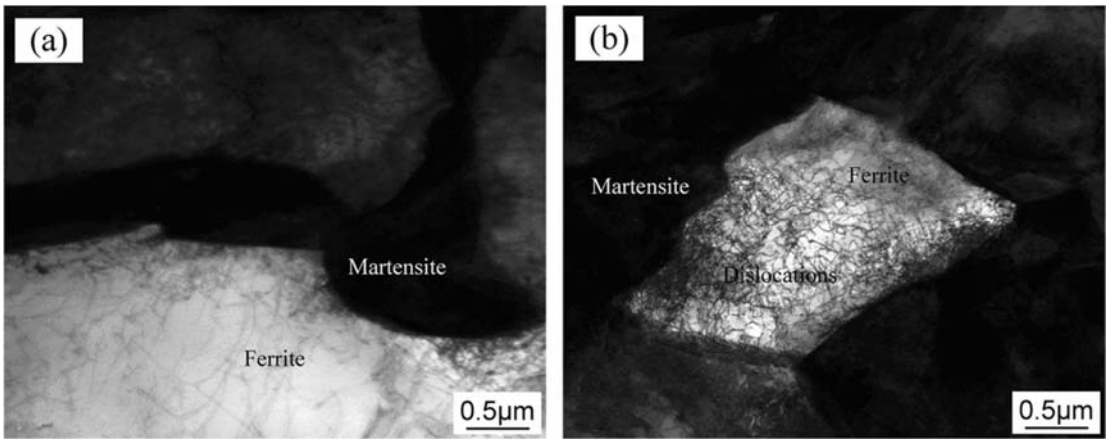

Figure 1.7: TEM images showing dislocations in ferrite associated with the formation of martensite during a) conventional annealing and b) rapid annealing [63].

The efficiency of applying high heating rates in combination with other thermal treatments, such as Q&P was also proved in [45,47,58]. Liu *et al*. [45] analyzed the effect of two different heating rates (5 ºC/s and 300 ºC/s) during the Q&P treatment for various peak temperatures and soaking times. Due to the grain refinement and the large martensite volume fraction, the fast heating leads to a higher YS compared to the slow one. However, absence of soaking or annealing at lower temperatures results in a YS reduction in both conditions, mainly caused by the softening of the ferrite matrix through recrystallization. On the contrary, increasing both soaking time and peak temperature increases significantly the yield strength, because of the higher martensite volume fraction. De Knijf *et al.* [58] also studied the influence of heating rate on the microstructure and properties on Q&P, but in this case prior to treatment. It was observed that the rapid heating before traditional Q&P treatment enhanced both strength and ductility significantly being more pronounced after high heating rates, 1000 ºC/s (**Figure 1.8** a). The study of the fracture surface revealed that after conventional Q&P treatment (10 ºC/s) with and without soaking, the fracture mode was quasi-cleavage formed by dimples and cleavage facets, being the former caused by the plastic deformation accommodated by RA, while the latter by the presence of high C martensite (**Figure 1.8** b & c). Nevertheless, the use of high heating rates modified the fracture behavior to a ductile mode, where fracture surface consisted mainly of dimples (**Figure 1.8** d & e). The transition from a quasi-cleavage to a ductile fracture mode was associated with the reduction of grain size in both, austenite and martensite. Moreover, due to the short time of the processing, there were undissolved carbides in the microstructure and, therefore, the tempered martensite formed present a low C content and, finally, some recrystallized ferrite appears as a consequence of shifting transition temperatures (A_{C1} and A_{C3}) to the higher values.

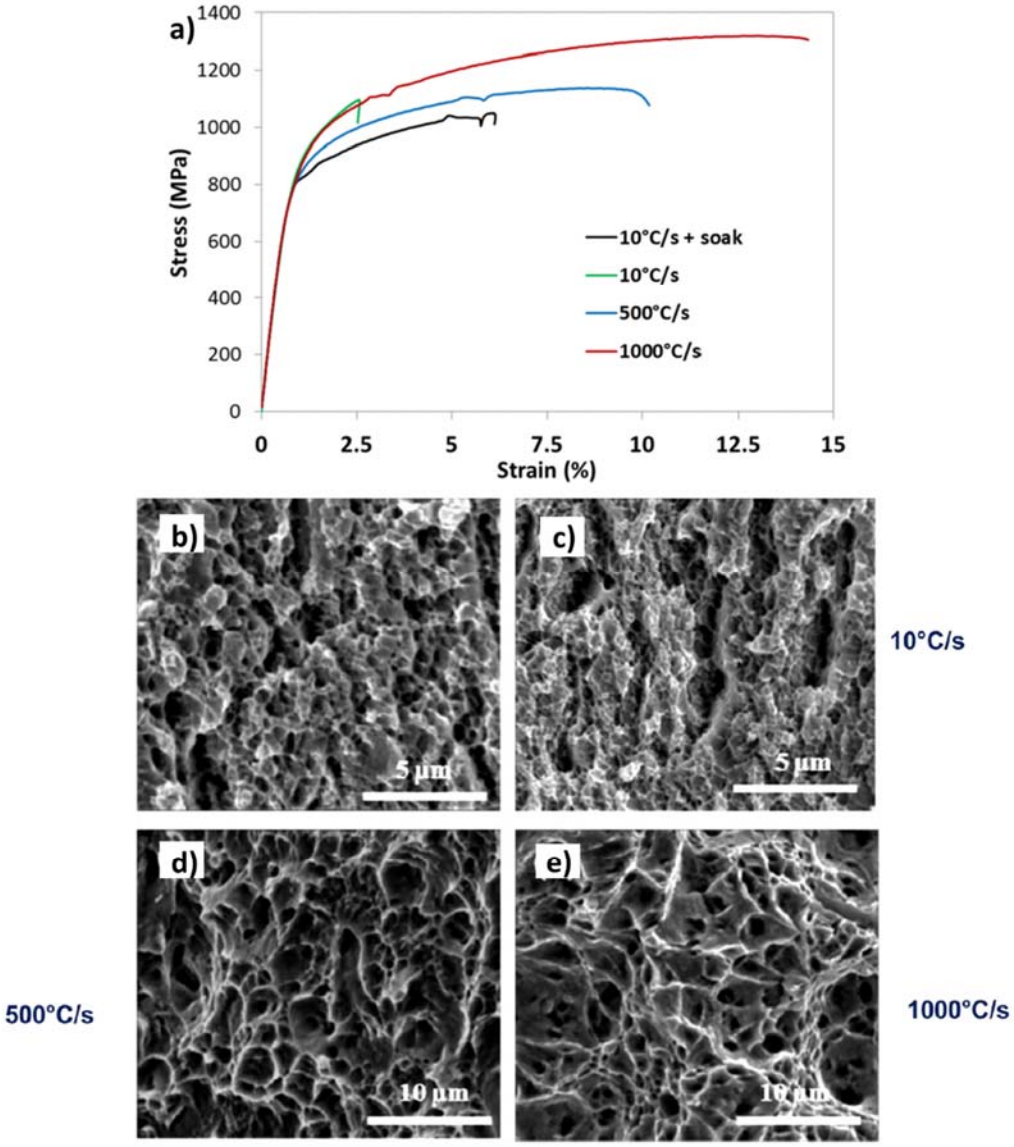

Figure 1.8: a) Tensile test curves on 25 mm sub-size samples of steel 0.25%C–1.5%Si–3%Mn after applying high heating rates followed by Q&P treatment; Fracture surfaces of tensile test samples after conventional Q&P heat treatment b) and after heating at c) 10 ºC/s, d) 500 ºC/s and d) 1000 ºC/s [58].

1.3.1.3.2. Properties of individual microconstituents

The main body of research focuses entirely on macro-mechanical properties of the UFH processed steels. However, the AHSS are complex steels formed by various phases. It is well-known that macro-mechanical response of the multi-phase materials is determined by morphology, architecture and properties of the individual microconstituents [1]. The latter

depend, in turn, on their internal lattice structure (i.e. defect density) [65], which are greatly affected by the processing parameters. In order to study mechanical behavior of individual microconstituents, nanoindentation technique needs to be employed. It has been largely used for different steels to characterize the materials behavior at micro-scale, being a reliable method. For instance, in [66,67], Ohmura *et al.* studied the dependence of the matrix strength with the tempering temperature for various Fe-C binary systems with a martensitic matrix. A matrix softening was observed for all conditions, when tempering temperature increased, due to the reduction in the dislocation density. Mazaheri *et al.* reported that ferrite nanohardness was significantly lower than that measured in martensite in DP steels [68]. However, nanohardnes values in both microconstituents were affected by the processing route, decreasing with increasing intercritcal holding time. Authors claimed that variations of ferrite grain size and martensite carbon content with intercritical holding as main reasons for decrease in hardness. Moreover, the martensite to ferrite hardness ratio greatly affects the macro-mechanical properties of the system, as the higher the ratio, the higher the strength of the material. Yielding is directly linked to the soft phase present in the microstructure, in this case ferrite. However, martensite introduces additional dislocations due to the volume expansion produced by its transformation, hardening the ferrite. The maximum strength is related to the volume fraction of the hard phase. On the other hand, the greater the difference in nanohardness between phases, the lower the ductility of the system, as there is higher strain localization at the interfaces [68]. Similar results were reported in [69]. In [70], authors carried out an investigation on commercial DP steels. Their outcomes clearly denoted a significant dispersion on the hardness results for both, ferrite and martensite, caused by the difference in dislocation density within grains, the inhomogeneous distribution of alloying elements in the interior of grains and/or the effect of the microstructure present underneath the grain tested. Nanoindentation studies were also performed on TRIP steels to analyze the mechanical response of the different phases. Furnémont and coworkers analyzed the effect of the chemical composition on two different steels [71]. It was shown that ferrite and martensite were the softest and hardest phase, respectively, independently on the alloying elements. The hardness of the ferritic matrix increased with the silicon content due to the solid-solution strengthening. Martensite presented the highest nanohardness values because of the high carbon content (~ 0.6–1 wt. %), as it is known that martensite hardness strongly depends on the carbon content [72], as it distorts the lattice introducing high dislocation density [71]. He *et al.* [73] studied the mechanical stability of different phases, mainly retained austenite (RA) and ferrite in a TRIP steel. They showed that austenite presents

higher nanohardness than ferrite, although the possible austenite to martensite transformation should be taken into account in the analysis of the results. Nonetheless, it was observed a much greater dispersion of the nanohardness values on RA compared to ferrite, caused by different mechanical stabilities of the austenitic grains, which was greatly affected by its Mn content, as Mn enriched austenite requires high loads to transform into martensite. Even in third generation steels, such as Q&P, nanoindentation was used to characterize the internal structure of the material [14]. It was demonstrated that during the partitioning step carbon diffuses from martensite into austenite, hardening the latter phase due to solid solution.

Nevertheless, up to date there have been no systematic studies on the properties of the individual microconstituents in the UFH processed steels. Understanding the effect of the UFH parameters on the properties of individual microconstituents and their effect on the overall mechanical performance of UFH steels could provide the research community with a valuable tool for the microstructural design in AHSS using ultrafast heating. In this PhD thesis, the effect of different processing parameters, such as heating rate and soaking time, on the properties of the individual microconstituents formed after ultrafast heating as well as of the bulk material was thoroughly studied. This work is included in section 4.3 corresponding to the paper titled “The effect of soaking time after ultrafast heating on the microstructure and mechanical behavior of a low carbon steel” by Valdes-Tabernero *et al.* published in *Materials Science and Engineering A 765 (2019) 138276*. The paper is focused on the evolution of the microstructure with soaking time and its relation with the micro- and macro-mechanical response of the low carbon steel.

1.3.2. **Role of initial microstructure**

The influence of the initial microstructure on the final microstructure of the UFH treated steels has been broadly studied in the literature. Therefore, the scope of this section is to make an overview of the effects of the initial materials condition on aspects such as the recrystallization or the morphology and formation of the different phases. In [44], Azizi *et al.* studied the relation between microstructure and properties on DP chemical composition (Fe-C-Mn) with three different initial microstructures. The first one (I) was a fully martensitic structure subjected to 80 % cold rolling. The second condition (II) was similar

to the first one but tempered at 550 ºC for 2 hours prior to the 80 % cold rolling in order to promote carbide particles. Finally, the third one (III) was tempered before and after cold rolling to form a more equiaxed grains. All conditions were heated at 300 ºC/s to 750 ºC and hold for 10 seconds. The (III) processing resulted in more carbides at ferrite grain boundaries which, in turn, provoke a higher fraction of austenite (martensite upon cooling) during the rapid heating. The competition between ferrite and austenite during the growing stage ended up in a finer microstructure, and, therefore, an improved combination of strength and ductility was achieved [44]. In another work [40], authors also investigated the effect of cold and hot rolling on the transformation temperatures. They demonstrated that, whereas in cold rolled (CR) microstructures the increase in A_{C1} temperature due to the increase in heating rate can be suppressed, in hot rolled (HR) condition the increment of heating rate was always accompanied by an increment of both A_{C1} and A_{C3}. While in the former case, there was a balance between the existence of preferable sites for austenite nucleation (non-recrystallized ferrite, carbides, fragmented pearlite lamella…) and the delay of the austenite formation due to the lack of time, in HR there were not favorable places for austenite formation, being only a thermally activated process. Moreover, the increment of heating rate in the HR case resulted in a fine and homogeneous distribution of ferrite and martensite. However, in the CR structures, the increasing heating rate transforms the microstructure from a uniform dispersion of martensite in the matrix to the banded morphology, as it can be seen in **Figure 1.9**. This is caused because austenite preferentially forms at the interface of pearlite colonies, which are elongated during cold rolling. Hence, austenite grows consuming the elongated colonies in first place, as carbon needs to travel a short distance and those are carbon enriched zones [25,40]. Nevertheless, the amount of banded martensite can be controlled reducing the deformation and/or the heating rate. The effect of cold rolling also affects the recrystallization kinetics, as it was shown by Bandi *et al.* in [36] and by Nakada and coauthors in [74]. In the first study, researchers investigated the effect of incrementing the cold rolling from 50 % to 75 % before reheating at 50 ºC/s. They observed that less holding time for a given temperature was required for the complete recrystallization of the microstructure. Therefore, the recrystallization kinetics was faster. Similar results were published in [74], where authors analyzed steels subjected to various cold rolling reductions (0%, 20%, 40, 60%) at two heating rates (0.083 y 100 ºC/s). They observed that the increment in deformation leads to a high degree of matrix recrystallization at the given temperature. In both cases, the effect was related to the high energy stored in the system due to the high amount of accumulated deformation, thus presenting more driving force for

recrystallization. Moreover, a high CR reduction ratio drives to the formation of elongated grains with a higher amount of grain boundaries providing more nucleation sites for recrystallization [36]. The more nucleation zones, the finer the resultant microstructure, as there is a competition between the grains during their growth during fast treatment. This also affects the final mechanical properties of the material. It was observed that the strength was enhanced without a significant reduction of elongation with increasing cold rolling reduction ratio [74].

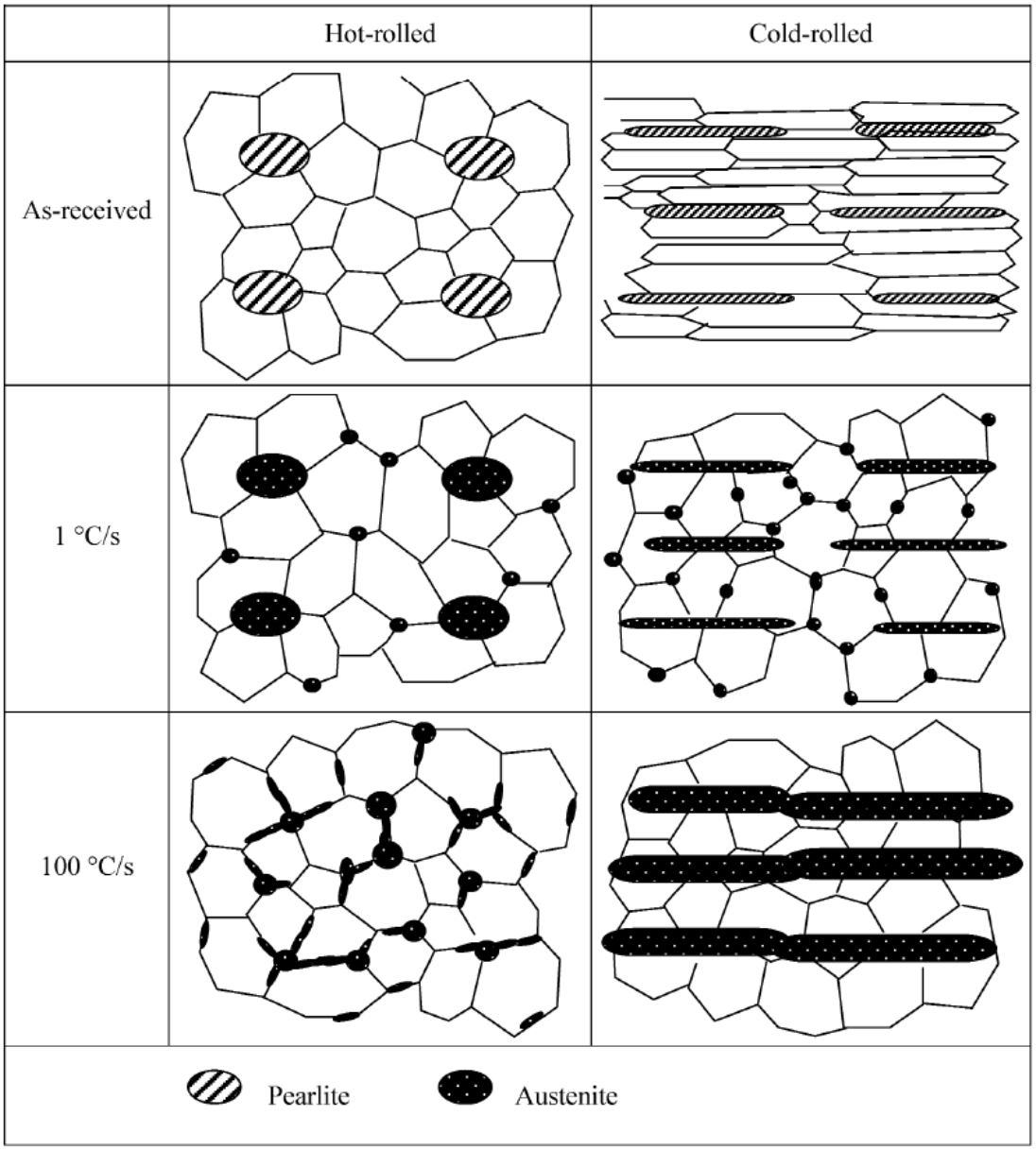

Figure 1.9: Schematic illustration of the microstructure evolution in a cold-rolled Fe-C-Mn-Mo steel annealed with different heating rates to holding temperature [25].

The evolution of grain size was analyzed in [21], where two microstructures, one formed by ferrite and pearlite (F + P) and another composed by ferrite and martensite (F + M), were compared. Both initial conditions were subjected to cold rolling with 50 % reduction ratio. Then both materials were heated to 300 ºC isothermally held at this temperature for 30 s to simulate a preheating stage in some industrial annealing lines. Afterwards the specimens were heated to 860 ºC with various heating rates (10 – 1200 ºC/s). After analyzing the average ferritic grain (AFG) size, it was observed that it was reduced with heating rate,

although the effect was more pronounced in the F + P microstructure. However, the maximum AFG size measured was considerably coarser in the F + P than in the F + M (**Figure 1.10** a)). The latter observation can be rationalized based on two effects: 1) the phase distribution in the initial microstructure has a great influence on the grain size, and 2) the interaction between fine particles and grain boundaries, which can take place during preheating stage, as particles may suppress the grain boundary migration. On the other hand, above 400 ºC/s, the AFG tended to reach a plateau due to the shorter time given to nuclei for growth during treatment. Authors also observed that the martensite fraction increased faster in the F + P than in the F + M counterpart (**Figure 1.10** b)), due to the existence of preferable places for austenite to grow (carbides and cementite platelets). Similar behavior was reported by Pedraza *et al.* in [43], where they compared the austenite formation in a F + P microstructure and the same alloy after spheroidization treatment during heating at 200 ºC/s. In the latter case, the phase transformation was slower due to the presence of more Fe_3C carbides in the interior of the matrix, which did not contribute to the austenite nucleation. Nevertheless, if the heating rate is too high, *i.e.* above 800 ºC/s, the fraction of austenite and, therefore, martensite is significantly reduced, because of the shift of A_{C3} temperature to higher values, thus reducing the fraction of austenite formed during heating, as it is shown in **Figure 1.10** b) [21].

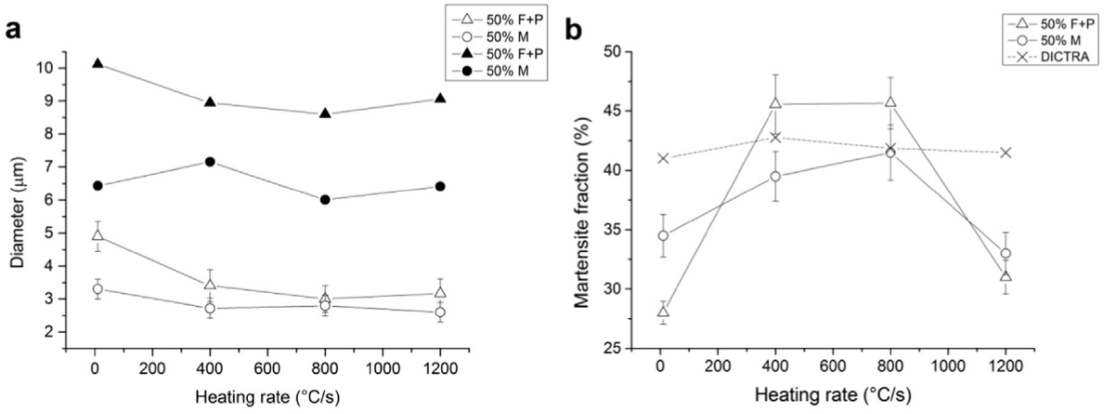

Figure 1.10: a) Average ferritic grain size (lower set, outlined marks) and maximum ferritic grain size (upper set, filled marks); b) Martensite phase fraction [21].

In [75], authors studied the effect of initial microstructure on the hardness of a C-Si-Mn steel. The two conditions analyzed present an initial microstructure composed by ferrite and pearlite (F + P) and ferrite and martensite (F + M). The hardness was maintained unchanged

in both conditions, when the material was reheated below 500 ºC at different heating rates, 140 ºC/s, 360 ºC/s and 1500 ºC/s (zone I in **Figure 1.11**). However, further increase in temperature up to 800 ºC at 140 ºC/s produced a decrease in the hardness in both conditions, F + P and F + M, being more pronounced in the latter one (zone II). This effect was attributed to the onset of recovery and recrystallization in the initial microstructures. On the other hand, the hardness was slightly reduced in the F + M condition when heating rate was increased to 360 ºC/s in that temperature range, and it was completely suppressed in the F + P one at 1500 ºC/s. Moreover, when temperature was increased to the intercritical region (zone III), the hardness was raised in both conditions because of the martensite formation. Nevertheless, above A_{C3} the hardness of the F + M sample slightly decreased due to the grain growth of the parent austenite which formed coarse martensite, while for the F + P case the hardness reduction was delayed. The latter effect can be explained by the pinning effect of the undissolved carbides which come from initial pearlite.

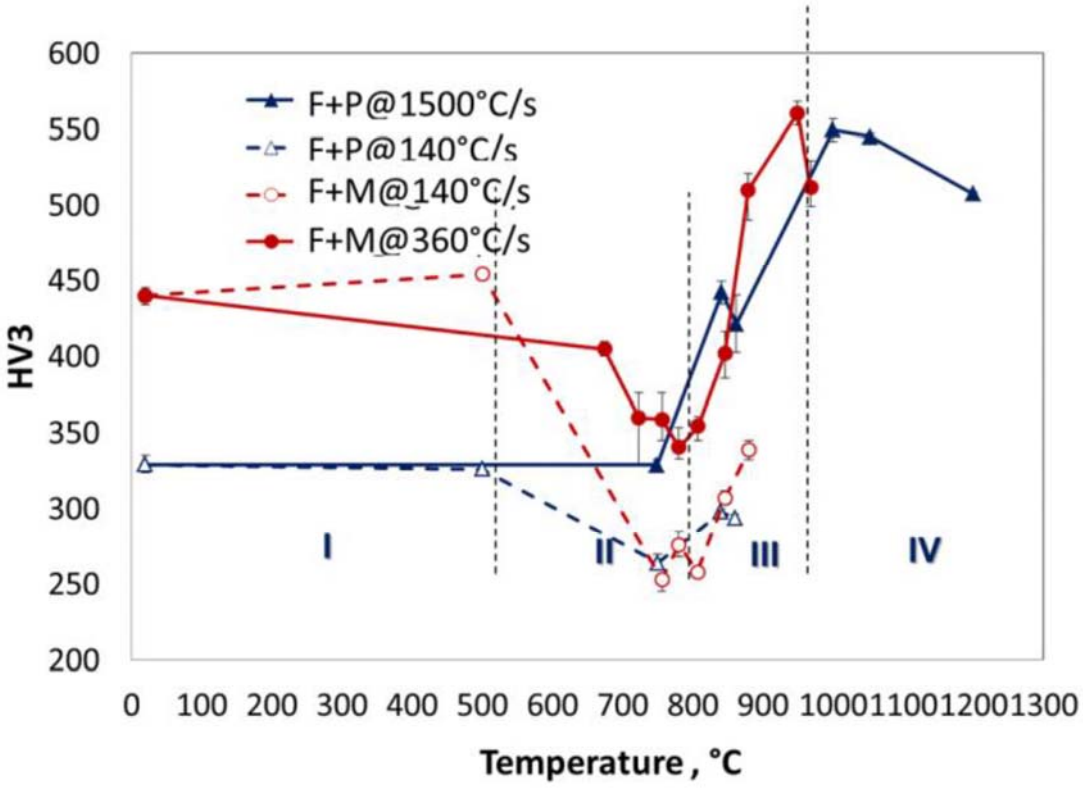

Figure 1.11: Hardness vs peak temperature for different heating rates and initial microstructures [75].

1.3.3. Effect of other heat treatment parameters

During rapid treatments there are other parameters in addition to the heating rate, that need to be considered carefully in order to obtain the desired materials behavior, as they can greatly modify the microstructure and properties. The maximum temperature achieved during treatment, the soaking time at the peak temperature or the cooling rate, among others, are aspects which should be taken into account with great care, although any of these concepts has not been thoroughly investigated yet. For instance, there are no systematic studies on the influence of the isothermal soaking on the microstructure and properties, being, in most of the studies as short as possible (0.2 – 3 s) [18,21,52,76]. However, in [44] authors studied the effect of different holding times (1, 60 and 300 s) during intercritical annealing at 300 ºC/s on martensite and ferrite. They reported that martensite reached the paraequilibrium after soaking for 60 s. Moreover, increasing from 10 to 60 s, martensitic islands doubled in size (1 to 2 μm). On the other hand, in the 10 to 60 s time range, the percentage of ferritic grains larger than 3 μm passed from a 32 to a 38 % reaching 46 % after 300 s. Their main goal was to achieve an ultrafined grained (UFG) microstructure, but, longer soaking times (60 – 300 s) were inadequate. Nevertheless, the increment of holding time raised the mechanical properties, mainly caused by the higher fraction of martensite. The coarsening of the grains and the martensite fraction formed during rapid heating followed by soaking and quenching was also reported by Puype *et al.* in [77]. In this case, the material was subjected to a full austenitization at two heating rates, 10 ºC/s and 1000 ºC/s. It was shown that the final martensitic microstructure after UFH treatment was determined by two key parameters: nucleation rate of austenitic grains and their growth rate. At low heating rate, the amount of martensite formed was higher than at ultrafast heating rate, when no soaking was applied. Nonetheless, the microstructure of the steel heated at 1000 ºC/s without soaking was characterized by fine austenitic nuclei (i.e. fine martensitic grains formed upon quenching), which did not have enough time to grow in the first stages. When soaking time during UFH treatment was increased to 60 s, the austenitic nuclei grew faster than those formed during heating at 10 ºC/s, leading to a higher final fraction of martensite. This observation was related to the dominance of the austenite growth over the nucleation process, which prevailed at the low heating rate [78]. Similar results were obtained during the analysis of the grain size evolution. For no soaking, slow heating resulted in a coarser grain size compared to the high heating rates, due to the time given for the structure to develop. However, when the soaking time was increased to 30 s, the positive

grain refinement produced by high heating rates was erased. The latter was related to the delayed (or partially suppressed) recrystallization during UFH treatment in comparison with the conventional (10 ºC/s) one, which provided higher internal energy resulting in higher driving force for grain growth. (**Figure 1.12**). After 60 s, both conditions presented similar size. These outcomes were in a good agreement with the statement proposed in [45], where it was suggested that fast heating (300 ºC/s) and short holding times at an intercritical temperature would produce a microstructure with a higher volume fraction of finer austenite compared to the conventional heating rates (5 ºC/s). However, in [35] Massardier did not appreciate a significant change in the grain size for 0 - 5 s holding times, which was related to the initial microstructure. The effect of soaking time on the retained austenite was studied by Liu [45] at different peak temperatures (770 ºC – 850 ºC) for two holding times, 30 and 120 s, during a Q&P treatment carried out at 300 ºC/s. They observed that the maximum volume fraction of retained austenite was similar for both soaking times, being ~ 16 %. This value was reached during soaking for 30 s at 810 ºC, whereas the longer soaking time 120 s was required at 790 ºC. This difference can be attributed to higher fraction of prior austenite formed during intercritical annealing for longer time, the complete dissolution of cementite present in the initial microstructure and the longer time for carbon to diffuse into the austenite. A detailed study of the influence of soaking time on the recrystallization, recovery and phase transformation during ultrafast heating is included in this PhD Thesis in section 4.2. It corresponds to the paper titled “The effect of heating rate and soaking time on microstructure of an advanced high strength steel” by Valdes-Tabernero *et al.* published in *Materials Characterization 155 (2019) 109822*. In this work, in addition to analysis of the microstructure formed during high heating rates (800 ºC/s), the microstructure evolution during conventional heating is also included for comparison.

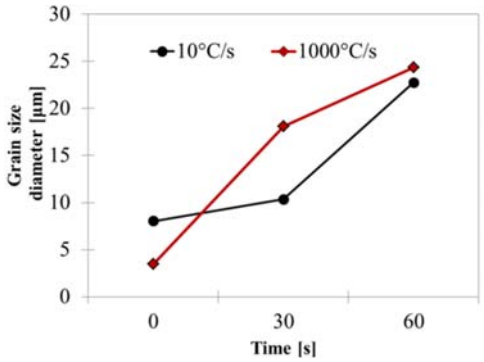

Figure 1.12: Influence of the isothermal soaking time on the prior austenite grain size in steel with 0.15%C; 1.7%Mn; 0.26%Si; 1%Al (mass) heated to 900 °C at 10 °C/s and 1000 °C/s [77].

The influence of the peak temperature on the microstructure and properties was investigated sporadically. For instance, Stockemer reported in [79] a growth in grain size from 3.5 to 4.8 µm in a low carbon steel, when temperature was increased from 620 ºC to 763 ºC. Nonetheless, Massardier *et al.* [35] suggested that heating in the intercritical region could lead to significant grain refinement even if complete recrystallization before the formation of austenite occured. However, heating above A_{C3} led to a rapid grain growth eliminating the beneficial grain refinement effect produced in the intercritical regime. The differences between both investigations can lay in the heating and cooling rates employed. While in the former study the heating rate used was 200 ºC/s and cooling rate 15 ºC/s, in the latter case, heating and cooling rates were 1000 ºC/s and 250 ºC/s, respectively. The growth of austenite grains with temperature and its dependence on heating rate observed were in a good agreement with the results reported by Vercruysse [80], where he studied the effect of the temperature increment from 760 ºC to 840 ºC for various heating rates (400 ºC/s y 1000 ºC/s) in a DP steel. The martensite grain size growth from 2.5 µm at 760 ºC to 3.5 µm at 840 ºC, when heating at 400 ºC/s was applied, whereas at 1000 ºC/s the maximum grain size was 3 µm. Moreover, he reported that increasing peak temperature resulted in a lower fraction of non-recrystallized ferrite and a higher fraction of martensite independently on the applied heating rate. Thus, the mechanical strength was enhanced with peak temperature, as it strongly depends on the martensite fraction formed. On the other hand, the amount of retained austenite was negatively affected. This was shown by Xu *et al.* in [37], where the peak temperature was varied from 800 ºC to 860 ºC. The reduction in the percentage of RA was associated with the austenite grain growth provoked by the increase in temperature, hence, the carbon concentration was reduced which, in turn, reduced the stability of the

austenite. The decrease in RA affected the ductility of the material, as the TRIP effect was less pronounced. Moreover, as % C in RA was low, the retained austenite transformed into martensite at lower strains, producing a steeper decrease in the strain hardening behavior [37]. The formation of austenite during isothermal holding at different peak temperatures for two heating rates (1 ºC/s and 100 ºC/s) was investigated by Huang et al. in [25]. At 775 ºC, the austenite in equilibrium was 25 % and 50 %, respectively, while at 800 ºC, at 1 ºC/s the austenite fraction increased to 40 % and at 100 ºC/s to 80 %. Similar outcomes were reported elsewhere [78]. In [45], authors examined the impact of elevating the peak temperature from 790 to 830 ºC on the tempered martensite developed after Q&P treatment. They reported that the increasing peak temperature led to a higher fraction of austenite, therefore, more tempered martensite was developed during the partitioning step. The role of the maximum temperature achieved during ultrafast heating treatments (i.e. peak temperature) is also studied in this PhD Thesis. The thorough investigation is included in section 4.4, corresponding to the paper titled "The sensitivity of the microstructure and properties to the peak temperature in an ultrafast heat treated low carbon-steel" by Valdes-Tabernero *et al.* published in *Materials Science and Engineering A 776 (2020) 138999*. In this work, different heat treatments with the combination of different peak temperatures (860 - 900 ºC) and two different short soaking times (≤ 1.5 s) are applied to the low carbon steel, and their effect on microstructure evolution and properties at both, micro and macro-levels, is investigated.

The effect of cooling rate on microstructure and properties has not been studied in a consistent manner. For instance, Stockemer *et al.* observed in [79] that, the temperature at which the full recrystallization of the microstructure occured was independent on the heating rate (40 – 300 ºC/s), when the cooling rate employed was equal to 15 ºC/s. Nonetheless, an increment of the peak temperature to achieve full recrystallization was required when the cooling rate was raised up to 1000 ºC/s. Authors claimed that the recrystallization continues during slow cooling. They also mentioned that the cooling step can affect the final mechanical properties. In this case, both yield and ultimate tensile strength significantly increased with cooling rate, but elongation was reduced by half. The latter was caused by the increase of interstitial carbon content. This effect could be suppressed if slow cooling rates (- 15 ºC/s) were applied above 400 ºC to enhance precipitation after annealing, and afterwards, increased cooling rate to -150 ºC/s. In addition, Massardier *et al.* [35] showed that grain refinement can be achieved during cooling, from 6 µm at -15 ºC/s to 4 µm at -250 ºC/s. Authors suggested that this effect was caused by the $\gamma \rightarrow \alpha$ transformation which

occurred during cooling. Hence, the higher the cooling rate, the lower the time for grains to grow. They demonstrated that high cooling rates were not required during the entire cooling stage to produce grain refinement, only from 920 to 650 ºC, corresponding to the $\gamma \rightarrow \alpha$ transformation. This was because the cooling rate has similar effect as the heating rate over the transformation temperatures. Hence, in [35] the maximum cooling rate should be applied only above 650 ºC. An increasing cooling rate shifted the transformation to lower temperatures affecting nucleation (increase in nucleation site density) and growth (mainly controlled by carbon diffusion) of ferrite grains and, consequently, the final grain size [26].

It should also be noted that the application of high heating rates on small strips can cause different distortions in the material due to two main facts: 1) the volume change caused by the phase transformations during heating, and 2) the thermal stresses associated with the high difference in temperature achieved in a short time during the process. While the first effect cannot be avoided unless appropriate heat treatment parameters are applied, the second type of distortions can be minimized by replacing the one-step heating cycle by two-steps heating cycle. The two-step heating cycles can include a preheating stage, as it was reported by Castro Cerda *et al.* in [54], who introduced an isothermal soaking step at 300 °C and 400 °C for 30 s during heating of a low carbon steel to the intercritical temperature. The temperature selected for the preheating stage was lower than the starting recrystallization temperature. It was shown that intermediate holding times at temperatures below recrystallization starting point had negligible effects on the initial microstructure and texture, but reduced the thermal stresses associated with the process. Therefore, this approach can be used without reducing the benefits provoked by the effect of the high heating rate. On the other hand, in [47], Liu and co-workers also studied the effect of applying two different heating rates during the heating ramp on the microstructure and properties of the low carbon steel analyzed. The first stage of the heating was carried out at 0.5 ºC/s from room temperature to 690 ºC and from that point to 790 ºC the heating was raised up to 300 ºC/s. The resultant microstructure presented a fully recrystallized structure with more spheroidized particles in the interior of the ferrite, whereas the microstructure entirely heated at 300 ºC/s was composed by non-recrystallized ferrite and deformed pearlite colonies. Moreover, the two-step heating not only affected the austenite volume fraction (i.e. martensite after quenching), showing a significant reduction from 59 % to 17 % compared to 300 ºC/s counterpart, but also its spatial distribution, changing from a homogeneous distribution to a banded one. As a result, the one-step heating at 300 ºC/s led to a higher

strength due to the higher fraction of martensite, but similar ductility, as the banded martensite distribution observed in the two – step process increased the difference in the amount of plastic deformation accommodate by each constituent leading to the formation of voids at the early stages of deformation [47].

2. MOTIVATION AND OBJECTIVES

2. Motivation and objectives

From the state of the art, it is clearly seen that the UFH processing is a very promising technique for manufacturing AHSS. A body of research focused on UFH processing and its effect on microstructure and mechanical properties exists in the current literature. Particularly, the influence of heating rate on the microstructure and basic mechanical properties of the UFH processed steels has been understood to satisfactory level. However, there are no systematic studies focused on the effect of soaking time and peak temperature on the microstructure and properties of steels subjected to UFH treatment. A requirement for further improvement of mechanical properties via intelligent microstructural design is, thus, to achieve fundamental understanding of the processing - microstructure - property relationship in this type of steels.

Therefore, the main goal of this work is to gain fundamental understanding of the effect of soaking time and peak temperature on the microstructure and properties of an UFH treated low carbon steel. This knowledge will allow to develop a concept of microstructural design via UFH treatments to achieve enhanced combination of mechanical and functional properties in steels. The following partial objectives can be derived from the general one:

- To understand the joint effect of ultrafast heating rate, peak temperature and soaking time at the peak temperature on the microstructure of the UFH treated low carbon steel on different scales (meso, nano).

- To analyze the effect of microstructure evolved during UFH treatment on the properties of individual microconstituents and on the macro-mechanical response of the material.

- To establish the processing-microstructure-properties relationship for the UFH treated steels with complex microstructures.

- Based on the outcomes of the experimental work, to derive a recipe for intelligent microstructural design in low carbon steels via UFH treatment.

3. MATERIALS AND METHODS

3. Materials & Methods

3.1. Material

The low carbon steel selected for this investigation was laboratory cast by CRM Group (Belgium). The chemical composition of the material is shown in **Table 3.1**. Alloys with this composition are typically used in the automotive sector as transformation induced plasticity (TRIP) assisted steels, which belong to the 1st generation of AHSS [81–83].

Table 3.1: Chemical composition of the studied material (wt. %).

C(%)	Mn(%)	Al(%)	Si(%)
0.19	1.61	1.06	0.50

The cast ingots were cut into blocks of 40 mm in thickness. They were reheated to 1250 ºC for 1 hour, and hot rolled to 14 mm in 3 passes with a finishing rolling temperature equal to 1050 ºC. The material was then reheated to 1250 ºC and subsequently hot rolled to 2 mm in 2 passes with a finishing rolling temperature of 1050 ºC. Then, it was cooled down in water to a coiling temperature of 600'ºC. Finally, the sheets were subjected to 50% cold rolling reduction to a final thickness of 1 mm. The supplied sheets presented a microstructure formed by 76 % of ferrite and 24 % of pearlite (**Figure 3.1**). They had final dimensions of 1200 mm in length and 200 mm in width.

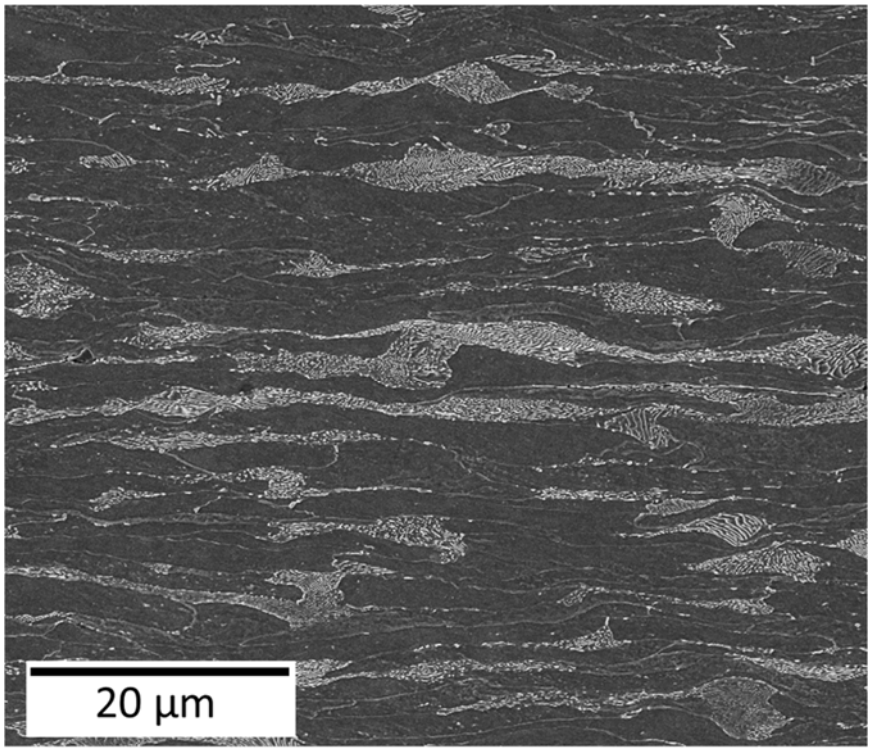

Figure 3.1: Initial ferritic-pearlitic microstructure of the steel after cold rolling with 50 % reduction ratio.

3.2. Heat treatment experiments

Two kinds of heating experiments were performed: a) dilatometry measurements to determine phase transformation temperatures and the formation of austenite at different intercritical temperatures; b) annealing tests to various intercritical temperatures with varying soaking time followed by quenching. Both types of experiments are described in detail below.

3.2.1. Dilatometry

The phase transformations that takes place during heating above certain temperatures were measured by dilatometry. The technique records the change in length of a sample during heating, cooling or isothermal soaking. The lattice parameter of the different phases, ferrite and austenite, varies in a linear way with temperature. However, ferrite (bcc) contains 2

atoms in a unit cell with a lattice parameter of 0.286 nm, while austenite (fcc) contains 4 atoms in a unit cell with a lattice parameter equal to 0.356 nm, for 727 ºC in pure iron [84]. Hence, austenite presents a higher density than ferrite. Due to the difference in density between phases, it is possible to measure a contraction by dilatometry during heating, when austenite starts to form above the A_{C1} temperature.

For these experiments, specimens with dimensions of 10 x 5 x 1 mm^3 were machined from the as-received material. Tests were carried out in a Bähr DIL805A/D dilatometer (Bähr-Thermoanalyse GmbH, Hüll-Horst, Germany). A *K*-type thermocouple was welded to the midsection of each specimen to measure their temperature during experiment. The sample expansion/contraction during heating/cooling was recorded.

Two different types of experiments were performed: continuous heating and isothermal soaking. Continuous heating was carried out in order to determine the phase transformation temperatures A_{C1} and A_{C3} of the studied steel as a function of heating rate. As increasing heating rate shifts the recrystallization temperature to the higher values than the equilibrium one or the one measured at conventional heating rates [21,33]. Specimens were heated up to 1100 ºC with different heating rates (1, 10, 50 and 200 ºC/s) and holding time equal to 0.2 s (**Figure 3.2**). Heating rates above 200 ºC/s were not applied due to instability of the system in that range of heating rates. The material was then cooled down to room temperature at -300 ºC/s.

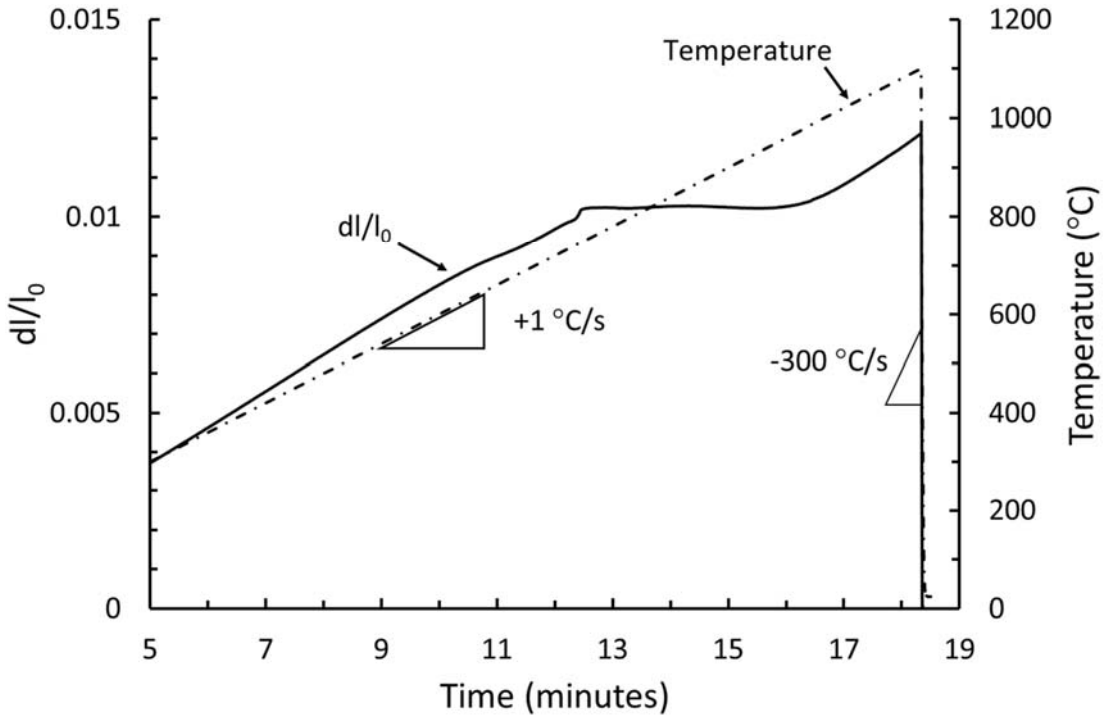

Figure 3.2: Example of continuous heating performed at 1 ºC/s.

Isothermal annealing was performed to analyze the austenitization kinetics at different temperatures for the same heating rate. Specimens were heated from room temperature to different temperatures in the intercritical region (860 ºC, 880 ºC and 900 ºC) at 200 ºC/s and soaked for 600 seconds. The specimens were then heated to a maximum temperature of 1100 ºC at 200 ºC/s and soaking time equal to 0.2 s (**Figure 3.3**). The material was then cooled down to room temperature at -300 ºC/s to freeze the microstructure formed.

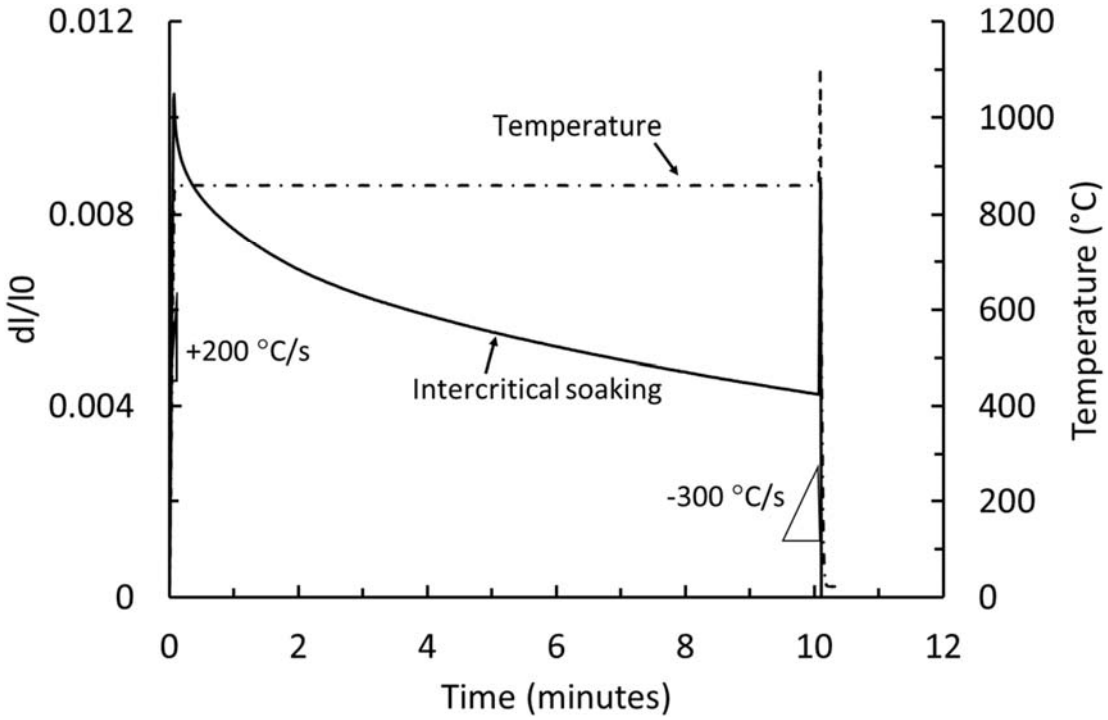

Figure 3.3: Example of isothermal soaking at 860 ºC after heating at 200 ºC/s.

The data obtained from the dilatometry experiments was processed applying the lever rule (**Figure 3.4**) [85]. The phase fractions formed at different temperatures and/or soaking times can be determined in this way. The A_{C1} and A_{C3} temperatures, during continuous heating, were determined through the intersection method at 5 % volume fraction of the transformed phase.

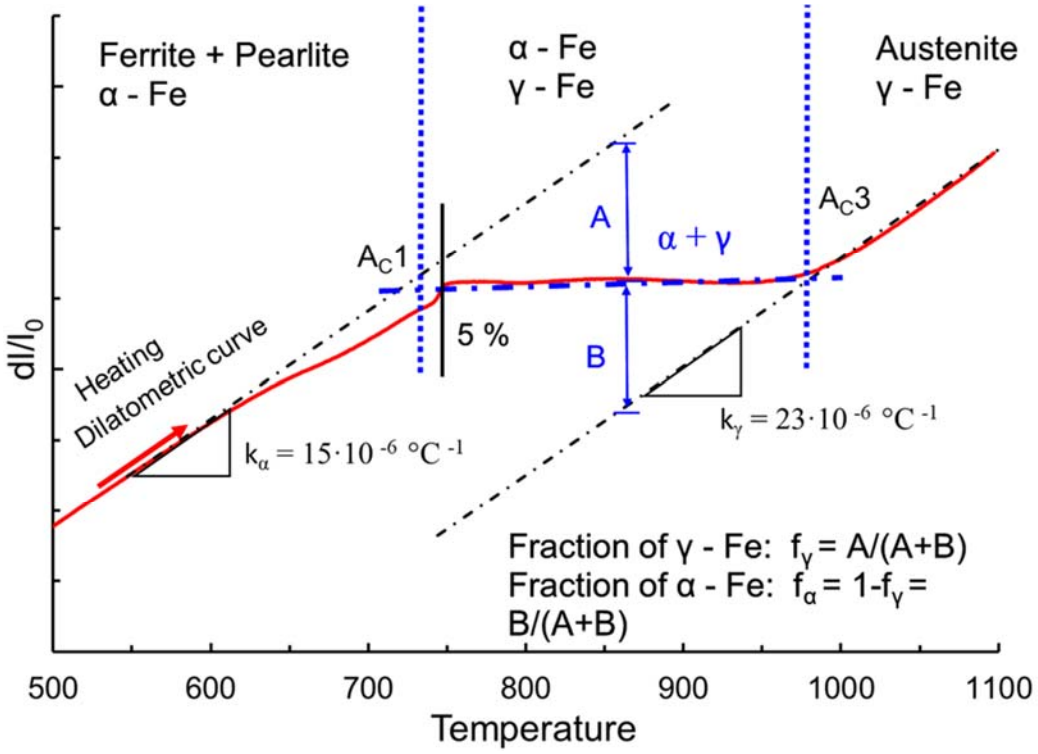

Figure 3.4: Schematic diagram of an experimental dilatometry curve (measured at 1 ºC/s) to calculate A_{C1} and A_{C3} temperatures and phase fractions via tangent intersection principle and lever rule. F_α and f_γ are the volume fractions of ferrite and austenite, respectively; k_α and k_γ are the thermal expansion coefficients of ferrite and austenite, respectively.

3.2.2. Intercritical heat treatments

For the intercritical heat treatments, strips of 100 x 10 x 1 mm^3 were machined along the rolling direction and heat treated in a thermo-mechanical simulator Gleeble 3800. A *K*-type thermocouple was spot-welded to the midsection of each specimen. Two different types of heat treatment were applied. In both types, the thermal cycle was divided into five stages. On the first and second stages, the specimens were heated at 10 ºC/s to 300 ºC, followed by a soaking period of 30 s at 300 ºC. These stages simulate a preheating in some industrial continuous annealing lines to reduce the thermal stresses during heating. The third stage is heating from 300 ºC to the peak temperature of 860 ºC at two different heating rates, 10 ºC/s (conventional heating or CH) and 800 ºC/s (ultra-fast heating or UFH) followed by soaking at 860 ºC for 0.2 s. The processed specimens will be referred to as CH10-0.2s and UFH800-0.2s (UFH860-0.2s), respectively. Such a short soaking time (0.2 s) allows to eliminate the

effect of annealing time on the microstructure and to focus entirely on the effect of heating rate. The last stage was to cool down the material to room temperature at ~160 ºC/s. The peak temperature of 860 ºC for intercritical annealing was selected based on the outcomes of the dilatometry measurements.

To study the effect of soaking time at both heating rates (CH and UFH), additional heat treatments were performed with higher soaking time (1.5 s and 30 s). The new generated conditions are referred to as CH10-1.5s and CH10-30s for the CH treatment, and UFH800-1.5s (UFH860-1.5s) and UFH800-30s (UFH860-30s) for the UFH treatment. All applied thermal cycles are schematically presented in (**Figure 3.5**).

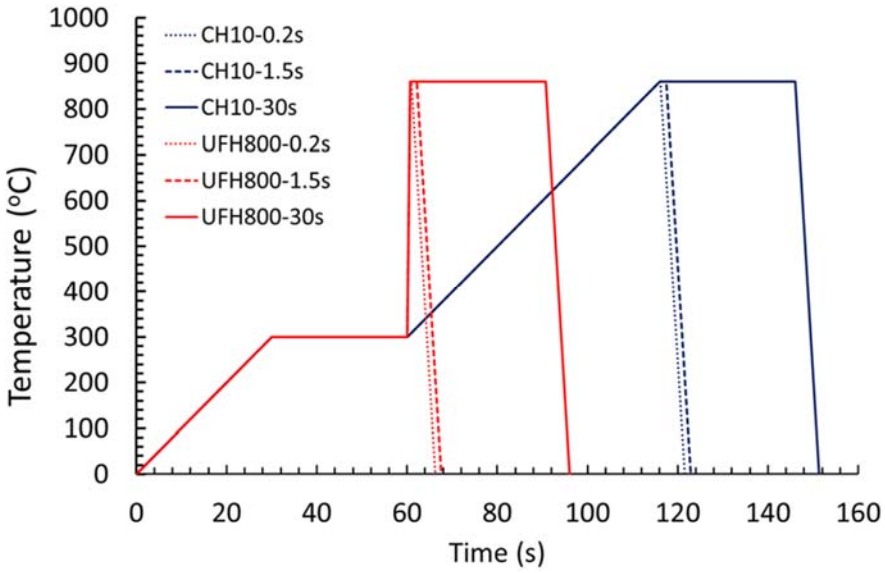

Figure 3.5: Schematic representation of the different heat treatments with peak temperature of 860 ºC applied to the studied material.

In order to study the effect of peak temperature during UFH treatment, additional heat treatments were carried out varying exclusively the peak temperatures to 880 ºC and 900 ºC. For both peak temperatures, the soaking times were 0.2 and 1.5 seconds. The new conditions are referred to as UFH880-0.2s and UFH880-1.5s for the 880 ºC peak temperature and UFH900-0.2s and UFH900-1.5s for the 900 ºC one. **Figure 3.6** a) and b) represents the new thermal treatments performed.

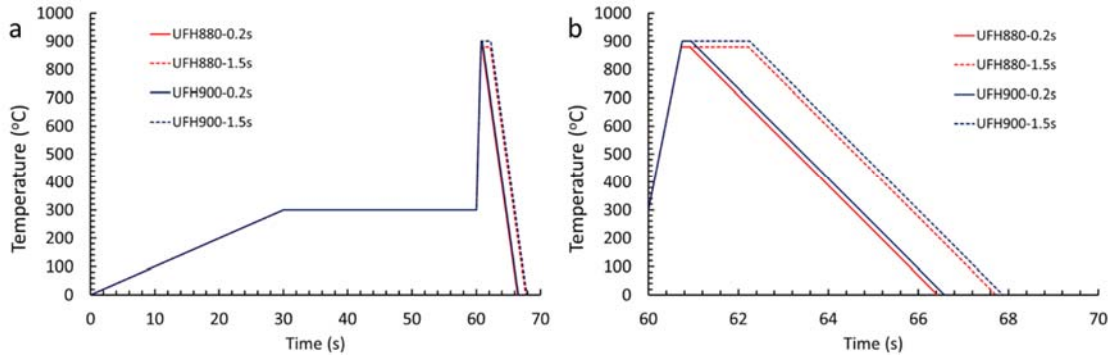

Figure 3.6: a) Representation of the thermal treatments performed to study the effect of the peak temperature; b) Detailed representation of image a).

In all samples, a minimum length of 10 mm of the homogeneously heat treated zone was verified by microhardness measurements and optical microscopy analysis.

The specimens processed by the Gleeble thermo-mechanical simulator were then subjected to a thorough microstructural and mechanical characterization.

3.3. Microstructural characterization

3.3.1. Optical microscopy

Optical microscopy observations were carried out using an Olympus BX-51 light microscope equipped with a digital camera. Specimens for microstructural analysis were cut from the strips, and subsequently ground and polished to a mirror-like surface, using 3 and 1 μm diamond paste with final polishing using OP-U (colloidal silica) for 40 minutes. The polished specimens were etched with 3 vol.% Nital solution for ~ 10 s. The RD-ND plane was characterized.

3.3.2. Scanning electron microscopy (SEM)

Specimens for scanning electron microscopy (SEM) studies were ground and polished to a mirror-like surface, using 3 and 1 μm diamond paste with final polishing using OP-U (colloidal silica) for 40 minutes. The polished specimens were etched with 3 vol.% Nital

solution for 10 s. Due to low availability reasons, the microstructure was examined using three different equipments: a FEI Quanta™ 450 FEG-SEM, a FEI Quanta™ Helios NanoLab 600i and a SEM EVO MA15 operating, in all cases, at an accelerating voltage of 15 kV. Microstructure was observed on the RD–ND plane.

3.3.3. Electron backscatter diffraction (EBSD) analysis

Specimens for EBSD analysis were prepared following the same procedures as for SEM, with final polishing using OP-U (colloidal silica) for 40 minutes. Orientation imaging microscopy (OIM) studies were performed using a FEI Quanta™ Helios NanoLab 600i equipped with a NordlysNano detector controlled by the AZtec Oxford Instruments Nanoanalysis (version 2.4) software. The data were acquired at an accelerating voltage of 18 kV, a working distance of 8 mm, a tilt angle of 70º, and a step size of 65 nm in a hexagonal scan grid. The orientation data were post-processed using HKL Post-processing Oxford Instruments Nanotechnology (version 5.1©) software and TSL Data analysis version 7.3 software. Data clean-up routines can be used to compensate in part for unsolved patterns [86]. The post-processing routine followed in this work is described below. First, IQ standardization with a minimum grain size of 4 pixels was applied. This clean up algorithm changes the IQ of all points in a grain to the maximum IQ found among all points belonging to that grain. Afterwards, the neighbor IQ correlation algorithm was employed, which implies that if a particular point has a value below 0.1, then the IQ of the nearest neighbors are checked to find the neighbor with the highest IQ. The orientation and IQ of the particular point are reassigned to match the orientation and IQ of the neighbor with the maximum IQ. After the cleaning procedure, different grains were defined as a minimum of 4 pixels with a misorientation higher than 5º and a confidence index (CI) higher than 0.1. Grain boundaries having a misorientation ≥ 15º were defined as high-angle grain boundaries (HAGBs), whereas low-angle grain boundaries (LAGBs) had a misorientation <15º. Moreover, in order to quantify the volume fractions of transformed/untransformed grains and recrystallized/recovered ferritic grains a two-step partitioning procedure described in [87] was employed. In this procedure, grains with high (> 70°) and low (≤70°) grain average image qualities are separated in a first step, allowing to distinguish between untransformed (ferrite) and transformed (martensite) fractions, respectively. In the second step, recrystallized and non-recrystallized ferritic grains are separated using the grain orientation

spread (GOS) criterion: grains with orientation spread below 1º are defined as the recrystallized grains, while grains with an orientation spread above 1º are defined as the non-recrystallized ones [88]. On the other hand, grain average misorientation (GAM) criterion can be used as well to separate recrystallized from recovered fractions of ferrite [55]. However, comparison of these two different criteria via analysis of numerous EBSD scans carried out in this work has shown, that the GOS criterion yields better results. The density of geometrically necessary dislocations (GNDs) was calculated from the local misorientations following the procedure described in [89]. Microstructure was observed on the plane perpendicular to the sample transverse direction (the RD–ND plane).

3.3.4. Texture

Textures are represented as orientation distribution functions (ODFs) using Bunge notation [90]. The ODFs were derived from the EBSD scans by superimposing Gaussian distributions with a half-width of 5°. The resulting ODF was represented as a series expansion of spherical harmonics functions with a maximum rank of the expansion coefficient L =16. Texture and grain size calculations were made using scans having area of ~6000 μm^2 which contains at least 1100 grains.

3.3.5. X-ray diffraction (XRD) analysis

X-ray diffraction (XRD) experiments were carried out to determine the retained austenite volume fraction and its carbon concentration. Specimens with a surface of 10 x 5 mm^2 were prepared following the same procedure as for the EBSD analysis (Section 3.3.3). The measurements were performed using a Bruker D8 Advance diffractometer (Bruker AXS, Karlsruhe, Germany) equipped with a VANTEC position sensitive detector and using Co K_α radiation (λ = 1.78897 Å), an acceleration voltage of 45 kV and current of 35 mA. The measurements were performed in the 2θ range from 45 º to 130º with a step size of 0.035º and a counting time per step of 3 s. The volume fraction of retained austenite was calculated using the Jatczak model as described in [91]. The austenite carbon concentration, X_C, was estimated from its lattice parameter, a_γ. The latter was determined from the austenite peak position as [92]:

$$a_\gamma = 0.3556 + 0.00453\ X_c + 0.000095\ X_{Mn} + 0.00056\ X_{Al} \quad (3.1)$$

where a_γ is the austenite lattice parameter in nm and X_I represents the concentration of the alloying element *I* in wt. %. The effect of silicon and phosphorous is not taken into account, as it is negligible compared to other elements considered in Eq. **(3.1)**.

The XRD characterization was performed on samples CH10-0.2s, UFH800-0.2s, UFH800-1.5s and UFH800-30s.

3.3.6. Transmission electron microscopy (TEM)

In order to characterize the microstructure developed at nanoscale, transmission electron microscopy (TEM) technique was employed. Samples were manually ground to a thickness of 100 μm and disks of 3 mm in diameter were subsequently punched out. The disks were further thinned in a Struers Tenupol-5 via twin-jet electropolishing until a central hole appeared. The used electrolyte was composed of 4 % vol. $HClO_4$ in 63 % water-diluted CH_3COOH under 21 V at 20 ºC and a flow rate equal to 17 for the Struers device. TEM images were acquired in a Jeol (S)TEN JEM-2200FS operated at 200 kV and equipped with an aberration corrector of the objective lens (CETCOR, CEOS GmbH) and a column electron energy filter (omega type).

TEM characterization was performed on samples CH10-0.2s, UFH800-0.2s, UFH800-1.5s and UFH800-30s.

3.3.7. Transmission Kikuchi diffraction (TKD)

In the last decades, nanocrystalline structures, such as ultra-fined grained (UFG) materials, metal-oxides or thin films have rapidly developed due to the superior mechanical properties and their interesting magnetic and electronic features [93]. However, as a result of the grain size reduction, the actual techniques present some difficulties to characterize such fine microstructures. This has happened with EBSD, which has been the most commonly technique to analyze nanocrystalline structures in a rapid manner. The other option, when

EBSD is not sufficient to resolve small features, is to use transmission electron microscopy. Nevertheless, TEM presents some drawbacks, as the large time and high skills required to analyze the specimens. Moreover, with TEM images it can be difficult to differentiate between grains and measure grain sizes.

In order to carry out reliable and a thorough characterization of nanoscale constituents in a rapid manner, in 2012 Keller *et al.* proposed, a novel approach called transmission EBSD (t-EBSD) [94]. It is based on performing an EBSD analysis in transmission mode. The method requires very thin samples, similar to those for TEM characterization, and a conventional SEM equipped with EBSD detector. The specimen is placed perpendicular to the normal EBSD configuration, as it is shown in **Figure 3.7**. Due to the low thickness of the sample, typical SEM voltages are enough for electrons to interact with the material and pass through, to finally be captured by the EBSD detector. This configuration allows to obtain the diffraction pattern from the bottom surface of the specimen. Hence, the caption "electron backscattered diffraction" is no longer valid, being more suitable the term "transmission Kikuchi diffraction" (TKD).

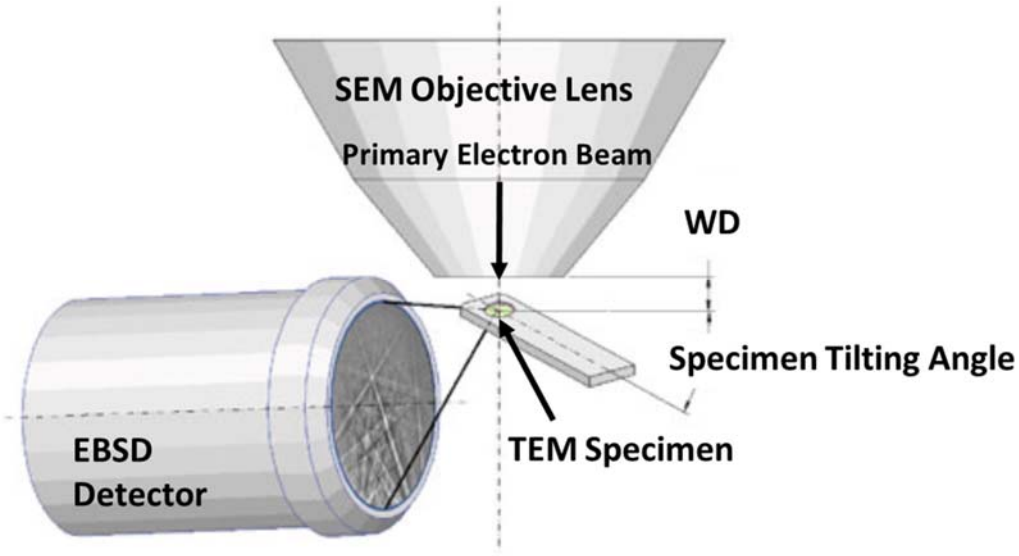

Figure 3.7: Set-up for TKD characterization of TEM specimen [95].

TKD offers better spatial resolution than EBSD (< 10nm), allowing the resolution of nanoscale microstructural constituents having 10-30 nm in size [96,97]. It has been successfully used to analyze oxides and nitrides in aluminum alloys [98] and stainless steels [99,100], martensite and retained austenite in bainitic steels [101] as well as highly deformed Al and Ti alloys [102–104] and NiO multilayers [105].

One of the problems of the TKD technique is the localized area analyzed, leading to statistically insignificant data. Therefore, it is not a suitable technique if the goal is to measure the volume fractions of different phases present in the microstructure, as the data is not truly representative. In order to have enough information, the area scanned should be enlarged, increasing the measuring time significantly, as the step size used is around 5-20 nm [95,104,105]. Moreover, the TKD results highly depend on the quality of the studied samples. If the electropolishing step is inhomogeneous, there are significant differences in the foil thickness through the sample. If a local area is too thick, the electrons are unable to pass through and reach the detector, as their initial energy is orders of magnitude less compared to the ones generated in TEM which results in the non-indexed areas. Similar effect occurs when the foil is too thin, as too many electrons cross the specimen and reach the detector [95,96]. Therefore, the specimen preparation is critical to obtain reliable results.

In this work, the specimens were prepared following the same procedure described in TEM (Section 3.3.6), as the exact same region of the analyzed samples was observed by both techniques, TEM and TKD.

TKD data were collected by an EDAX-TSL EBSD system attached to a FEI Quanta™ 450-FEG-SEM, under the following conditions: accelerating voltage of 30 kV, working distance of 4 mm, tilt angle of - 40°, a beam current of 2.3 nA corresponding to FEI spot and aperture sizes of 5 and 30 μm respectively. TKD measurements were performed with the step size of 10 nm. The orientation data were post-processed using TSL Data analysis version 7.3 software. The post-processing routine followed is similar to the one described in Section 3.3.3. In the first step, the IQ standardization with a minimum grain size of 4 pixels was applied. Secondly, the neighbor IQ correlation algorithm was used. Grains were defined as a minimum of 4 pixels with a misorientation higher than 5º and a confidence index (CI) higher than 0.1.

TKD characterization was performed on samples CH10-0.2s, UFH800-0.2s (UFH860-0.2s), UFH800-1.5s (UFH860-1.5s) and UFH800-30s (UFH860-30s).

3.4. Mechanical characterization

3.4.1. Hardness testing

Hardness measurements were performed on the RD–ND plane for all heat treated samples after metallographic preparation by grinding and polishing using 1 μm diamond paste as final step. Tests were carried out in a Shimadzu HMV Hardness Tester, according to the ASTM E92-17 Standard. The penetrator was a diamond square base pyramid with at angle of 136º. Tests were done applying a load of 4.9 N for 15 s.

3.4.2. Uniaxial tensile testing

Uniaxial tensile testing was carried out in order to obtain the mechanical behavior of the material studied. Dog bone sub-size tensile samples were machined from the homogeneously heat treated zone of the processed strips. Tensile axis was parallel to the rolling direction (RD) (**Figure 3.8**). The samples had a gauge length of 4 mm, a gauge width of 1 mm and a thickness of 1 mm. They were carefully ground and mechanically polished with 3 μm, 1 μm diamond paste for 40 minutes. Tensile tests were carried out at room temperature using a Kammrath&Weiss testing module equipped with a 1 kN load cell at a constant cross head speed corresponding to the initial strain rate of 10^{-3} s^{-1} until failure. At least three specimens were tested for each condition and the results were found to be reproducible. A very thin (~15 μm) decarburized layer formed on the surface of all heat treated strips was removed before any mechanical testing.

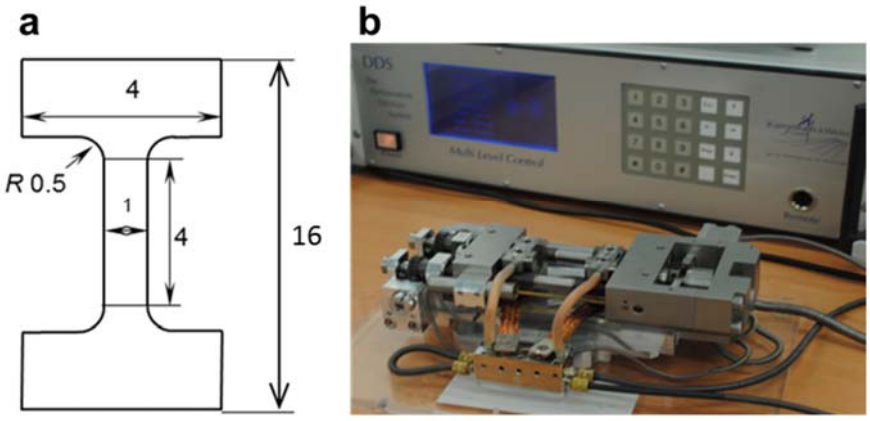

Figure 3.8: a) Geometry of tensile specimens; b) Kammrath&Weiss testing module.

3.4.3. Nanoindentation testing

Nanoindentation tests were performed on a HysitronTI950 Triboindenter using a Berkovich tip on square areas having a size of ~10 x 10 μm^2, which were *a priori* analyzed by EBSD (as described in Section 3.3.3) to identify the individual microstructural constituents. At least ten areas were subjected to testing for each material's condition. In order to target specific phases/grains, these square areas were scanned, using the scanning probe microscopy (SPM) mode of the instrument prior to the nanoindentation. In SPM mode, the nanoindenter tip is in contact with the surface of the tested material scanning it, giving the topography of the sample. Nanoindentation tests were carried out in displacement control mode, at a constant strain rate ($\dot{\varepsilon}=\dot{h}/h$) of 0.07 s^{-1}, where h is the penetration depth and $\dot{h}$ the penetration rate of indenter. At least 20 indents were performed on each phase, at an imposed maximum depth of 150 nm. The nanohardness was determined from the analysis of the load–displacement curves using the Oliver and Pharr method [106]. Surfaces for nanoindentation had a low roughness ($\leq$ 5 nm), suitable for performing nanoindentation measurements at the prescribed maximum depth of 150 nm

4. PUBLISHED PEER-REVIEWED MANUSCRIPTS

4. Published peer-reviewed manuscripts

4.1. Effect of ultrafast heating on the properties of the microconstituents in a low-carbon steel

M. A. Valdes-Tabernero*, F. Vercruysse, I. Sabirov, R.H. Petrov, M.A. Monclus, J.M. Molina-Aldareguia, *Metallurgical and Materials Transactions A* 49 (2018), 3145-3150.

DOI: https://doi.org/10.1007/s11661-018-4658-4

4.2. The effect of heating rate and soaking time on microstructure of an advanced high strength steel

M. A. Valdes-Tabernero*, C. Celada-Casero, I. Sabirov, A. Kumar, R.H. Petrov, *Materials Characterization* 155 (2019) 109822.

DOI: https://doi.org/10.1016/j.matchar.2019.109822

Materials Characterization 155 (2019) 109822

Contents lists available at ScienceDirect

Materials Characterization

journal homepage: www.elsevier.com/locate/matchar

The effect of heating rate and soaking time on microstructure of an advanced high strength steel

M.A. Valdes-Tabernero[a,*], C. Celada-Casero[b], I. Sabirov[a], A. Kumar[b], R.H. Petrov[b,c]

[a] IMDEA Materials Institute, Calle Eric Kandel 2, Getafe 28906, Madrid, Spain
[b] Department of Materials Science and Engineering, Delft University of Technology, Mekelweg 2, 2628 CD Delft, the Netherlands
[c] Department of Electrical Energy, Metals, Mechanical Constructions & Systems, Ghent University, Technologiepark 46, 9052 Ghent, Belgium

ARTICLE INFO

Keywords:
Steel
Ultrafast heating
Microstructure
Transmission Kikuchi diffraction
Texture

ABSTRACT

This work focuses on the effect of soaking time on the microstructure during ultrafast heat treatment of a 50% cold rolled low carbon steel with initial ferritic-pearlitic microstructure. Dilatometry analysis was used to estimate the effect of heating rate on the phase transformation temperatures and to select an appropriate intercritical temperature for final heat treatments. A thorough qualitative and quantitative microstructural characterization of the heat treated samples is performed using a wide range of characterization techniques. A complex multiphase, hierarchical microstructure consisting of ferritic matrix with embedded martensite and retained austenite is formed after all applied heat treatments. In turn, the ferritic matrix contains recrystallized and non-recrystallized grains. It is demonstrated that the ultrafast heating generally results in finer microstructure compared to the conventional heating independently on the soaking time. There is a significant effect of the soaking time on the volume fraction of martensite of the ultrafast heated material, while in the samples heated with conventional heating rate it remains relatively unchanged during soaking. Recrystallization, recovery and phase transformations occurring during soaking are discussed with respect to the applied heating rate.

1. Introduction

Steels have been the most widely used materials all over the world and are likely to remain a key material of choice in construction and manufacturing. Steel manufacturing is a multistage process, where the heat treatment of (semi-)final product (in form of sheet, rod, wire) to a great extent determines its microstructure and, hence, its properties. The current approach for steel heat treatment is based on homogenization of microstructure at elevated temperatures (either at austenitic or intercritical temperatures) and cooling with controlled rate often followed by further treatment to form the required microstructure [1]. In 2011, Cola et al. [2] proposed an idea to apply ultrafast heat treatment for manufacturing advanced high strength steels (AHSS) with microstructures as heterogeneous as those processed via conventional heat treatments. This treatment was initially referred to as 'flash processing' [2], and other terms such as 'ultrashort annealing' [3] and 'ultrafast heating' [4–7] are widely used for this process in the recent literature. Ultrafast heat treatment is based on heating the material with the heating rate in the range of 100 to 1000 °C/s to an intercritical temperature, very short soaking at this temperature followed by quenching. The whole process lasts just a few seconds and, therefore, is characterized by significantly reduced energy consumption compared to the conventional heat treatments [8].

The current state of the art in the effect of ultrafast heat treatment on the microstructure and properties of steels can be summarized as follows. The final microstructure of the ultrafast heat treated steels is determined by three major heat treatment parameters: heating rate, peak temperature and soaking time. Ultrafast heating typically results in grain refinement in interstitial free (IF) [9] and low carbon steels [3–5,10,11], thus, leading to higher mechanical strength. Increasing heating rate shifts the recrystallization temperature to higher values than the one measured at conventional heating rates of 10–20 °C/s. Recovery and recrystallization processes concurrently occur during ultrafast heating, and increasing the heating rate decreases the recrystallized fraction of ferrite for a given temperature [5–7,12–14]. The martensite volume fraction in the heat treated steel tends to increase with increasing peak temperature [15]. The initial microstructure strongly influences the properties of steels after ultrafast heat treatment [5]. Particularly, the steels with the initial ferritic-pearlitic microstructure showed lower strength and higher ductility compared to the

* Corresponding author.
E-mail address: miguelangel.valdes@imdea.org (M.A. Valdes-Tabernero).

https://doi.org/10.1016/j.matchar.2019.109822
Received 27 April 2019; Received in revised form 1 July 2019; Accepted 15 July 2019
Available online 16 July 2019

steels with the initial ferritic-martensitic microstructure [5]. The pre-heating stage at temperatures of 300–400 °C has minor effects on the microstructure evolution during ultrafast heating, though increase of pre-heating temperature results in lower volume fraction of austenite, and hence martensite upon quenching, due to cementite spheroidization [12].

Microstructure evolution in steels during ultrafast heating and short soaking at the peak temperature is a very complex phenomenon, as it involves simultaneously recovery, recrystallization, grain growth, phase transformations and diffusion of alloying elements with carbon playing the key role. In most of the basic studies, the isothermal soaking time was taken as short as possible, 0.1–0.2 s [5,7,12,13]. Such short soaking times cannot be reached during UFH processing of steel on the existing industrial lines and this is a significant obstacle for implementation of the ultrafast heating in steel industry. It was reported that longer isothermal soaking time (30 s) can erase the positive grain refining effect of the ultrafast heating [16]. However, in the current literature there are no systematic studies on the effect of the isothermal soaking time at the peak temperature on the microstructure and properties of steel after ultrafast heating. Fundamental understanding of microstructure evolution is required to enable an easy determination of the optimum soaking parameters for microstructural design in the ultrafast heat treated steels. Therefore, the main objective of the present work is to thoroughly study the effect of soaking time on the microstructure evolution during ultrafast heating of a low carbon steel. Conventional heating of the steel followed by detailed microstructural characterization is also performed for comparison.

2. Material and experimental procedures

2.1. Material

A low carbon steel with chemical composition of 0.19% C, 1.61% Mn, 1.06% Al, 0.5% Si (in wt%) was selected for this investigation. Alloys with this composition are typically used in the automotive sector as transformation induced plasticity (TRIP) assisted steels, which belong to the 1st generation of AHSS [17–19]. Two kinds of heating experiments were performed: a) dilatometry measurements to determine phase transformation temperatures, and b) annealing tests to the intercritical temperature with varying soaking time followed by quenching. Both types of experiments are described in detail below.

2.2. Dilatometry experiments

As increasing heating rate shifts the recrystallization temperature to the higher values than the equilibrium one or the one measured at conventional heating rates [5,13]. Dilatometry measurements were carried out to determine the phase transformation temperatures A_{C1} and A_{C3} of the studied steel as a function of heating rate. For these experiments, specimens with dimensions of 10x5x1 mm^3 were machined from the as-received material. Tests were carried out in a Bähr DIL805A/D dilatometer (Bähr-Thermoanalyse GmbH, Hüll-Horst, Germany). Specimens were heated up to 1100 °C with different heating rates (1, 10, 50 and 200 °C/s) and holding time equal to 0.2 s. Heating rates above 200 °C/s were not applied due to instability of the system in that range of heating rates. A *K*-type thermocouple was welded to the midsection of each specimen to measure their temperature during experiment. The material was then cooled down to room temperature at −300 °C/s. The sample expansion/contraction during heating/cooling was recorded, and the obtained dilatometry curves were analyzed. The tangent intersection method was applied to determine the start (A_{C1}) and finish (A_{C3}) temperatures of austenite formation.

2.3. Intercritical heat treatments

For the intercritical heat treatments, strips of 100 mm in length and 10 mm in width were machined along the rolling direction and heat treated in a thermo-mechanical simulator Gleeble 3800. A *K*-type thermocouple was spot-welded to the midsection of each specimen. Two different types of heat treatment were applied. In both types, the thermal cycle was divided into five stages. On the first and second stages, the specimens were heated at 10 °C/s to 300 °C, followed by a soaking period of 30 s at 300 °C. These stages simulate a preheating in some industrial continuous annealing lines to reduce the thermal stresses during heating. The third stage is heating from 300 °C to the peak temperature of 860 °C at two different heating rates, 10 °C/s (conventional heating or CH) and 800 °C/s (ultra-fast heating or UFH) followed by soaking at 860 °C for 0.2 s. The processed specimens will be referred to as CH10-0.2s and UFH800-0.2s, respectively. Such a short soaking time (0.2 s) allows to eliminate the effect of annealing time on the microstructure and to focus entirely on the effect of heating rate. The last stage was to cool down the material to room temperature at ~160 °C/s. The peak temperature of 860 °C for intercritical annealing was selected based on the outcomes of the dilatometry measurements (see Section 3.1).

To study the effect of soaking time at both heating rates (CH and UFH), additional heat treatments were performed with higher soaking time (1.5 s and 30 s). The new generated conditions are referred to as CH10-1.5s and CH10-30s for the CH treatment, and UFH800-1.5s and UFH800-30s for the UFH treatment. All applied thermal cycles are schematically presented in (Fig. 1). In all samples, a minimum length of 10 mm of the homogeneously heat treated zone was verified by microhardness measurements.

2.4. Microstructural characterization

A thorough microstructural characterization of the samples heat treated in a thermo-mechanical simulator (Fig. 1) was performed. Specimens for scanning electron microscopy (SEM) studies were ground and polished to a mirror-like surface applying standard metallographic techniques with final polishing using OP-U (colloidal silica). The polished specimens were etched with 3 vol% Nital solution for 10 s. Examination of the microstructure was performed using a FEI Quanta™ 450 FEG-SEM operating at an accelerating voltage of 15 kV. Microstructure was observed on the RD–ND plane.

Specimens for electron backscatter diffraction (EBSD) analysis were ground and polished following the same procedure as for SEM images. Orientation imaging microscopy (OIM) studies were performed using a FEI Quanta™ Helios NanoLab 600i equipped with a NordlysNano detector controlled by the AZtec Oxford Instruments Nanoanalysis (version 2.4) software. The data were acquired at an accelerating voltage of 18 kV, a working distance of 8 mm, a tilt angle of 70°, and a step size of

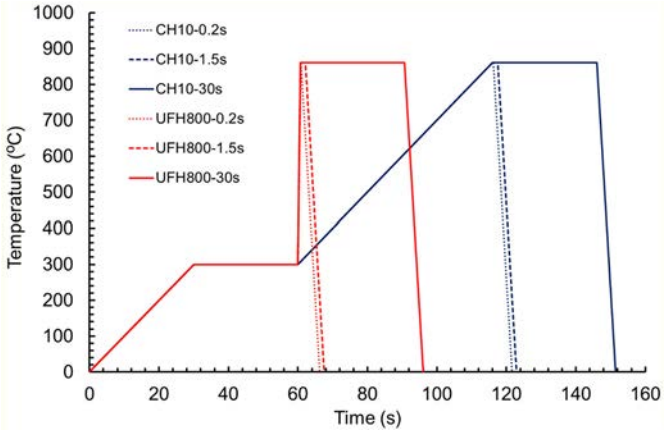

Fig. 1. Schematic representation of the different heat treatments applied to the studied material.

65 nm in a hexagonal scan grid. The orientation data were post-processed using HKL Post-processing Oxford Instruments Nanotechnology (version 5.1©) software and TSL Data analysis version 7.3 software. Grains were defined as a minimum of 4 pixels with a misorientation higher than 5°. Grain boundaries having a misorientation ≥15° were defined as high-angle grain boundaries (HAGBs), whereas low-angle grain boundaries (LAGBs) had a misorientation < 15°. Textures are represented as orientation distribution functions (ODFs) using Bunge notation [20]. The ODFs were derived from the EBSD scans by superimposing Gaussian distributions with a half-width of 5°. The resulting ODF was represented as a series expansion of spherical harmonics functions with a maximum rank of the expansion coefficient L = 16. Texture and grain size calculations were made using scans having area of ~6000 μm^2 which contains at least 1100 grains. The volume fractions of transformed/untransformed grains and recrystallized/recovered ferritic grains were determined by a two-step partitioning procedure described in [5,21]. In this procedure, grains with high (> 70°) and low (≤70°) grain average image qualities are separated in a first step, allowing to distinguish between untransformed (ferrite) and transformed (martensite) fractions, respectively. In the second step, recrystallized and non-recrystallized ferritic grains are separated using the grain orientation spread criterion: Grains with orientation spread below 1° are defined as the recrystallized grains, while grains with an orientation spread above 1° are defined as the non-recrystallized ones [22]. It should be noted that another grain average misorientation based criterion was employed in our recent report [14] for separation of recrystallized/non-recrystallized grains. Comparison of these two different criteria via analysis of numerous EBSD scans carried out in this work has shown, that the criterion utilized in the present manuscript yields better results. The microstructure was characterized on the plane perpendicular to the sample transverse direction (the RD–ND plane).

X-ray diffraction (XRD) experiments were carried out to determine the retained austenite volume fraction and its carbon concentration. Specimens with a surface of 10 × 5 mm^2 were prepared following the same procedure as for the EBSD analysis. The measurements were performed using a Bruker D8 Advance diffractometer (Bruker AXS, Karlsruhe, Germany) equipped with a VANTEC position sensitive detector and using Co K_α radiation (λ = 1.78897 Å), an acceleration voltage of 45 kV and current of 35 mA. The measurements were performed in the 2θ range from 45° to 130° with a step size of 0.035° and a counting time per step of 3 s. The volume fraction of retained austenite was calculated using the Jatczak model as described in [23]. The austenite carbon concentration, X_c, was estimated from its lattice parameter, a_γ. The latter was determined from the austenite peak position as [24]:

$$a_\gamma = 0.3556 + 0.00453\,X_c + 0.000095\,X_{Mn} + 0.00056\,X_{Al} \quad (1)$$

where a_γ is the austenite lattice parameter in nm and X_i represents the concentration of the alloying element *i* in wt%. The effect of silicon and phosphorous is not taken into account, as it is negligible compared to other elements considered in Eq. (1).

In order to carry out a thorough characterization of nanoscale constituents in a rapid manner, in 2012 Keller et al. proposed a novel approach called transmission Kikuchi diffraction (TKD) analysis [25]. It is based on performing an EBSD analysis in transmission mode. The method requires very thin samples, similar to those for TEM characterization, and a conventional SEM equipped with EBSD detector. It can also be combined with transmission electron microscopy (TEM) analysis. Due to the low thickness of sample, typical SEM voltages are sufficient for electrons to interact with the material and pass through, to finally be captured by the EBSD detector. TKD offers better spatial resolution (< 10 nm) than EBSD, allowing the resolution of nanoscale microstructural constituents having 10–30 nm in size [26,27]. It has been successfully used to analyze oxides and nitrides in aluminium alloys [28] and stainless steels [29,30], as well as martensite and retained austenite in bainitic steels [31]. In this work, for TKD and TEM studies, the samples were ground to a thickness of 100 μm and disks of 3 mm in diameter were subsequently punched out. The disks were further thinned in a Struers Tenupol-5 via twin-jet electropolishing until a central hole appeared. The used electrolyte was composed of 4% vol. $HClO_4$ in 63% water-diluted CH_3COOH under 21 V at 20 °C and a flow rate equal to 17. TKD data were collected by an EDAX-TSL EBSD system attached to a FEI Quanta™ 450-FEG-SEM under the following conditions: accelerating voltage of 30 kV, working distance of 4 mm, tilt angle of - 40°, a beam current of 2.3 nA corresponding to the FEI spot size of 5, aperture size of 30 μm. TKD measurements were performed with the step size of 10 nm. The orientation data were post-processed using TSL Data analysis version 7.3 software. TEM images were acquired in a Jeol (S)TEN JEM-2200FS operated at 200 kV and equipped with an aberration corrector of the objective lens (CETCOR, CEOS GmbH) and a column electron energy filter (omega type). XRD, TEM and TKD measurements were performed on samples CH10-0.2s, UFH800-0.2s, UFH800-1.5s and UFH800-30s.

3. Results and discussion

3.1. Dilatometry

Fig. 2a represents the typical dilatometry curves for the samples tested with different heating rates. The A_{C1} temperature was determined at 5% volume fraction of the transformed phase calculated by the lever rule (as shown in Fig. 2b). Such relatively high percentage of the transformed phase was selected as a criterion due to complexity of the microstructure evolution during heating, which involves various processes (carbide dissolution, recovery and recrystallization of ferrite, formation of austenite as observed in [32–34] and described in Section 3) resulting in A_{C1} temperature range. Once the sample is fully austenitic at the A_{C3} phase transformation temperature, the expansion becomes linear with the temperature. The martensite start temperature M_s corresponds to the point on the dilatation curve, where the contraction of austenite during quenching is replaced by expansion due to the formation of martensite. As it is seen from Table 1, all three transformation temperatures, A_{C1}, A_{C3} and M_s, tend to increase with the increasing heating rate.

For the A_{C1}, the pronounced increase from 738 to 781 °C occurs at the lower heating rates ranging from 1 °C/s to 50 °C/s. On the other hand, the A_{C3} temperature just slightly grows from 968 to 971 °C in that temperature range jumping up to 983 °C at 200 °C/s. It can be hypothesized, that this variation of the A_{C1} temperature is determined mainly by nucleation and growth rate of austenitic grains. The nucleation rate at the given elevated temperature grows with the increasing heating rate, since the latter suppresses the recovery effects, resulting in higher density of lattice defects at the given temperature, which, in turn, promote phase nucleation. The growth rate of the nucleated austenitic grains is controlled by carbon diffusion [7] and solute drag effect (by Mn atoms in the studied steel) [35]. Therefore, at the early stages of phase transformation, the austenite volume fraction at the given temperature decreases with increasing heating rate. Both factors result in increasing A_{C1} temperature with rising heating rate. It should be noted that similar results were earlier published in [36]. In this study, a linear dependency of A_{C1} on the heating rate (Fig. 3) on the semi-log plot is observed. Similar tendency of A_{C1} on the heating rate for ferritic-pearlitic microstructure has been reported in [37,38]. The nucleation and growth depend on the heating rate exponentially [38]. Moreover, the extrapolation of this behavior to low heating rates (0.2 °C/s) shows an equilibrium temperature of 720 °C, which is very close to the theoretical one (723 °C), thus confirming the linear character of this dependence. Therefore, this approach can also be used to predict the A_{C1} temperature at high heating rates. Particularly, for 800 °C/s, the A_{C1} temperature is about 808 °C (Fig. 3). On the other hand, the dependence of A_{C3} temperature on the heating rate is less pronounced. Similar observations were reported earlier in [39].

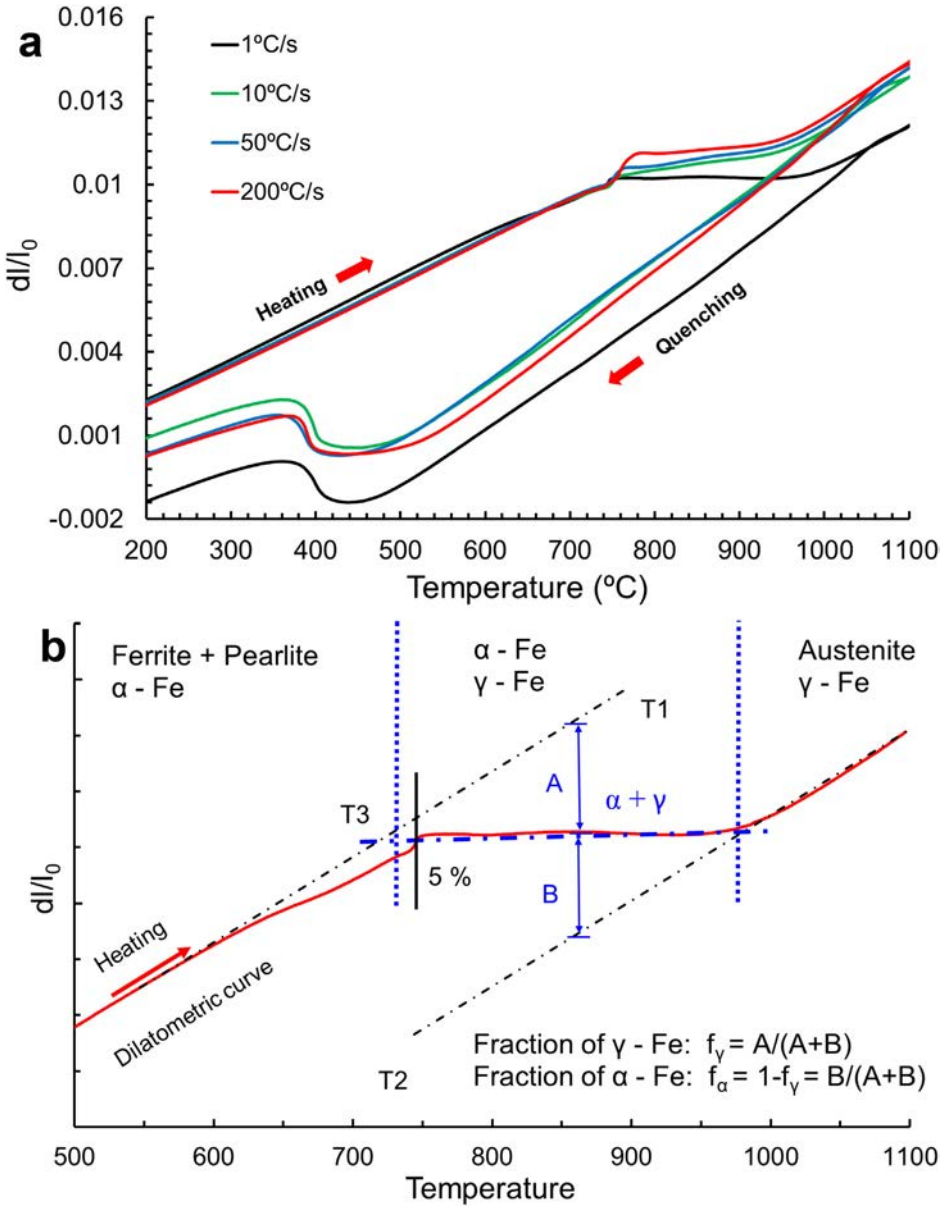

Fig. 2. a) Dilatometry curves from dilatometry tests with different heating rates; b) Schematic diagram of an experimental dilatometry curve (measured at 1 °C/s) to calculate A_{C1} and A_{C3} temperatures via tangent intersection principle and lever rule.

Table 1
Effect of the heating rate on the phase transformation temperatures: A_{C1}, A_{C3} and M_s.

Heating rate (°C/s)	A_{C1} (°C)	A_{C3} (°C)	M_s (°C)
1	738	968	483
10	760	969	489
50	781	971	498
200	793	983	530

Therefore, the intercritical temperature of 860 °C was selected as the peak temperature for both CH and UFH treatments (see Section 2.3).

Increasing heating rate during heat treatment with full austenitization followed by immediate cooling leads to increment of the M_s temperature. This effect is produced because the higher applied heating rate results in the higher amount of defects in the microstructure induced by cold rolling. As recovery is diffusion controlled [40], higher density of lattice defects is retained in the microstructure due to shorter time at elevated temperatures. This effect was observed previously in

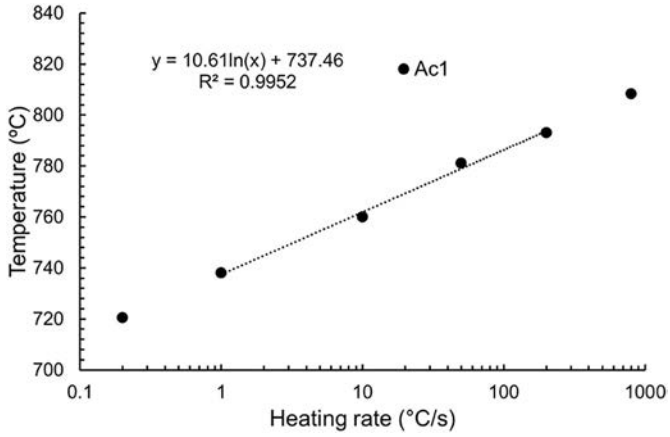

Fig. 3. Effect of heating rate on the A_{C1} temperature.

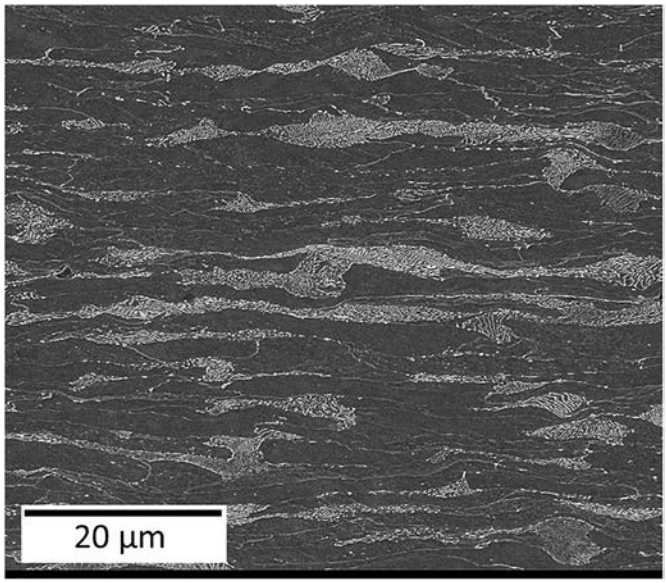

Fig. 4. Initial ferritic-pearlitic microstructure of the steel after 50% cold reduction, being ferrite in grey and pearlitic colonies in white.

[41,42]. In addition, at high heating rates carbides remain undissolved in the microstructure, leading to a formation of austenite with lower carbon content and, hence, a higher M_s compared to the conventional heating rates. Therefore, the steepest increment on M_s is produced, when heating rate grows from 50 °C/s to 200 °C/s leading to an increase of transformation temperature from 498 °C to 530 °C. On the other hand, in the range of lower heating rates from 1 to 50 °C/s the M_s temperature just slightly varies.

3.2. SEM characterization

The supplied material shows a typical cold rolled microstructure consisting of elongated grains of deformed ferrite with volume fraction of 76% and pearlite with volume fraction of 24% (Fig. 4).

The microstructure after CH treatment with soaking time of 0.2 s, 1.5 s and 30 s is presented in Fig. 5a,b,c, respectively, whereas remaining images illustrate the microstructure after UFH treatment. In all cases, the material presents a complex microstructure formed by a ferritic matrix (consisting of recrystallized and recovered ferritic grains) with embedded martensite and retained austenite grains. However, it strongly depends on the applied heat treatment parameters. During CH treatment, the material presents a similar microstructure independently on the soaking time, while the latter has very significant effect on the microstructure formed after UFH treatment.

CH treatment generates a ferritic matrix with homogeneous microstructure consisting of equiaxed grains, as previously observed in [5]. On the other hand, UFH results in the matrix microstructure consisting of fine equiaxed grains and larger elongated grains surrounded by martensitic grains. The large grains may grow from the heavily deformed ferrite located in the vicinity of pearlite colonies, as the latter are not able to accumulate high plastic strain during rolling. Hence, the higher energy stored in the heavily deformed ferritic areas leads to a faster grain growth [40]. Some Widmanstätten ferritic grains are also observed in the UFH samples after soaking for 1.5 and 30 s (marked by white arrows on Fig. 5h,i) possibly formed at the early stages of cooling. Those ferrite plates are surrounded by bainite.

Spheroidized cementite (SC) is also observed in samples UFH-0.2s and UFH-1.5s (marked by red dashed arrows on SEM micrographs presented on Fig. 5). It is related to the short time (0.2–1.5 s) of the heat treatment, as reported previously by Castro Cerdá et al. [5,43], and fully dissolved after soaking for 30 s. A very small region with spheroidized cementite particles was also observed in the CH-0.2 s sample, although its amount is negligible (Fig. 5a).

3.3. EBSD characterization

EBSD technique was used to precisely quantify and characterize the different microconstituents formed in the material after both heat treatments. The results of EBSD analysis are outlined in Table 2. CH treatment leads to a microstructure mainly formed by a ferritic matrix, whose volume fraction remains constant (~86–87%) and martensite volume fraction slightly increases from 10.6% to 12.5% with the soaking time. As volume fraction of ferrite does not vary with soaking time (i.e. the amount of intercritical austenite formed at the peak temperature does not depend on the soaking time), the martensite increment can be attributed to the partial transformation of austenite into martensite by deformation during sample preparation. This indicates that retained austenite is less stable caused by the homogenization of carbon distribution in its interior after longer soaking times. Although the UFH process generates similar microstructure with the same microstructural constituents, there are significant variations in the volume fractions of different phases with respect to the CH treatment. The volume fraction of ferrite noticeably decreases with increasing soaking time from 90.9% at 0.2 s to 75.9% at 30 s, while the volume fraction of martensite shows the opposite trend. As the volume fraction of retained austenite remains stable (2.1–2.2%), it is possible to assure that the decrease of ferrite fraction is directly associated to the formation of martensite. On the other hand, the difference in ferrite and martensite volume fractions between CH and UFH conditions can be explained by the spheroidization of cementite during heating. First, the nucleation of austenite occurs at the α/cementite interface [44]. With conventional heating (CH), the cementite spheroidizes [7] reducing the amount of preferable sites for austenite formation and resulting in longer soaking time to reach the equilibrium. The main fraction of the inter-critical austenite is transformed into martensite during cooling. On the other hand, during UFH treatment the peak temperature is reached in < 1 s which dramatically reduces the amount of spheroidized cementite and, thus, increases the driving force for austenite nucleation at the more favorable α/cementite interfaces.

The morphology of the ferritic matrix in the CH and UFH heat treated samples also presents significant differences. The EBSD analysis revealed both recrystallized and recovered grains in the ferritic matrix. Fig. 6 represents the fraction of recrystallized ferrite in the ferritic matrix for all analyzed conditions. It is seen that, while the CH treatment leads to a homogeneous ferritic matrix, where almost 90% of ferrite is recrystallized, the UFH processing generates a matrix microstructure formed by recrystallized and non-recrystallized (i.e. recovered) ferritic grains. After UFH treatment, the volume fraction of recrystallized ferrite increases from ~50% after 0.2 s to ~67% after 30 s. So, while the recrystallization process is completed during CH treatment already after soaking for 0.2 s, it is delayed during UFH process. Similar observations were previously reported in [43,45,46]. This effect is due to the competition of different processes, such as austenite formation and further grain growth, reducing the driving force for recrystallization. For short soaking time (0.2 s), the recrystallization is the controlling process, which results in a very low martensite volume fraction (Table 2), similar to the CH treatment, and a significant volume fraction of recrystallized ferrite present in the material (Fig. 6). However, after soaking for longer time (1.5–30 s), other processes become dominant over recrystallization, such as the nucleation and growth of austenite into ferrite and ferrite grain growth [10,16]. The first effect results in the higher volume fraction of martensite present in the UFH800-30s (Table 2) and the decrease in volume fraction of recrystallized ferrite with increasing soaking time from 1.5 to 30 s (Fig. 6). The latter effect is discussed more in detail below (Figs. 7 and 8).

Fig. 7 represents the IPF maps for recrystallized (a,b,c) and non-

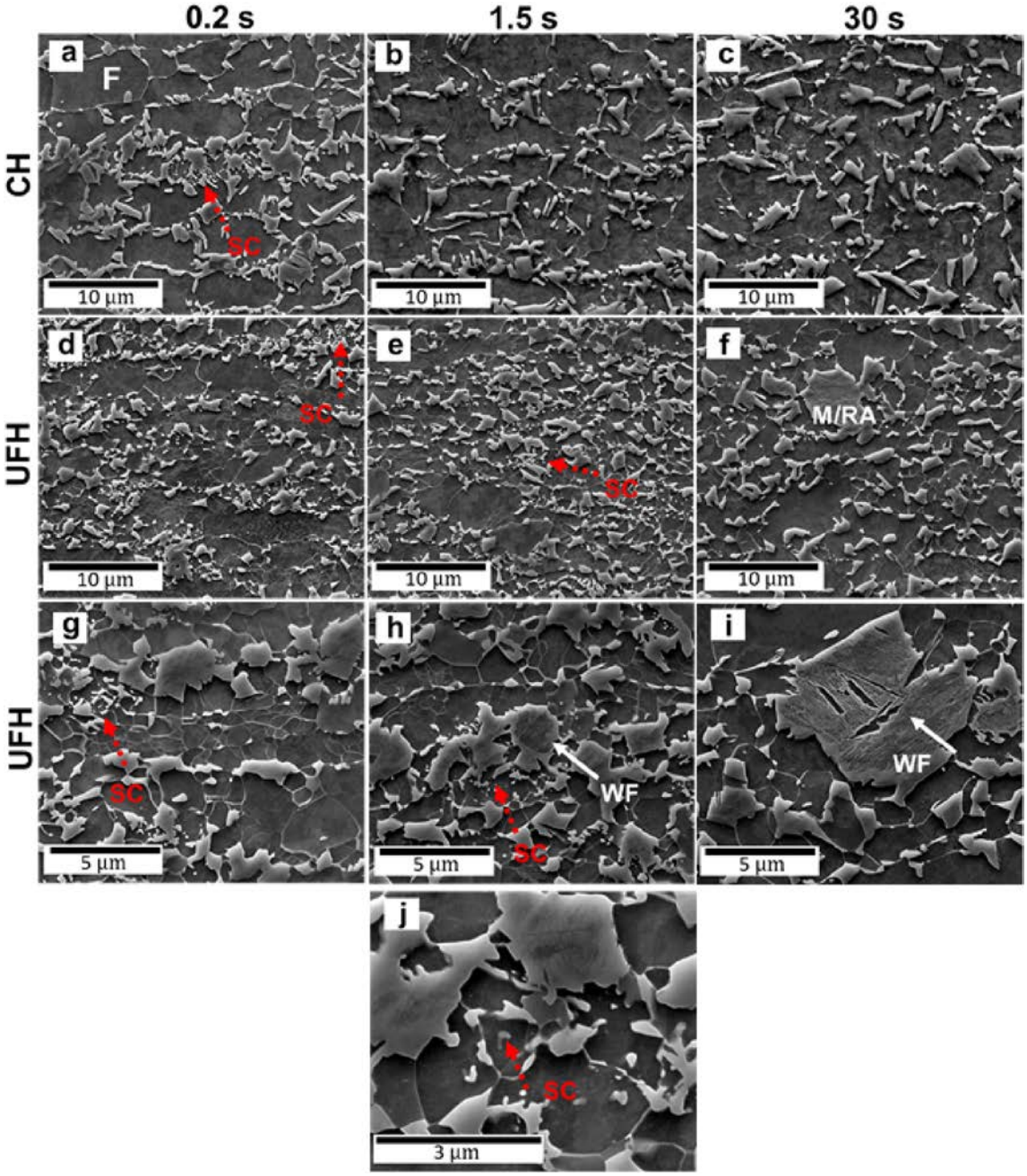

Fig. 5. SEM micrographs showing the effect of heating rate (10 and 800 °C/s) and soaking time (0.2 to 30 s) on the microstructure: a), b) and c) correspond to 10 °C/s for 0.2, 1.5 and 30 s, respectively; d), e) and f) correspond to 800 °C/s for 0.2, 1.5 and 30 s, respectively. Higher magnification images g), h) and i) show microstructures heated at 800 °C/s for 0.2, 1.5 and 30 s, respectively; j) higher magnification image of spheroidized cementite (SC) in the sample heated at 800 °C/s for 1.5 s. Spheroidized cementite is marked by dashed red arrows, while white arrows indicate Widmanstätten ferrite (WF). Ferrite is marked as F, and M/RA stands for martensite/retained austenite. Etched with Nital (3%). (For interpretation of the references to color in this figure legend, the reader is referred to the web version of this article.)

Table 2
Effect of the heating rate and soaking time on the volume fractions of phases present in the studied material.

Condition (s)	CH			UFH		
	0.2	1.5	30	0.2	1.5	30
Ferrite (%)	86.3 ± 2.4	87.4 ± 2.7	85.8 ± 1.6	90.9 ± 4.0	85.3 ± 2.8	75.9 ± 4.6
Martensite (%)	10.6 ± 1.7	10.8 ± 1.6	12.5 ± 1.6	6.9 ± 3.2	12.6 ± 3.1	22.0 ± 3.0
Retained austenite (%)	3.1 ± 0.7	1.8 ± 0.6	1.7 ± 0.1	2.2 ± 0.4	2.1 ± 0.3	2.1 ± 1.9

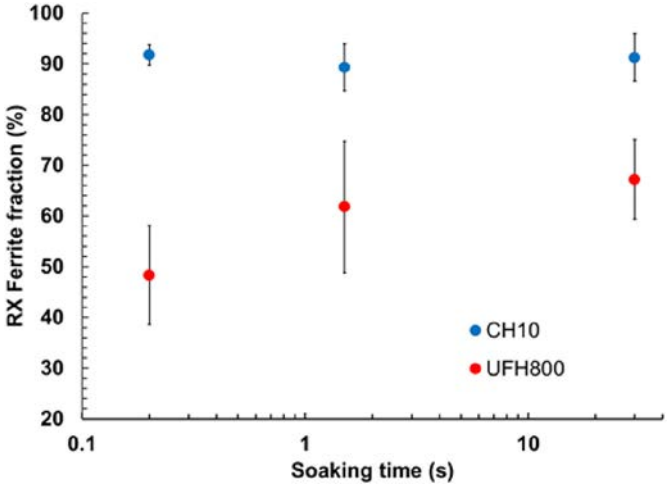

Fig. 6. Evolution of volume fraction of recrystallized ferrite with respect to the total fraction of ferrite with heating rate and soaking time.

recrystallized (d,e,f) ferrite after UFH for 0.2, 1.5 and 30 s, respectively. It is seen in Fig. 7a,b, that the vast majority of the grains are in the early stage of growth, presenting a size $\leq 1.5\,\mu m$, although it is possible to observe grains which have fully recrystallized and grown, i.e. grains without LAGBs and with low misorientations in their interior. This observation was also reported by Castro Cerda et al. [5]. When soaking time increases to 30 s, the fraction of fine grains decreases due to their growth, and the presence of larger grains is more evident (Fig. 7c). The non-recrystallized grains demonstrate significant misorientation in the interior of the grains indicating formation of substructure independently on the applied soaking time (Fig. 7d,e,f).

The evolution of the grain size distribution for recrystallized ferrite is clearly visible and quantified in Fig. 8a,b,c, where the grain size is plotted vs. the area fraction for the UFH800-0.2s, UFH800-1.5s and UFH800-30s, respectively (blue lines). It is observed that the mean peak shifts to higher values and widens. For instance, in the samples UFH800-0.2s and UFH800-1.5s the fraction of grains with a size below 1.5 μm is 52% and 56%, respectively, while after longer soaking it decreases to 36% indicating the growth of the small grains nucleated at shorter times. A second peak at higher grain size is noticeable indicating the presence of the large grains mentioned above. The intensity of the second peak decreases with soaking time, as the microstructure becomes more homogeneous (Fig. 8c). The histogram of grain size

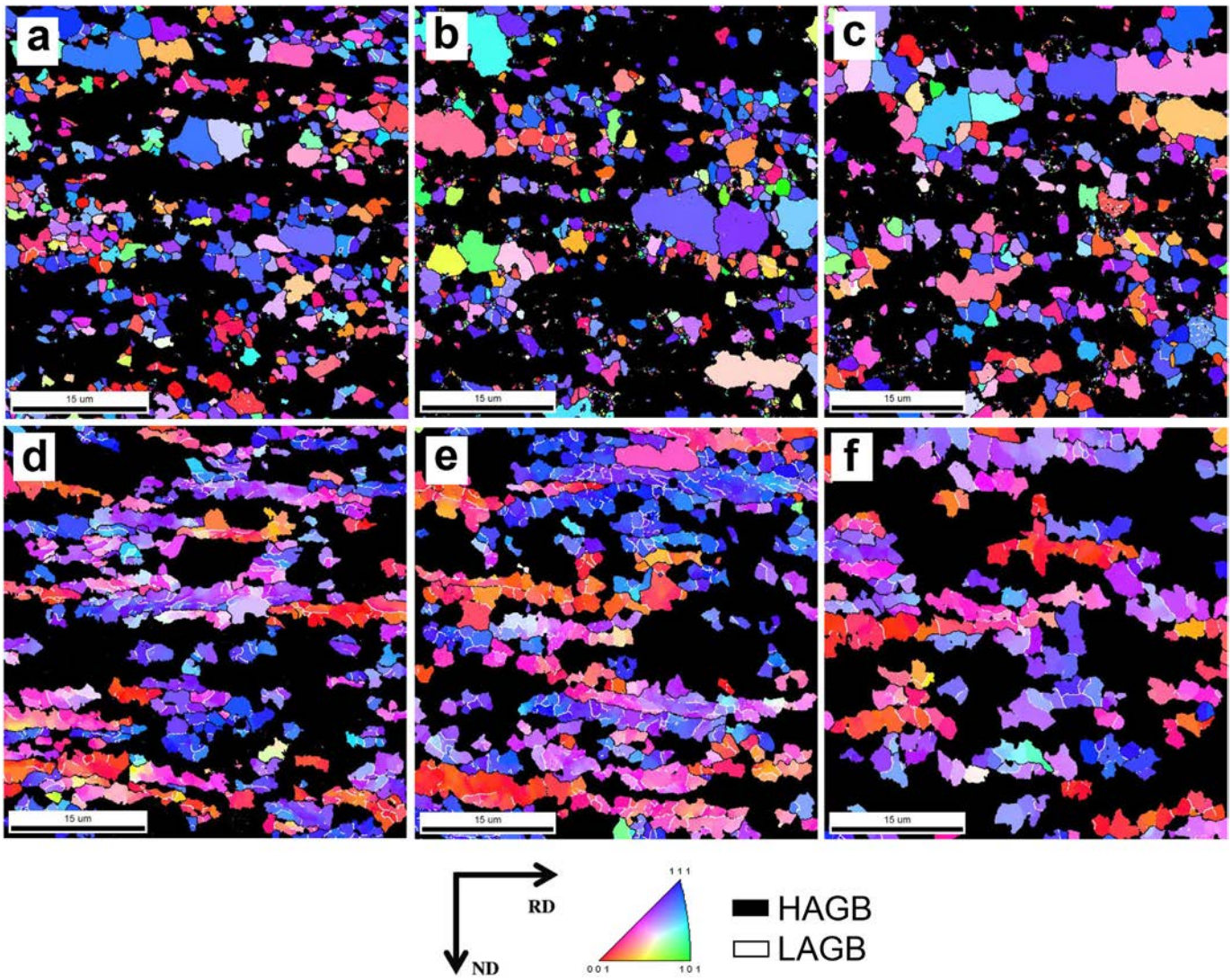

Fig. 7. IPF maps after UFH treatment showing the recrystallized (a, b, c) and non-recrystallized (d, e, f) ferrite after 0.2, 1.5 and 30 s, respectively. HAGBs are shown in black and LAGBs in white.

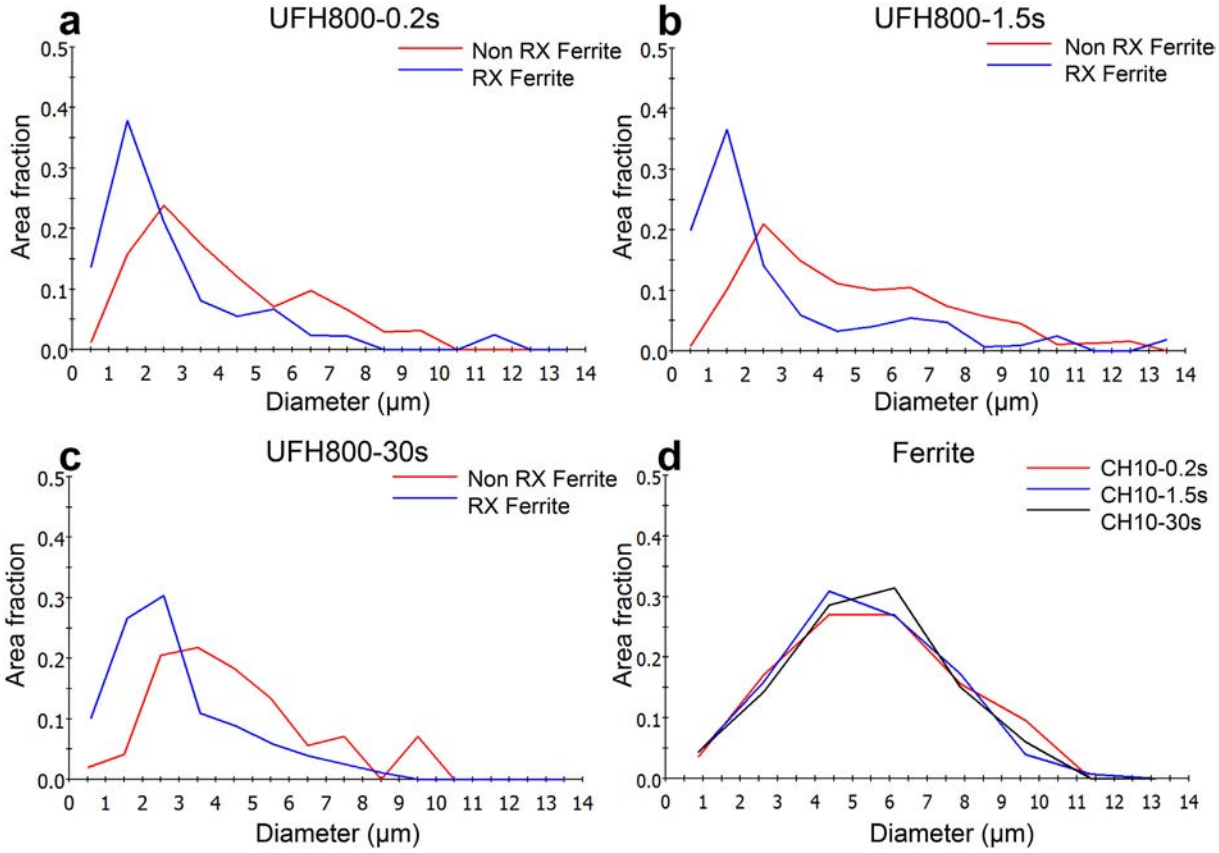

Fig. 8. a), b), c) Representation of the equivalent circle diameter (ECD) versus area fraction for recrystallized (RX) and non-recrystallized (Non RX) ferrite after UFH with soaking for 0.2, 1.5 and 30 s, respectively; d) grain diameter versus area fraction for ferrite after CH treatment. Data are obtained from the EBSD measurements. (For interpretation of the references to color in this figure, the reader is referred to the web version of this article).

distribution for non-recrystallized ferritic grains (red lines in Fig. 8) presents a similar character in comparison to the recrystallized ones. The primary peak shifts to the higher values becoming wider, when soaking time is increased. The fraction of grains having size above 2.5 μm increases from 59% at 0.2 s to 68% at 1.5 s to 73% after 30 s. This effect can be produced by the coalescence of grains after partial recrystallization indicated by the presence of HAGBs. Nevertheless, the non-recrystallized grains are larger compared to the recrystallized ones after all soaking times. On the other hand, the ferritic matrix in the CH condition is formed mainly by recrystallized equiaxed grains, and its microstructure is not affected by soaking time (Fig. 8d).

It is well known that high heating rates lead to a smaller grain size [6,10,13,47,48], as it is shown for the studied steel in Fig. 8. This is caused, among other reasons, by the short time given to the α/α interface to grow. On the one hand, after CH treatment the recrystallization and grain growth processes are completed independently on the applied soaking time. The grain size is also not affected by soaking time, as intercritical austenitic grains act as barriers for the ferritic grains suppressing their further growth. On the other hand, the UFH treated conditions show a bimodal distribution of grain size. The presence of the two differentiated regions on the histograms can be rationalized by the interplay of two main effects:

(1) the effect of the initial heterogeneous microstructure related to different amounts of strain accommodated by individual ferritic grains, as shown in Fig. 4;
(2) the effect of heating rate. A higher heating rate results in a recrystallization process taking place at higher temperatures, as discussed above, and, thus, in a higher nucleation rate due to the high density of defects [13,43,48].

The nuclei formed within the highly deformed areas possess higher driving force to grow and coalesce due to the high energy stored during cold rolling, resulting in the larger grains. On the other hand, nuclei generated within the less deformed regions present reduced driving force for growth. Moreover, due to the short time of the heat treatment, remains of individual cementite particles (which were not completely dissolved during inter-critical annealing) located at grain boundaries effectively pin grain boundaries suppressing grain growth and coalescence [49–51] (Fig. 5g,h,i). As the material is heated up to an intercritical temperature, another important factor comes into play: Formation of austenite and its growth competes for the energy stored in the material. The austenitic grains nucleate in carbon enriched areas, i.e. within pearlitic colonies. It can be assumed that the intensive nucleation of austenitic grains takes place within pearlitic colonies which were severely deformed, rotated or broken during cold rolling, resulting in reduction of distance between cementite plates. As is well known, the austenite nucleation rate is inversely proportional to the inter-lamellar spacing of pearlite [12]. The austenite grows firstly into the pearlite until it is dissolved and then into ferrite, as it is seen in Fig. 5. Competition of all these processes during UFH treatment results in the microstructure with finer grains (Figs. 5, 8).

Fig. 9 represents the equivalent circle diameter of martensite plotted versus area fraction. For the CH condition, at short soaking time (0.2 s) most of the martensite grains were formed from ultrafine austenitic grains, as the major peak lies below 1 μm (Fig. 9a). Increasing soaking time up to 1.5 s, the curve shifts to the right, indicating the growth of the earlier formed nuclei. Finally, after annealing for 30 s, the decrease of the main peak intensity is accompanied by increase in the area fraction at 3 μm, displaying that the austenite has entered the growth stage after the nucleation after short soaking times. In the case of the UFH800-0.2s, the curve is similar to the CH condition with the same

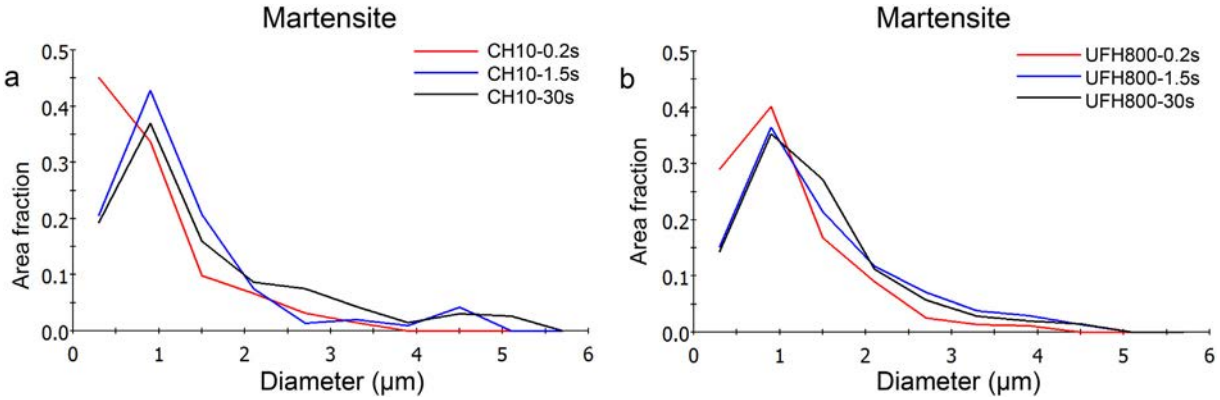

Fig. 9. Martensite ECD vs area fraction for CH (a) and UFH (b) for different soaking times: 0.2 s, 1.5 s and 30 s.

soaking time. However, the fraction of larger grains having a size of 4–5 μm increases. This behavior can indicate that the austenite nucleation is accompanied by a growth, due to the fact that the material has higher energy compared to the CH condition because of the low amount of spheroidized cementite and the higher carbon gradients present in the material, both produced by the rapid heating. It is more pronounced after 1.5 s, where the main peak has reduced, but there is an increase of the fraction of larger grains. The result of this effect is the rise of the martensite fraction in the overall microstructure. Finally, after 30 s the peak spreads to higher values, as it happens in the ferrite, showing an intense growth of the austenite grains during soaking.

3.4. Texture analysis

To analyze evolution of the preferable crystallographic orientation of ferritic grains, texture analysis was carried out for all studied conditions. Fig. 10a represents the ideal positions of the most important texture components in BCC lattice, while Fig. 10b shows the orientation distribution function (ODF) of the initial cold-rolled material. Fig. 10c,d,e display the ODFs for the CH samples annealed for 0.2, 1.5 and 30 s, respectively, while Fig. 10e,f,g represent the UFH conditions soaked for 0.2, 1.5 and 30 s, respectively. The initial cold-rolled material is represented by the ND {111}‹uvw› and RD {hkl}‹110› fibers, with a maxima corresponding to {111}‹110› components. Similar texture was found previously in cold-rolled low carbon steels [52,53]. On the other hand, the CH samples (Fig. 10c,d,e) present an opposite curvature in the ND fiber compared to the initial cold-rolled microstructure and lower intensity in the RD fiber. Both effects can be associated with the recrystallization in the ferritic matrix [4]. In the UFH conditions (Fig. 10f,g,h), the ODFs display texture similar to the initial cold-rolled condition (Fig. 10b), with a strong intensity in the ND fiber components, indicating that complete recrystallization has been delayed. However, its intensity is reduced with increasing soaking time. This effect can be attributed to onset of recrystallization during intercritical annealing for > 1.5 s and increasing fraction of recrystallized grains with soaking time revealed by EBSD analysis (Fig. 6, Section 3.3), as the initial ND fiber grains in the cold rolled steel present the higher stored energy [54].

The alpha fiber in the UFH treated material is also affected by soaking time. While a significant fraction of gamma fiber components recrystallized during UFH due to higher energy stored during cold rolling (compared to the alpha fiber components) [55,56], a lower fraction of alpha possesses energy (i.e. driving force) sufficient for recrystallization. So the RD fiber intensity is retained to large extent during UFH treatment.

3.5. XRD analysis

XRD measurements were carried out to analyze the evolution of retained austenite and its carbon content with soaking time. The results are listed in Table 3 and compared to the values obtained by TKD (see Section 3.6).

After short annealing (soaking for 0.2 s), the CH sample presents a higher retained austenite fraction compared to the UFH condition. The CH treatments lead to phase fractions closer to the ones at the equilibrium condition since there is more time for the austenite to nucleate and grow (Table 2). In the CH10-0.2s sample, taking into account fractions of both phases (i.e. retained austenite measured by XRD in Table 3 and martensite determined by EBSD in Table 2), the total fraction of austenite formed during intercritical annealing is close to 20%. The effect of soaking time on the retained austenite volume fraction for the UFH samples has two different trends. For short soaking times (0.2 s, 1.5 s), both nucleation and growth of intercritical austenite take place, as it is observed from the martensite fraction (see Section 3.3). Then, the volume fraction of austenite rises slightly from 6.6% to 6.9% with increasing time within the short range (Table 3). This effect indicates, that the nucleation stage plays a more important role compared to the growth stage, as there is a significant austenite fraction, which retains after rapid cooling, with a carbon concentration similar to the CH condition. Eventually, when the soaking time increases up to 30 s, the austenite fraction at the peak temperature increases due to the longer time to nucleate and grow, as there is a significant fraction of martensitic grains having a size below 1 μm (Fig. 9), but its carbon concentration decreases up to 0.7% reducing the amount of retained austenite down to 5.2%.

The volume fractions of retained austenite measured by XRD (Table 3) are considerably higher than the values determined by EBSD (Table 2). This effect is produced by the large difference in the depth of the analyzed area being approximately 1 μm for XRD and 50 nm for EBSD [57]. As is well known, the metastable retained austenite generates a local increase in volume during transformation into martensite [58]. As phase transformation on the surface allows an easier accommodation of this volume change, the surface retained austenite grains are more prone to phase transformation during sample preparation, that reduces the amount of retained austenite detected by EBSD [57]. Meanwhile, XRD is able to detect retained austenite present in the bulk material, which has not transformed into martensite. Moreover, it should be noted that although the spatial resolution of the EBSD is reasonably high (65 nm in step size), it is not sufficient for detection of the finest austenite grains present in the microstructure, revealed by TEM analysis (see Section 3.6). Similar conclusions were drawn for other steel grades containing metastable austenite, such as Q&P steels in [59,60].

3.6. TEM and TKD analysis

To study the evolution of microstructure during soaking on nanoscale, TKD analysis combined with TEM characterization were

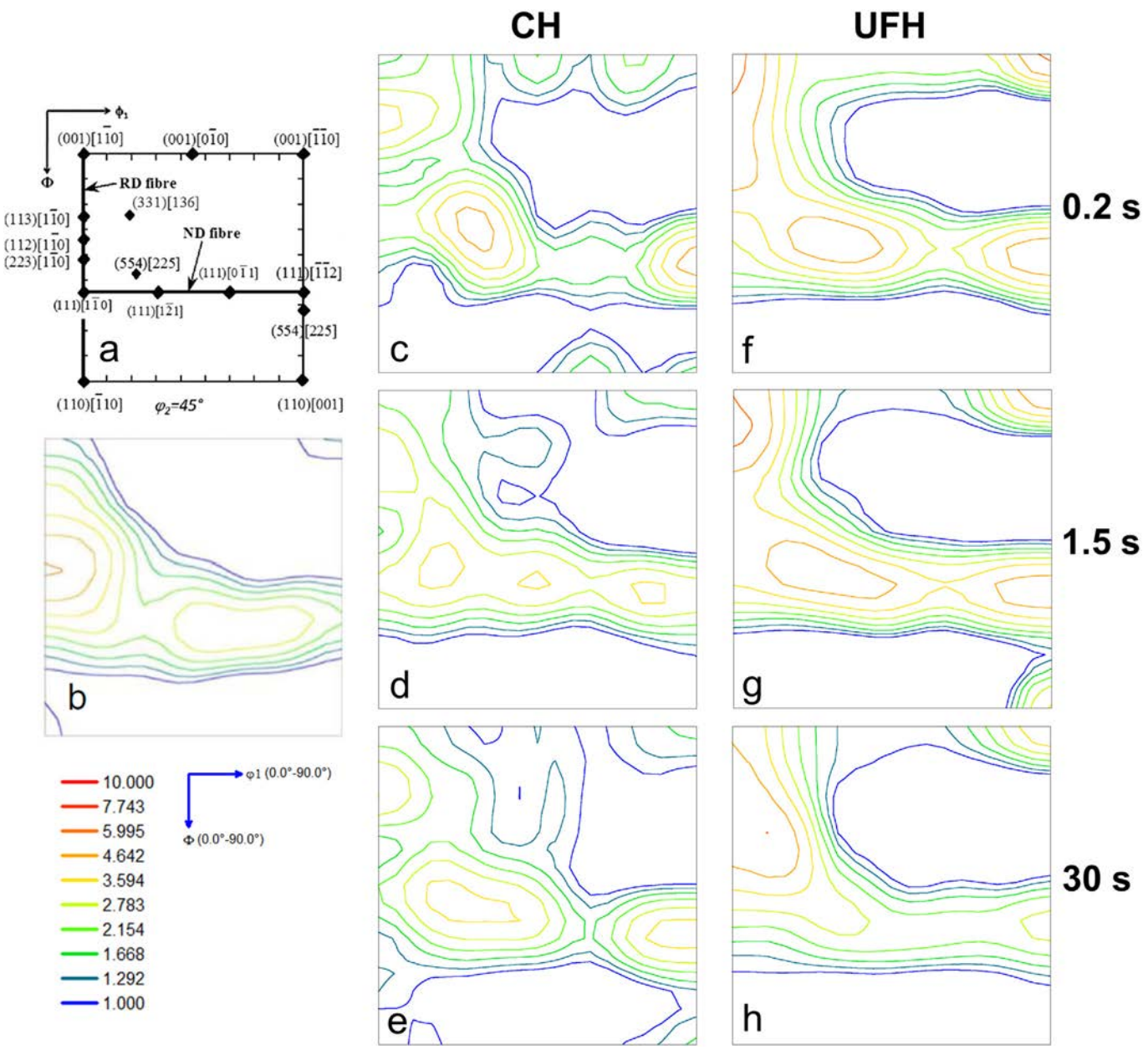

Fig. 10. Effect of heating rate and soaking time on the orientation distribution function (ODF) of the studied material for $\varphi_2 = 45^\circ$ in the Euler space; a) ideal BCC texture components for $\varphi_2 = 45^\circ$ in the Euler space; b) ODF of the initial cold rolled material, reproduced from [5]; c), d) and e) ODF corresponding to the CH conditions annealed for 0.2, 1.5 and 30 s, respectively; f), g) and h) correspond to the UFH conditions soaked for 0.2, 1.5 and 30 s, respectively.

Table 3
Effect of the heating rate and soaking time on the retained austenite volume fraction and its carbon content measured by XRD and TKD analysis.

Condition	XRD		TKD
	(%)	% C (wt.)	(%)
CH10-0.2s	7.9	0.77	4.8
UFH800-0.2s	6.6	0.80	8.1
UFH800-1.5s	6.9	0.77	4.9
UFH800-30s	5.2	0.70	4.4

carried out on CH10-0.2s and UFH after 0.2, 1.5 and 30 s samples. Fig. 11 represents the phase maps of the different samples analyzed by TKD. They are in a good accordance with the outcomes of the EBSD measurements presented above (see Section 3.3). Larger ferritic grains are observed in the CH10-0.2s samples (Fig. 11a) compared to those seen in the UFH samples (Fig. 11b,c,d). In addition, the CH treatment results in equiaxed ferritic grains without LAGBs in their interior (Fig. 11a) due to the longer treatment time, while the UFH leads to an inhomogeneous microstructure with varying grain size and a higher fraction of LAGBs (Fig. 11b,c,d).

Values of retained austenite volume fraction measured by TKD are provided in Table 3. They are higher compared to those determined by EBSD. This effect is caused by higher spatial resolution of the TKD technique, which enables to resolve nanoscale microstructural constituents having 10–30 nm in size [27]. Discrepancies between the volume fractions of retained austenite determined by XRD and those measured by TKD should also be noted. Unlike in the XRD measurements, a very local area is analyzed by TKD which leads to statistically insignificant data. Moreover, the TKD results highly depend on the quality of the studied samples. If the electropolishing step is inhomogeneous, there are significant differences in the foil thickness

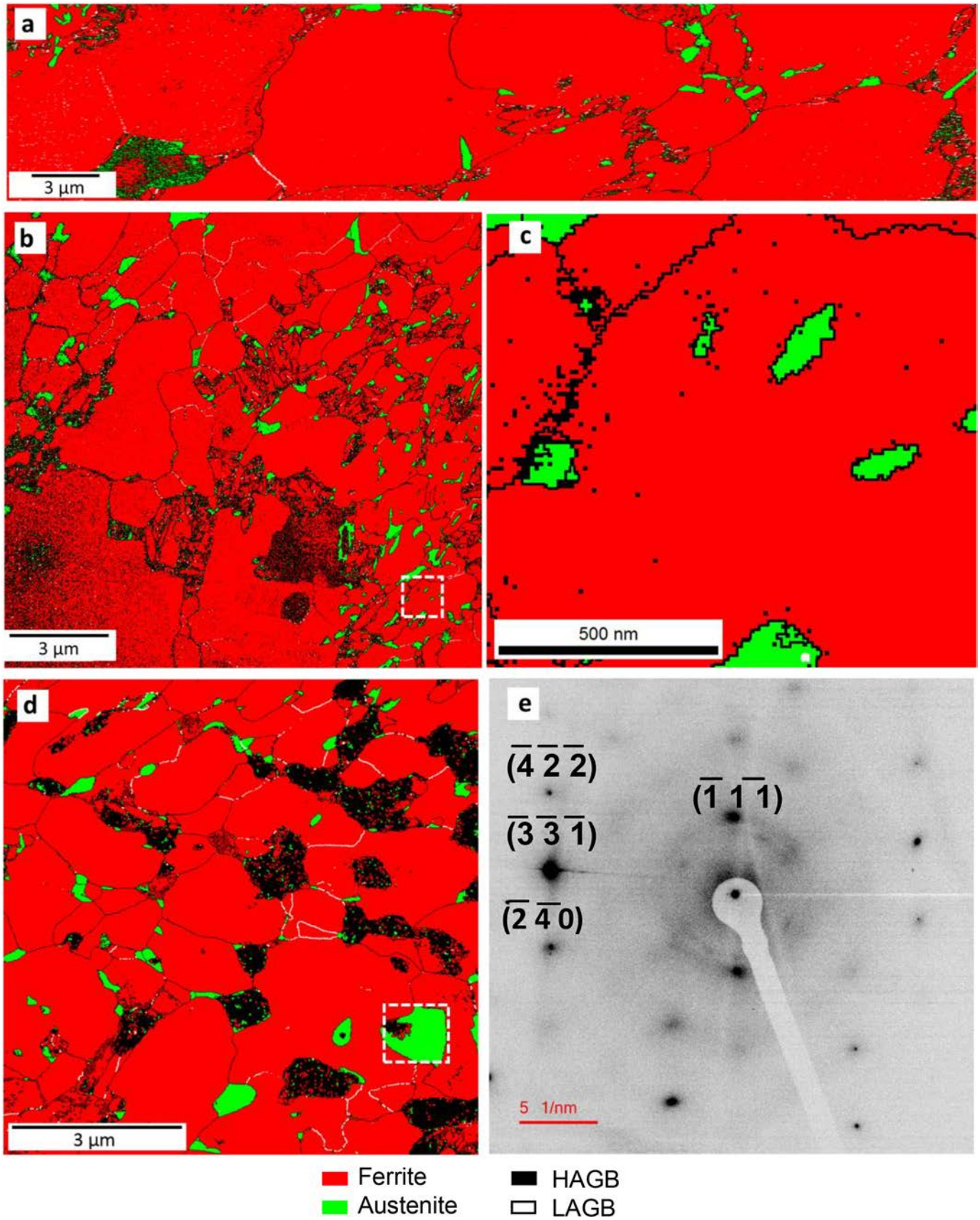

Fig. 11. Phase maps obtained from TKD analysis in a) CH10-0.2s and UFH for 0.2 s (b & c), and 1.5 s (d)). Figure c) shows a detailed region in figure b). Figure e) represents the diffraction pattern of the austenite marked in figure d). Ferrite is shown in red and austenite in green. HAGBs are represented in black and LAGBs in white. Large regions in black are areas with a confidence index (CI) lower than 0.1. (For interpretation of the references to color in this figure legend, the reader is referred to the web version of this article.)

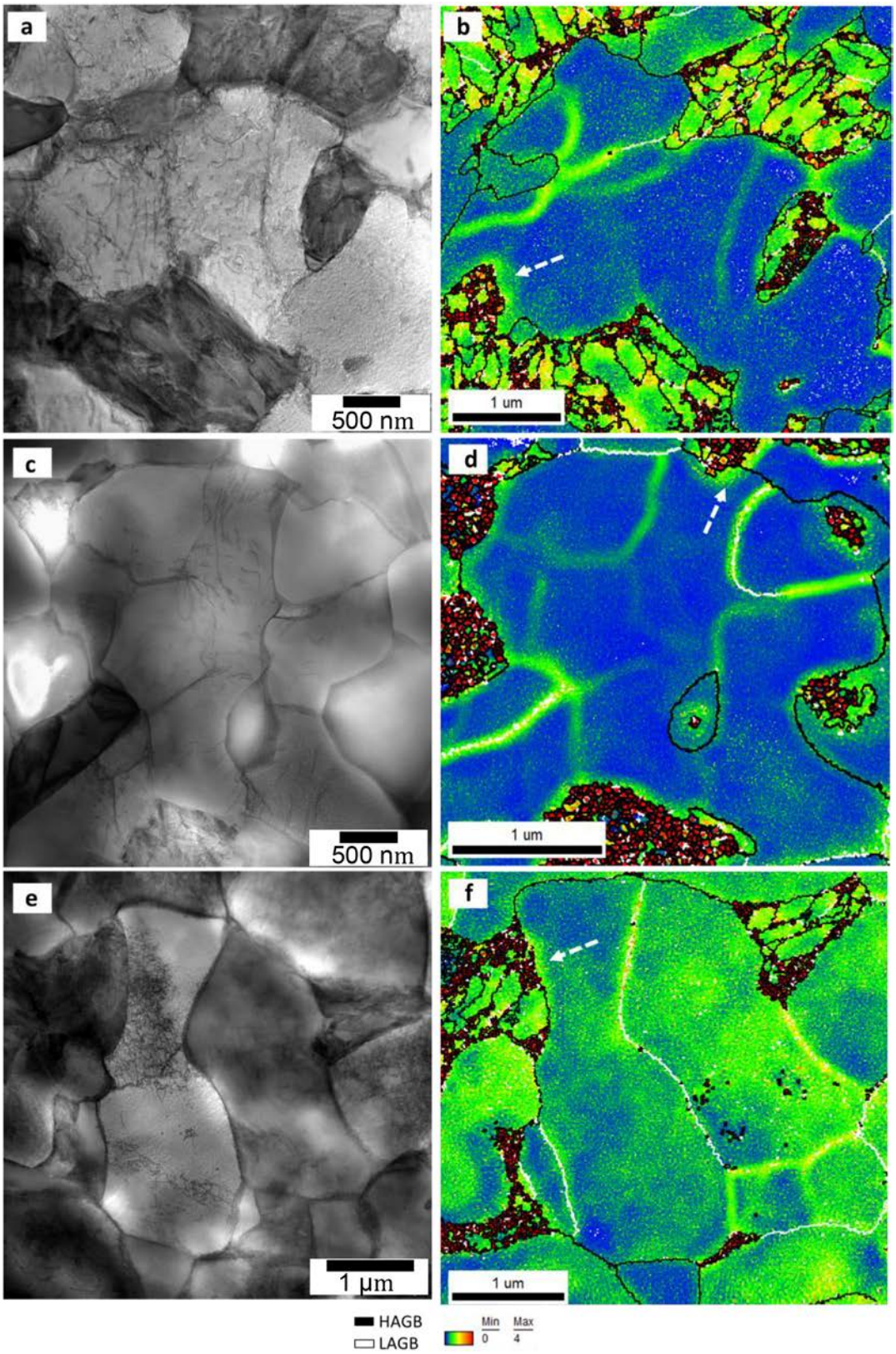

Fig. 12. TEM images after UFH treatment for a) 0.2 s, c) 1.5 s and e) 30 s; KAM maps for b) 0.2 s, d) 1.5 s and f) 30 s obtained from the TKD analysis. White dashed arrows indicate the increase in misorientation in the ferritic matrix due to the martensite formation (HAGBs in black, LAGBs in white).

through the sample. If a local area is too thick, the electrons are unable to pass through and reach the detector, as their initial energy is orders of magnitude less compared to the ones generated in TEM which results in the non-indexed areas. Similar effect occurs when the foil is too thin, as too many electrons cross the specimen and reach the detector [26,61]. Diffraction patterns were taken from different austenitic regions observed by TKD in all samples, in order to prove the presence of austenite in the material, as it is shown in Fig. 11e).

Fig. 12a,c,e shows TEM images illustrating microstructure evolution during UFH treatment of the steel within the non-recrystallized areas (as discussed in Sections above). Fig. 12b,d,f illustrate the corresponding KAM maps of the corresponding regions extracted from the TKD analysis. Formation of dislocation walls and other configurations is observed after UFH 0.2 s treatment, which are represented in form of lines with local misorientation < 1° on KAM maps (Fig. 12a,b). Dislocation walls associated to recovery were reported elsewhere [49,62]. Longer soaking time of 1.5 s allows further dislocation climb and rearrangement and onset of LAGBs formation (Fig. 12c,d). Finally, annealing for 30 s results in formation of an energetically favorable substructure in the grain interior (Fig. 12e) with local misorientation at LAGBs reaching 4° (Fig. 12f). In Fig. 12e,f, enhanced local dislocation density and increased local misorientation are clearly seen also in the ferritic matrix near the martensite/ferrite interface (marked by white arrows). It is related to accommodation of the plastic micro-strain induced by the volume expansion due to the austenite/martensite transformation during rapid cooling. This observation was reported earlier for DP steels [63].

The outcomes of this study clearly indicate that the microstructure of the low carbon steel is very sensitive to the soaking time at the peak temperature during UFH treatment. This provides an additional tool for microstructural design in carbon steels by manipulating also the soaking time in addition to the heating rate [5] and initial microstructure [12] of steels. Grain size, volume fraction of martensite, volume fraction of non-recrystallized and recrystallized ferrite can be optimized via the correct balance of the heat treatment parameters, so steels with the excellent combination of high strength and ductility can be manufactured [5]. The approach can be applied to all carbon steels.

4. Conclusions

The effect of heating rate and soaking time on the microstructure of the heat-treated low carbon steel was studied using SEM, EBSD, XRD, TKD and TEM techniques. The following conclusions can be drawn.

1. A complex multiphase, hierarchic microstructure mainly consisting of ferritic matrix with embedded martensite and retained austenite is formed after all applied heat treatments. There is significant effect of soaking time on the microstructure of the UFH treated steel, while it does not affect the microstructure evolved in the CH treated material.
2. There is a strong effect of heating rate on the microstructure of the ferritic matrix. The CH treatment results in the ferritic matrix consisting mainly of equiaxed recrystallized grains independently on the soaking time, while fine recrystallized grains and larger non-recrystallized (i.e. recovered) ferritic grains are present in all UFH treated conditions. The fraction of recrystallized ferritic grains generally tends to increase with increasing soaking time. Combined TEM and TKD study proved directly that the recovery process starts with formation of dislocation walls via dislocation climb and rearrangement, which gradually transform into LAGBs.
3. Volume fraction of martensite tends to increase with increasing soaking time during UFH treatment due to suppression of cementite spheroidization, which, in turn, reduces the amount of energetically favorable sites for austenite nucleation and results in longer soaking time to reach the equilibrium at the inter-critical peak temperature.
4. Based on the outcomes of the XRD analysis, it is possible to conclude that UFH treatments results in slightly lower amount of retained austenite compared to CH treatment. The amount of retained austenite and carbon content therein tend to slightly decrease with increasing soaking time after UFH treatment due to lower carbon gradients in the material before rapid cooling.
5. TKD analysis allows to precisely identify and analyze the retained austenite nanograins and other nanoscale elements of the complex microstructure along with the local misorientations due to dislocation generation and rearrangement.
6. TKD and TEM proved that local volume expansion due to austenite-martensite phase transformation during rapid cooling induces dislocations into the ferritic grains.

Data availability statement

The raw/processed data required to reproduce these findings cannot be shared at this time as the data also forms part of an ongoing study.

Acknowledgements

MAVT acknowledges gratefully the financial support by IMDEA Innovation Award. IS would like to acknowledge MAT4.0-CM project funded by Madrid region under programme S2018/NMT-4381.

References

[1] N. Fonstein, Advanced High Strength Sheet Steels: Physical Metallurgy, Design, Processing, and Properties, Springer, 2015, https://doi.org/10.1007/978-3-319-19165-2.
[2] T. Lolla, G. Cola, B. Narayanan, B. Alexandrov, S.S. Babu, Development of rapid heating and cooling (flash processing) process to produce advanced high strength steel microstructures, Mater. Sci. Technol. 27 (2011) 863–875, https://doi.org/10.1179/174328409x433813.
[3] R.H. Petrov, J. Sidor, W.J. Kaluba, L.A.I. Kestens, Grain refinement of a cold rolled TRIP assisted steel after ultra short annealing, Mater. Sci. Forum 715–716 (2012) 661–666, https://doi.org/10.4028/www.scientific.net/MSF.715-716.661.
[4] R.H. Petrov, J. Sidor, L.A.I. Kestens, Texture formation in high strength low alloy steel reheated with ultrafast heating rates, Mater. Sci. Forum 702–703 (2012) 798–801, https://doi.org/10.4028/www.scientific.net/MSF.702-703.798.
[5] F.M. Castro Cerda, C. Goulas, I. Sabirov, S. Papaefthymiou, A. Monsalve, R.H. Petrov, Microstructure, texture and mechanical properties in a low carbon steel after ultrafast heating, Mater. Sci. Eng. A 672 (2016) 108–120, https://doi.org/10.1016/j.msea.2016.06.056.
[6] F.M. Castro Cerda, F. Vercruysse, T.N. Minh, L.A.I. Kestens, A. Monsalve, R.H. Petrov, The effect of heating rate on the recrystallization behavior in cold rolled ultra low carbon steel, Steel Res. 87 (2016) 1–9, https://doi.org/10.1002/srin.201600351.
[7] F.M. Castro Cerda, I. Sabirov, C. Goulas, J. Sietsma, A. Monsalve, R.H. Petrov, Austenite formation in 0.2% C and 0.45% C steels under conventional and ultrafast heating, Mater. Des. 116 (2017) 448–460, https://doi.org/10.1016/j.matdes.2016.12.009.
[8] http://www.flashbainite.com/
[9] L.A.I. Kestens, A.C.D. Reis, W.J. Kaluba, Y. Houbaert, Grain refinement and texture change in interstitial free steels after severe rolling and ultra-short annealing, Mater. Sci. Forum 467–470 (2004) 287–292, https://doi.org/10.4028/www.scientific.net/MSF.467-470.287.
[10] V. Massardier, A. Ngansop, D. Fabrègue, S. Cazottes, J. Merlin, Ultra-rapid inter-critical annealing to improve deep drawability of low-carbon, al-killed steels, Metall. Mater. Trans. A. 43 (2012) 2225–2236, https://doi.org/10.1007/s11661-012-1096-6.
[11] P. Gobernado, R.H. Petrov, L.A.I. Kestens, Recrystallized {311}(136) orientation in ferrite steels, Scr. Mater. 66 (2012) 623–626, https://doi.org/10.1016/j.scriptamat.2012.01.056.
[12] F.M. Castro Cerda, C. Goulas, I. Sabirov, L.A.I. Kestens, R.H. Petrov, The effect of the pre-heating stage on the microstructure and texture of a cold rolled FeCMnAlSi steel under conventional and ultrafast heating, Mater. Charact. 130 (2017) 188–197, https://doi.org/10.1016/j.matchar.2017.06.010.
[13] M. Ferry, D. Muljoni, D.P. Dunne, Recrystallization kinetics of low and ultra low carbon steels during high-rate annealing, ISIJ Int. 41 (2001) 1053–1060, https://doi.org/10.2355/isijinternational.41.1053.
[14] M.A. Valdes-Tabernero, F. Vercruysse, I. Sabirov, R.H. Petrov, M.A. Monclús, J.M. Molina-Aldareguia, Effect of ultrafast heating on the properties of the micro-constituents in a low-carbon steel, Metall. Mater. Trans. A. 49 (2018) 3145–3150, https://doi.org/10.1007/s11661-018-4658-4.
[15] F. Vercruysse, Third generation advanced high strength steel by ultrafast annealing, Master thesis University of Ghent, 2016.
[16] A. Puype, Developing of advanced high strength steel via ultrafast annealing, Master thesis University of Ghent, 2014.
[17] L. Barbé, K. Verbeken, E. Wettinck, Effect of the addition of P on the mechanical properties of low alloyed TRIP steels, ISIJ Int. 46 (2006) 1251–1257, https://doi.org/10.2355/isijinternational.46.1251.
[18] E.M. Bellhouse, J.R. McDermid, Effect of continuous galvanizing heat treatments on the microstructure and mechanical properties of high Al-low Si transformation induced plasticity steels, Metall. Mater. Trans. A Phys. Metall. Mater. Sci. 41 (2010) 1460–1473, https://doi.org/10.1007/s11661-010-0185-7.
[19] B.C. De Cooman, Structure-properties relationship in TRIP steels containing carbide-free bainite, Curr. Opin. Solid State Mater. Sci. 8 (2004) 285–303, https://doi.org/10.1016/j.cossms.2004.10.002.

[20] O. Engler, V. Randle, Introduction to Texture Analysis: Macrostructure, Microstructure and Orientation Mapping, CRC Press, Boca Raton, 2009 2nd ed.
[21] R.H. Petrov, L.A.I. Kestens, Advanced high-strength steels: electron backscatter diffraction (EBSD), Encycl. Iron, Steel, their Alloy, 2015, pp. 46–69, , https://doi.org/10.1081/E-EISA-120050786.
[22] Y. Cao, H. Di, J. Zhang, J. Zhang, T. Ma, R.D.K. Mishra, An electron backscattered diffraction study on the dynamic recrystallization behavior of a nickel – chromium alloy (800H) during hot deformation, Mater. Sci. Eng. A 585 (2013) 71–85, https://doi.org/10.1016/j.msea.2013.07.037.
[23] C.F. Jatczak, Retained austenite and its measurement by X-ray diffraction, SAE Tech. Pap. (1980), https://doi.org/10.4271/800426.
[24] N.H. van Dijk, A.M. Butt, L. Zhao, J. Sietsma, S.E. Offerman, J.P. Wright, S. van der Zwaag, Thermal stability of retained austenite in TRIP steels studied by synchrotron X-ray diffraction during cooling, Acta Mater. 53 (2005) 5439–5447, https://doi.org/10.1016/j.actamat.2005.08.017.
[25] R.R. Keller, R.H. Geiss, Transmission EBSD from 10 nm domains in a scanning, J. Microsc. 245 (2012) 245–251, https://doi.org/10.1111/j.1365-2818.2011.03566.x.
[26] P.W. Trimby, Orientation mapping of nanostructured materials using transmission Kikuchi diffraction in the scanning electron microscope, Ultramicroscopy 120 (2012) 16–24, https://doi.org/10.1016/j.ultramic.2012.06.004.
[27] P.W. Trimby, Y. Cao, Z. Chen, S. Han, K.J. Hemker, J. Lian, X. Liao, P. Rottmann, S. Samudrala, J. Sun, J.T. Wang, J. Wheeler, J.M. Cariney, Characterizing deformed ultrafine-grained and nanocrystalline materials using transmission Kikuchi diffraction in a scanning electron microscope, Acta Mater. 62 (2014) 69–80, https://doi.org/10.1016/j.actamat.2013.09.026.
[28] N. Mortazavi, C. Geers, M. Esmaily, V. Babic, M. Sattari, K. Lindgren, P. Malmberg, B. Jönsson, M. Halvarsson, J.E. Svensson, I. Panas, L.G. Johansson, Interplay of water and reactive elements in oxidation of alumina-forming alloys, Nat. Mater. 17 (2018) 610–617, https://doi.org/10.1038/s41563-018-0105-6.
[29] N. Mortazavi, M. Esmaily, M. Halvarsson, The capability of Transmission Kikuchi Diffraction technique for characterizing nano-grained oxide scales formed on a FeCrAl stainless steel, Mater. Lett. 147 (2015) 42–45, https://doi.org/10.1016/j.matlet.2015.02.008.
[30] D. Wang, H. Kahn, F. Ernst, A.H. Heuer, “Colossal” interstitial supersaturation in delta ferrite in stainless steels: (II) low-temperature nitridation of the 17-7 PH alloy, Acta Mater. 124 (2017) 237–246, https://doi.org/10.1016/j.actamat.2016.11.004.
[31] C. Hofer, V. Bliznuk, A. Verdiere, R.H. Petrov, F. Winkelhofer, H. Clemens, S. Primig, High-resolution characterization of the martensite-austenite constituent in a carbide-free bainitic steel, Mater. Charact. 144 (2018) 182–190, https://doi.org/10.1016/j.matchar.2018.07.011.
[32] M. Kulakov, W.J. Poole, M. Militzer, The effect of the initial microstructure on recrystallization and austenite formation in a DP600 steel, Metall. Mater. Trans. A Phys. Metall. Mater. Sci. 44 (2013) 3564–3576, https://doi.org/10.1007/s11661-013-1721-z.
[33] R.R. Mohanty, O.A. Girina, N.M. Fonstein, Effect of heating rate on the austenite formation in low-carbon high-strength steels annealed in the intercritical region, Metall. Mater. Trans. A. 42 (2011) 3680–3690, https://doi.org/10.1007/s11661-011-0753-5.
[34] J. Huang, W.J. Poole, M. Militzer, Austenite formation during intercritical annealing, Metall. Mater. Trans. A. 35 (2004) 3363–3375, https://doi.org/10.1007/s11661-004-0173-x.
[35] J.B. Seol, D. Raabe, P.P. Choi, Y.R. Im, C.G. Park, Atomic scale effects of alloying, partitioning, solute drag and austempering on the mechanical properties of high-carbon bainitic–austenitic TRIP steels, Acta Mater. 60 (2012) 6183–6199, https://doi.org/10.1016/j.actamat.2012.07.064.
[36] V.N. Gridnev, Y.Y. Meshkov, S.P. Oshkaderov, Austenite transformation point in rapidly heated steel and iron, Phys. Met. Metallogr. 18 (1964) 135–136.
[37] H. Li, K. Gai, L. He, C. Zhang, H. Cui, M. Li, Non-isothermal phase-transformation kinetics model for evaluating the austenization of 55CrMo steel based on Johnson – Mehl – Avrami equation, Mater. Des. 92 (2016) 731–741, https://doi.org/10.1016/j.matdes.2015.12.110.
[38] N. Li, J. Lin, D.S. Balint, T.A. Dean, Experimental characterisation of the effects of thermal conditions on austenite formation for hot stamping of boron steel, J. Mater. Process. Technol. 231 (2016) 254–264, https://doi.org/10.1016/j.jmatprotec.2015.12.008.
[39] W.L. Haworth, J.G. Parr, The effect of rapid heating on the alpha-gamma transformation of iron, Trans AMS 58 (1965) 476–488.
[40] G. Gottstein, Physical Foundations of Materials Science, Springer, 2004, https://doi.org/10.1007/978-3-662-09291-0.
[41] A.S. Sastri, D.R.F. West, Effect of austenitizing conditions on kinetics of martensite formation in certain medium-alloy steels, J. Iron Steel Inst. 203 (1965) 138–145.
[42] A. Ankara, Strength of austenite and its effect on martensite transformation, J. Iron Steel Inst. 208 (1970) 819–823.
[43] F.M. Castro Cerda, L.A.I. Kestens, A. Monsalve, R.H. Petrov, The effect of ultrafast heating in cold-rolled low carbon steel: recrystallization and texture evolution, Metals (Basel) 6 (2016) 288–299, https://doi.org/10.3390/met6110288.
[44] G. Speich, A. Szirmae, M. Richards, Formation of austenite from ferrite and ferrite-carbide aggregates, Trans. AIME 245 (1969) 1063–1073.
[45] J. Stockemer, P. Vanden Brande, Recrystallization of a cold-rolled low-carbon steel by cold-plasma-discharge rapid annealing, Metall. Mater. Trans. A. 34 (2003) 1341, https://doi.org/10.1007/s11661-003-0245-3.
[46] R.H. Petrov, F. HajyAkbary, J. Sidor, M.J. Santofimia, J. Sietsma, L.A.I. Kestens, Ultra-fast annealing of high strength steel, Int. Virtual J. Mach. Technol. Mater. 8 (2012) 68–71.
[47] D. Muljono, M. Ferry, D.P. Dunne, Influence of heating rate on anisothermal recrystallization in low and ultra-low carbon steels, Mater. Sci. Eng. A 303 (2001) 90–99, https://doi.org/10.1016/S0921-5093(00)01882-7.
[48] T. Senuma, K. Kawasaki, Y. Takemoto, Recrystallization behavior and texture formation of rapidly annealed cold-rolled extralow carbon steel sheets, Mater. Trans. 47 (2006) 1769–1775, https://doi.org/10.2320/matertrans.47.1769.
[49] F.J. Humphreys, M. Hatherly, Recrystallization and Related Annealing Phenomena, (2004), https://doi.org/10.1016/B978-008044164-1/50015-3.
[50] G.S. Rohrer, Introduction to grains, phases, and interfaces - an interpretation of microstructures, Trans. AIME 175 (1948) 15–51, https://doi.org/10.1007/s11661-010-0215-5.
[51] V. Massardier, A. Ngansop, D. Fabrègue, J. Merlin, J. Capelle, F.V. Cedex, Microstructure and mechanical properties of low carbon Al-killed steels after ultra-rapid annealing cycles, Mater. Sci. Forum 642 (2010) 3368–3373, https://doi.org/10.4028/www.scientific.net/MSF.638-642.3368.
[52] B. Hutchinson, Development and control of annealing textures in low-carbon steels, Int. Met. Rev. 29 (1984) 25–42, https://doi.org/10.1179/imtr.1984.29.1.25.
[53] R.K. Ray, J.J. Jonas, R.E. Hook, Cold rolling and annealing textures i∼ low carbon and extra low carbon steels, Int. Met. Rev. 39 (1994) 129–1720, https://doi.org/10.1179/imr.1994.39.4.129.
[54] I.L. Dillamore, P.L. Morris, C.J.E. Smith, B. Hutchinson, Transition bands and recrystallization in metals, Procedings R. Soc. London A. 329 (1972) 405–420, https://doi.org/10.1098/rspa.1972.0120.
[55] I. Samajdar, B. Verlinden, P. Van Houtte, D. Vanderschueren, γ-Fibre recrystallization texture in IF-steel: an investigation on the recrystallization mechanisms, Mater. Sci. Eng. A 238 (1997) 343–350, https://doi.org/10.1016/S0921-5093(97)00455-3.
[56] J. Kang, B. Bacroix, H. Réglé, K.H. Oh, H. Lee, Effect of deformation mode and grain orientation on misorientation development in a body-centered cubic steel, Acta Mater. 55 (2007) 4935–4946, https://doi.org/10.1016/j.actamat.2007.05.014.
[57] G.K. Tirumalasetty, M.A. van Huis, C. Kwakernaak, J. Sietsma, W.G. Sloof, H.W. Zandbergen, Deformation-induced austenite grain rotation and transformation in TRIP-assisted steel, Acta Mater. 60 (2012) 1311–1321, https://doi.org/10.1016/j.actamat.2011.11.026.
[58] P.G. Xu, Y. Tomota, Y. Arakaki, S. Harjo, H. Sueyoshi, Evaluation of austenite volume fraction in TRIP steel sheets using neutron diffraction, Mater. Charact. 127 (2017) 104–110, https://doi.org/10.1016/j.matchar.2017.02.028.
[59] I. de Diego-Calderón, D. De Knijf, M.A. Monclús, J.M. Molina-Aldareguia, I. Sabirov, C. Föjer, R.H. Petrov, Global and local deformation behavior and mechanical properties of individual phases in a quenched and partitioned steel, Mater. Sci. Eng. A 630 (2015) 27–35, https://doi.org/10.1016/j.msea.2015.01.077.
[60] D. De Knijf, R.H. Petrov, C. Föjer, L.A.I. Kestens, Effect of fresh martensite on the stability of retained austenite in quenching and partitioning steel, Mater. Sci. Eng. A 615 (2014) 107–115, https://doi.org/10.1016/j.msea.2014.07.054.
[61] S. Suzuki, Features of transmission EBSD and its application, J. Minearls, Met. Mater. Soc. 65 (2013) 1254–1263, https://doi.org/10.1007/s11837-013-0700-6.
[62] R.D. Doherty, D.A. Hughes, F.J. Humphreys, J.J. Jonas, D. Juul Jensen, M.E. Kassner, W.E. King, T.R. McNelley, H.J. McQueen, A.D. Rollett, Current issues in recrystallization: a review, Mater. Sci. Eng. A 238 (1997) 219–274, https://doi.org/10.1016/S0921-5093(97)00424-3.
[63] M. Calcagnotto, D. Ponge, E. Demir, D. Raabe, Orientation gradients and geometrically necessary dislocations in ultrafine grained dual-phase steels studied by 2D and 3D EBSD, Mater. Sci. Eng. A 527 (2010) 2738–2746, https://doi.org/10.1016/j.msea.2010.01.004.

4.3. The effect of soaking time after ultrafast heating on the microstructure and mechanical behavior of a low carbon steel

M.A. Valdés-Tabernero*, R.H. Petrov, M.A. Monclús, J.M. Molina-Aldareguia, I. Sabirov. *Materials Science and Engineering A* 765 (2019) 138276.

DOI: https://doi.org/10.1016/j.msea.2019.138276

Materials Science & Engineering A 765 (2019) 138276

Contents lists available at ScienceDirect

Materials Science & Engineering A

journal homepage: www.elsevier.com/locate/msea

The effect of soaking time after ultrafast heating on the microstructure and mechanical behavior of a low carbon steel

M.A. Valdes-Tabernero[a,*], R.H. Petrov[b,c], M.A. Monclus[a], J.M. Molina-Aldareguia[a], I. Sabirov[a]

[a] IMDEA Materials Institute, Calle Eric Kandel 2, Getafe, 28906, Madrid, Spain
[b] Department of Materials Science and Engineering, Delft University of Technology, Mekelweg 2, 2628CD, Delft, the Netherlands
[c] Department of Electrical Energy, Metals, Mechanical Constructions & Systems, Ghent University, Technologiepark 46, 9052, Ghent, Belgium

ARTICLE INFO

Keywords:
Steel
Ultrafast heating
Microstructure
Mechanical properties
Nanoindentation
Pop-in

ABSTRACT

The main objective of this study is to understand the effect of the soaking time during the ultrafast heat treatment of a low carbon steel on its complex multi-phase microstructure, tensile mechanical behavior and properties of individual microconstituents. Tensile tests were performed to determine the macro-mechanical properties. Nanoindentation testing was carried out on individual microconstituents (martensite, recrystallized ferrite and non-recrystallized ferrite) identified *a priori* via EBSD analysis to measure their properties. It is shown that ultrafast heating combined with short soaking times results in improved macro-mechanical properties due to finer grain size and higher fraction of non-recrystallized ferrite, that has a higher nanohardness than recrystallized ferrite. Prolonged soaking times eliminate the advantages of the ultrafast heat treatment. This occurs because, even though a long soaking time promotes a higher volume fraction of martensite than a short one, it also induces substantial grain growth and complete recrystallization of the ferritic matrix. On the micro-scale, the ferritic grains show two different types of mechanical response. The recrystallized ferritic grains are prone to show pop-in events on the nanoindentation curves that are associated to dislocation nucleation events as a consequence of their low dislocation density, while non-recrystallized ferritic grains demonstrate a continuous response. The relationship between microstructure and mechanical properties on the macro- and micro-scales is discussed with respect to the microstructure, which in turn strongly depends on the applied heating rate and soaking time. A general recipe for microstructural design to improve the tensile mechanical behavior of low carbon steels implementing controlled heating and soaking conditions is outlined.

1. Introduction

Steel is the most widely used material in the automotive sector [1]. However, the steel and automotive industries have been challenged by safety and carbon emission regulations imposed by the regulatory bodies. An improvement in the mechanical properties of steels is a potential solution to allow manufacturing of lighter components, thus reducing the total weight of the car, the fuel consumption and the carbon footprint. Moreover, the current paradigm in the steel processing industry is based on relatively long-time thermal treatments. This puts the steel sector at the top of the list of energy consumers and carbon dioxide emitters [2]. In order to decrease the required amount of energy and cut down the greenhouse emissions, new processing routes were developed over the last decade, such as the rapid heat treatment. It was firstly proposed by Lolla et al. [3] in 2011, who named it “flash processing”, while another term “ultra-fast heating” (UFH) has been used by other researchers [4,5]. The principle lies on the application of high heating rates ($\gg 100\ ^{\circ}C/s$) to heat the material instead of the conventional rates used nowadays ($\leq 10\ ^{\circ}C/s$) in combination with short soaking times. The rapid heating to an intercritical or fully austenitic peak temperature is followed by short soaking and immediate quenching to room temperature. The very short time required to perform the whole process ($\ll 10$ s) dramatically reduces the energy consumption [6] and has the potential of increasing the strength of the final product provided the final microstructure is carefully controlled.

The microstructure of the UFH processed steels depends on numerous factors including chemical composition, initial microstructure and the key heat treatment parameters (heating rate, peak temperature and soaking time) [7]. The main body of research in this field is focused on the effect of processing parameters on the microstructure of low carbon steels [8–12]. It has been demonstrated that UFH rates lead to the formation of a complex multiphase microstructure with ferrite,

* Corresponding author.
E-mail address: miguelangel.valdes@imdea.org (M.A. Valdes-Tabernero).

https://doi.org/10.1016/j.msea.2019.138276
Received 9 May 2019; Received in revised form 31 July 2019; Accepted 11 August 2019
Available online 12 August 2019
0921-5093/

martensite and some low amount of retained austenite as the main microconstituents. A heterogeneous microstructure was revealed in the ferritic matrix [13], as recrystallization and recovery processes occur simultaneously due to the shifting of recrystallization temperature to higher values [11,14]. As a result, the grain size is reduced [12]. The increase of peak temperature increases both the fractions of recrystallized ferrite and the austenite (i.e. martensite) [15]. The grain size also tends to increase with peak temperature [16]. As a consequence, the martensite formed after quenching is softer due to homogenization of the carbon distribution. On the other hand, the isothermal soaking time has always been kept as short as possible (< 0.5 s) [5,17] to avoid grain growth, which occurs during longer soaking [18], thus eliminating the grain refinement effect of the UFH treatment.

The effect of UFH on the mechanical properties has not been deeply studied yet. Higher mechanical strength without a significant reduction in ductility has been reported for ultrafast heated steels compared to conventionally heated ones [19,20]. These studies, however, focused entirely on their tensile mechanical properties. It is well-known that macro-mechanical response of multi-phase materials is determined by the morphology, architecture and properties of the individual microconstituents [21]. The latter depend, in turn, on their internal lattice structure (i.e. defect density) [22]. Up to date there have been no systematic studies on the properties of the individual microconstituents in ultrafast heated steels. Understanding the effect of the ultrafast heating parameters on them and their role on the overall mechanical properties of ultrafast heated steels could provide us with a valuable tool for the microstructural design of advanced high strength steels via optimization of the ultrafast heating process. Therefore, the main aim of this work is to study the effect of soaking time on the microstructure and properties of the individual microconstituents, as well as to link them to the properties of the low carbon steel at the macro-scale.

2. Material and experimental procedures

2.1. Material

The chemical composition of the low carbon steel selected for this investigation is shown in Table 1. Alloys with this composition are typically used in the automotive sector as transformation induced plasticity (TRIP) assisted steels. The material was supplied in the form of 50% cold rolled sheets with a thickness of 1 mm having a ferritic-pearlitic microstructure which consists of 76% of ferrite and 24% of pearlite.

2.2. Intercritical heat treatment

The material was subjected to different heat treatments using a thermo-mechanical simulator Gleeble 3800. Strips of 100 mm in length and 10 mm in width were machined along the rolling direction of the cold rolled sheet. A *K*-type thermocouple was spot-welded to the mid-section of each strip. Two different types of heat treatment were applied. In both types, the thermal cycle was divided into five stages. In the first and second stages, the specimens were heated at 10 °C/s to 300 °C, followed by a soaking period at 300 °C for 30 s. These stages simulate a preheating in some industrial continuous annealing lines to reduce the thermal stresses before heat treatment. The third stage is heating from 300 °C to the intercritical peak temperature of 860 °C at two different heating rates: 10 °C/s (conventional heating or CH) and 800 °C/s (ultra-fast heating or UFH) followed by soaking at 860 °C for 0.2 s. The processed specimens will be referred to as CH10-0.2s and UFH800-0.2s, respectively. Such a short soaking time (0.2 s) allows eliminating the effect of annealing time on the microstructure and mechanical properties, and to study entirely the effect of heating rate. The last stage was rapid cooling of the material to room temperature at ~300 °C/s, which is well above the critical cooling rate [23].

To study the effect of soaking time at the peak temperature, additional heat treatments with longer soaking time (1.5 s and 30 s) were performed for both CH and UFH. These conditions are referred to as CH10-1.5s and CH10-30s for the CH treatment, and UFH800-1.5s and UFH800-30s for the UFH treatment. In all samples, a minimum length of 10 mm of the homogeneously heat treated zone was verified by hardness measurements.

Table 1
Chemical composition of the studied material (wt. %).

C	Mn	Al	Si
0.19	1.61	1.06	0.50

2.3. Microstructural characterization

Microstructural characterization of the heat treated samples was performed through scanning electron microscopy (SEM) and electron backscatter diffraction (EBSD) analysis. Specimens were ground and polished to a mirror-like surface applying standard metallographic techniques with final polishing using OP-U (colloidal silica). For SEM characterization, polished specimens were etched with 3 vol% nital solution for ~10 s. The EBSD studies were performed using a FEI Quanta™ Helios NanoLab 600i equipped with a NordlysNano detector controlled by the AZtec Oxford Instruments Nanoanalysis (version 2.4) software. The data were acquired at an accelerating voltage of 18 kV, a working distance of 8 mm, a tilt angle of 70°, and a step size of 65 nm in a hexagonal scan grid. The orientation data were post-processed using HKL Post-processing Oxford Instruments Nanotechnology (version 5.1©) software and TSL Data analysis version 7.3 software. Grains were defined as a minimum of 4 pixels with a misorientation ≥ 5°. Grain boundaries having a misorientation ≥ 15° were defined as high-angle grain boundaries (HAGBs), whereas low-angle grain boundaries (LAGBs) had a misorientation < 15°. The volume fractions of transformed/untransformed grains and recrystallized/recovered ferritic grains were determined by a two-step partitioning procedure described in Ref. [24]. In this procedure, grains with high and low grain average image qualities are separated in a first step, allowing to distinguish between transformed (martensite) and untransformed (ferrite) fractions. In the second step, recrystallized and non-recrystallized ferritic grains are separated using the grain orientation spread criterion: Grains with orientation spread below 1° are defined as the recrystallized grains, while grains with an orientation spread above 1° are defined as the non-recrystallized ones [25]. The density of geometrically necessary dislocations (GNDs) was calculated from the local misorientations following the procedure described in Ref. [26]. Microstructure was observed on the plane perpendicular to the sample transverse direction (the RD–ND plane).

For transmission Kikuchi diffraction (TKD) and transmission electron microscopy (TEM) studies, the samples were ground to a thickness of 100 μm and disks of 3 mm in diameter were subsequently punched out. The disks were further thinned in a Struers Tenupol-5 via twin-jet electropolishing until a central hole appeared. The used electrolyte was composed of 4% vol. $HClO_4$ in 63% water-diluted CH_3COOH under 21 V at 20 °C and a flow rate equal to 17 for this Struers device. TKD data were collected by an EDAX-TSL EBSD system attached to a FEI Quanta™ 450-FEG-SEM, under the following conditions: accelerating voltage of 30 kV, working distance of 4 mm, tilt angle of - 40°, a beam current of 2.3 nA corresponding to FEI spot and aperture sizes of 5 and 30 μm respectively. TKD measurements were performed with a step size of 10 nm. The orientation data were post-processed using TSL Data analysis version 7.3 software. TEM images were acquired in a JEOL (S)TEM JEM-2200FS operated at 200 kV and equipped with an aberration corrector of the objective lens (CETCOR, CEOS GmbH) and a column electron energy filter (omega type).

2.4. Mechanical characterization

Vickers hardness tests were performed on the RD–ND plane for all heat treated samples after metallographic preparation by grinding and polishing using 1 μm diamond paste. Tests were done using a square base pyramid shaped diamond mounted in a Shimadzu HMV Micro Hardness Tester, applying a load of 4.9 N.

Dog bone sub-size tensile samples were machined from the homogeneously heat treated zone of the processed strips. Tensile axis was parallel to the RD. The samples had a gauge length of 4 mm, a gauge width of 1 mm and a thickness of 1 mm. They were carefully ground and mechanically polished using OP-U (colloidal silica) at the final stage. Tensile tests were carried out at room temperature using a Kammrath&Weiss testing module equipped with a 1 kN load cell at a constant cross head speed corresponding to an initial strain rate of 10^{-3} s^{-1} until failure. At least three specimens were tested for each condition, and the results were found to be reproducible. It should be noted that a very thin (~15 μm) decarburized layer formed on the surface of all heat treated strips was removed before any mechanical testing.

Nanoindentation tests were performed on a HysitronTI950 Triboindenter using a diamond Berkovich tip on square areas having a size of ~10 × 10 μm^2, which were *a priori* analyzed by EBSD (as described in Section 2.3) to identify the individual microconstituents. At least ten areas were tested for each material's condition. In order to target specific phases/grains, these square areas were scanned prior to nanoindentation, using the scanning probe microscopy (SPM) mode of the instrument. Nanoindentation tests were carried out in displacement control mode at a constant strain rate ($\dot{\varepsilon} = \dot{h}/h$) of 0.07 s^{-1}, where h is the penetration depth and $\dot{h}$ the penetration rate of indenter. At least 20 indents were performed on each microconstituent at an imposed maximum depth of 150 nm. The nanohardness was determined from the analysis of the load–displacement curves using the Oliver and Pharr method [27].

3. Results

3.1. Microstructural characterization

3.1.1. SEM analysis

Fig. 1 shows the evolution of the microstructure with soaking time of the CH (Fig. 1a–c) and UFH (Fig. 1d–f) samples. All conditions exhibit a heterogeneous microstructure with martensitic grains embedded into a ferritic matrix. EBSD analysis showed that some retained austenite is also present (see Section 3.1.2). Qualitative analysis of the SEM images shows that the heating rate plays a key role in the formation of the final microstructure. There is no significant effect of the soaking time on the microstructure of the CH samples (Fig. 1a–c), while its effect becomes apparent in the UFH samples (Fig. 1d–f). The UFH treatment with soaking times of 0.2 and 1.5 s generates a heterogeneous ferritic matrix formed by a mixture of fine and coarse grains, which are dispersed in the microstructure (Fig. 1d and e). Spheroidized cementite is also observed caused by the short time of the heat treatment (see Fig. 1d). Soaking for 30 s leads to a more homogeneous microstructure of the matrix with no cementite particles (Fig. 1f). Generally, the CH treatment produces a more homogeneous microstructure compared to the UFH one. There is no variation of microstructure through the thickness of all heat treated strips.

3.1.2. EBSD analysis

EBSD was used for the quantitative characterization of the multiphase microstructure developed in the material after all heat treatments. The results are summarized in Table 2. The microstructure formed after CH processing is mainly composed by a ferritic matrix, martensite and retained austenite. The ferrite fraction does not vary with soaking time (~86–87%). The ferritic matrix is composed of recrystallized (Rx) and non-recrystallized (non-Rx) ferritic grains. The vast majority of ferrite present in the CH material is recrystallized. It's volume fraction remains nearly constant (~90–92%) independently on the soaking time. On the other hand, the volume fraction of martensite slightly increases with soaking time from 10.6% at 0.2 s to 12.5% after soaking for 30 s, while the retained austenite shows the opposite trend decreasing from 3.1% to 1.7%, respectively. The UFH treatment results in a similar microstructure, but the volume fraction of microconstituents greatly varies with soaking time. In the UFH samples, the volume fraction of ferrite decreases significantly with soaking time from ~91% after 0.2 s to ~76% after 30 s. Moreover, the morphology of the ferritic matrix also evolves during soaking. In the UFH-0.2s sample, the matrix is mainly composed of non-Rx ferritic grains (~52%), while Rx ferritic grains dominate in the matrix of the UFH-30s sample, and volume fraction of the non-Rx grains drops down to ~ 33%. On the contrary, the volume fraction of martensite tends to increase with soaking time from ~7% to ~22% after 30 s. During UFH treatment, the volume fraction of retained austenite remains constant independently on the soaking time. Hence, the decrease of ferrite volume fraction is directly linked to the formation of martensite.

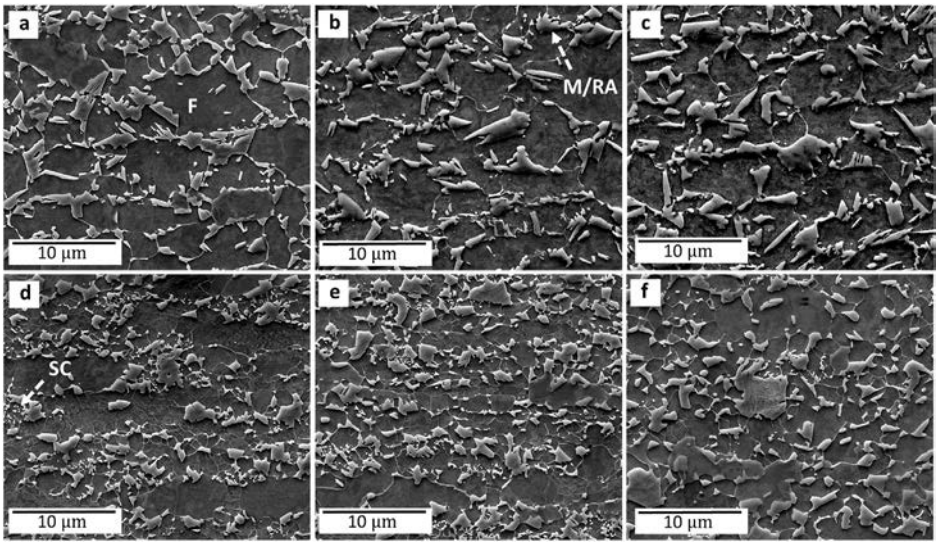

Fig. 1. SEM images showing the effect of heating rate (10 & 800 °C/s) and soaking time (0.2–30 s) on the microstructure: a), b) and c) correspond to 10 °C/s for 0.2, 1.5 and 30 s, respectively; d), e) and f) correspond to 800 °C/s for 0.2, 1.5 and 30 s, respectively. F: ferrite; M: martensite; RA: retained austenite; SC: spheroidized cementite.

Table 2
Effect of the heating rate and soaking time on the volume fraction of phases present in the studied material.

Heating rate	CH			UFH		
Soaking time (s)	0.2	1.5	30	0.2	1.5	30
Martensite (%)	10.6 ± 1.7	10.8 ± 1.6	12.5 ± 1.6	6.9 ± 3.2	12.6 ± 3.1	22.0 ± 3.0
Retained austenite (%)	3.1 ± 0.7	1.8 ± 0.6	1.7 ± 0.1	2.2 ± 0.4	2.1 ± 0.3	2.1 ± 1.9
Ferrite (%)	86.3 ± 2.4	87.4 ± 2.7	85.8 ± 1.6	90.9 ± 4.0	85.3 ± 2.8	75.9 ± 4.6
Rx ferrite	91.8 ± 2.0	90.3 ± 4.6	91.3 ± 4.7	48.4 ± 9.8	61.8 ± 13.0	67.2 ± 7.9
Non-Rx ferrite	8.2 ± 2.0	9.7 ± 4.6	8.7 ± 4.7	51.6 ± 9.8	38.2 ± 13.0	32.8 ± 7.9

Table 3
Hardness of the material in all studied conditions.

Heating rate	CH			UFH		
Soaking time (s)	0.2	1.5	30	0.2	1.5	30
Hardness (HV0.5)	241 ± 5	239 ± 6	264 ± 11	252 ± 4	245 ± 5	267 ± 10

3.2. Mechanical characterization

3.2.1. Macro-mechanical characterization

In order to characterize the mechanical properties of the steel after both heat treatments, hardness tests were performed for all studied conditions. Their outcomes are summarized in Table 3. It is seen that the UFH treatment leads to higher hardness values compared to the CH treatment for the given soaking time. The highest difference between CH and UFH is observed for 0.2 s, where the average hardness is 241 HV0.5 for the CH and 252 HV0.5 for the UFH conditions. This difference in average hardness is slightly reduced after 1.5 s soaking time (239 HV0.5 for CH versus 245 HV 0.5 for UFH), while soaking for 30 s results in similar hardness values, within error, for CH and UFH conditions, having average hardness values in the range of 264–267 HV 0.5.

In addition to the hardness tests, tensile tests of sub-size samples were performed for all studied conditions. The representative engineering stress - engineering strain curves are shown in Fig. 2. Data on mechanical properties determined from the engineering stress – engineering strain curves (0.2% proof strength $\sigma_{0.2}$, ultimate tensile strength σ_{UTS}, uniform elongation ε_u and elongation to failure ε_f) are listed in Table 4. It is seen that the UFH treatment leads to higher $\sigma_{0.2}$-values for any soaking time compared to the CH treatment. While after UFH treatments the $\sigma_{0.2}$-values are not affected by soaking time laying between 441 and 448 MPa, after CH treatments the $\sigma_{0.2}$ increases from 362 MPa after soaking for 0.2 s to 410 MPa after soaking for 30 s. Moreover, the UFH treatment leads to higher ultimate tensile strength compared to the CH treatment for the same soaking time. After soaking for 0.2 s, the σ_{UTS} is 926 MPa for the UFH sample, while it is 886 MPa for the CH counterpart. The difference in σ_{UTS} between treatments is reduced with increasing soaking time up to 1.5 s, where the UFH sample presents similar result as after 0.2 s, being 925 MPa, while σ_{UTS} in the CH sample increases to 900 MPa. Longer soaking time (30 s) induces a significant increase in the σ_{UTS} compared to the shorter soaking times for both CH and UFH being 960 and 1010 MPa, respectively.

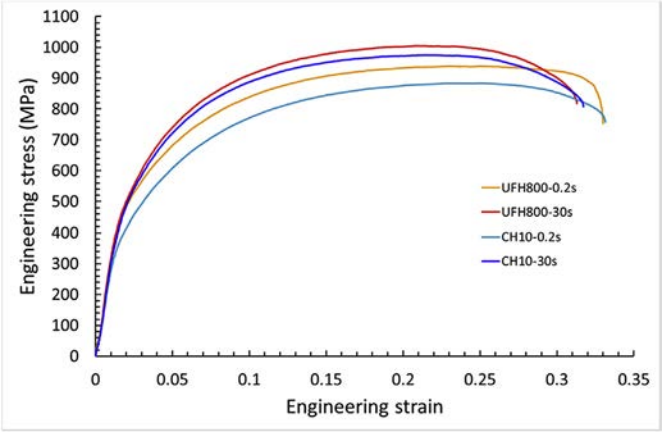

Fig. 2. Representative engineering stress – engineering strain curves for the CH and UFH samples after soaking for 0.2 and 30 s (For interpretation of the references to color in this figure, the reader is referred to the web version of this article).

3.2.2. Micro-mechanical characterization of individual microconstituents

In order to study the effect of the heating rate and soaking time on the mechanical properties of the individual microconstituents present in the material, nanoindentation tests on individual grains were performed. The individual microconstituents were determined *a priori* by EBSD analysis (Fig. 3a) and verified by SPM (Fig. 3b). The outcomes of the nanoindentation testing are summarized in Table 5. The nanohardness data are presented for ferrite and martensite. Retained austenite was not analyzed due to its low volume fraction and very small grain size (Table 2). Additionally, for the UFH samples, the nanohardness results for the ferritic matrix are presented separately for recrystallized (Rx) and non-recrystallized (non-Rx) ferritic grains. It should be mentioned that no nanohardness data are presented for non-Rx ferrite in the CH treated samples due to its low volume fraction (Table 2) that makes difficult to obtain reliable statistical data. The recrystallized ferritic grains present similar nanohardness between 2.6 and 2.8 GPa in all studied conditions. On the other hand, the UFH treatment leads to formation of the non-Rx ferrite with higher nanohardness compared to their recrystallized counterparts independently of the soaking time. The nanohardness of the non-Rx ferrite in the UFH sample does not vary with soaking time being in the range between 3.2 and 3.3 GPa. Martensitic grains showed the highest nanohardness in all studied conditions. In the UFH treated samples, martensite tends to soften with increasing soaking time. For a short soaking time (0.2 s) the martensite shows nanohardness of 7.6 GPa, which is reduced after longer soaking times to 7.4 GPa (after 1.5s) and finally to 6.1 GPa (after 30 s). On the other hand, evolution of the martensite hardness during CH treatment is ambiguous, having values of 8.1, 6.7 and 7.2 GPa for soaking times of 0.2, 1.5 and 30 s, respectively.

Two different types of mechanical response were observed on the nanoindentation curves (Fig. 3 c). While all load-depth curves from martensitic grains presented a continuous character, pop-ins were present in most of the curves from ferritic grains. Pop-ins are sudden penetration bursts during the loading segment of the test. Pop-ins might

Table 4
Tensile mechanical properties of the material in all studied conditions.

Heating rate	CH			UFH		
Soaking time (s)	0.2	1.5	30	0.2	1.5	30
$\sigma_{0.2}$	362 ± 1	391 ± 30	410 ± 3	444 ± 12	441 ± 8	448 ± 3
σ_{UTS}	886 ± 3	900 ± 28	960 ± 21	926 ± 20	925 ± 10	1010 ± 7
ε_u (%)	25 ± 1	21 ± 4	21 ± 1	24 ± 1	18 ± 2	21 ± 1
ε_f (%)	33 ± 1	31 ± 3	31 ± 2	33 ± 1	30 ± 2	29 ± 3

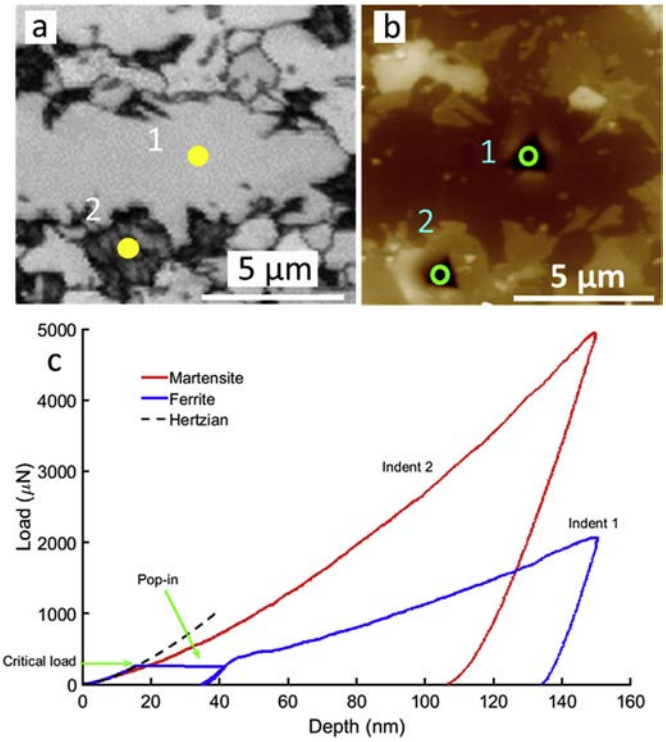

Fig. 3. a) Band slope EBSD map with marked spots (grains) for further nanoindentation; b) SPM image of the corresponding area with indents inside ferritic (1) and martensitic (2) grains; c) Representative load – depth curves for martensite (red), ferrite (blue) and Hertzian elastic contact solution (black). (For interpretation of the references to color in this figure, the reader is referred to the web version of this article).

have different origins but, in this case, are associated with a transition from an elastic to an elasto-plastic contact, that is typically encountered in crystals with a low dislocation density [22,28,29]. The lower the dislocation density, the larger the probability of indenting on a dislocation free volume and the larger the expected pop-in load. This is because, as proposed by Shim et al. [22], as the indenter penetrates, the stressed volume is enlarged, and so does the probability of finding a region which contains pre-existing dislocations, so that the indenter triggers their multiplication [30], thus generating the pop-in event.

Therefore, it becomes illustrative to analyze the range of pop-in loads observed in this case, as a signature of the dislocation density distribution in each phase. For this, we introduced a criterion of 3 nm as the minimum displacement discontinuity for identification of a pop-in Ref. [31]. In agreement with the hypothesis, pop-ins occurred in most of the Rx ferritic grains and in a slightly lower fraction of the non-Rx ones in all conditions. The results are plotted in Fig. 4. Fig. 4a represents the average pop-in load for Rx ferrite. It is seen that the pop-in load remains constant, with an average value of ~430 µN, in all cases. However, the standard deviation tends to decrease with soaking time for both heat treatments. On the other hand, Fig. 4b compares the pop-in load of Rx and non-Rx ferrite after the UFH treatment for different soaking times. In this case, the average pop-in load in the non-Rx grains is lower than the one measured in the Rx grains for any soaking time, but the difference is reduced with soaking time. It is interesting to note that the standard deviation in the non-Rx ferritic grains increases with soaking time, reaching similar values to the ones obtained for the Rx grains at 30 s.

4. Discussion

4.1. Microstructure – properties relationship in the UFH steel

The higher hardness measured in the steel after UFH treatment (Table 3) can be rationalized based on two factors. First, the suppression of recrystallization in ferrite during rapid heating [5,7,9,11,14,19] leads to a higher volume fraction of non-Rx ferrite, which shows higher nanohardness compared to the recrystallized one (Table 5) due its higher dislocation density. Second, rapid heating leads to reduced grain size compared to conventional treatments in low carbon steels [4,16,32] increasing the strength of the UFH treated material according to the Hall-Petch effect. However, the higher amount of martensite present in the CH material compared to the UFH one (Table 3) provides additional strengthening. A slight decrease of the average hardness in the UFH treated samples with increasing soaking time from 0.2 s to 1.5 s can also be noted, although the standard deviation is also higher. This outcome may be produced by the larger fraction of Rx ferrite and coarser grains compared to the UFH800-0.2s counterpart, but somewhat compensated by the higher martensite volume fraction. For longer soaking time (30 s), the hardness tends to increase in both CH and UFH samples (Table 3) as a result of the increased martensite fraction and the reduction of the ferritic volume fraction (Table 2). On the other hand, standard deviation is largely scattered, as indentations are greatly affected by the local microstructure within the plastic zone.

The growth in yield strength and ultimate tensile strength with soaking time observed in the CH samples (Table 4) can be associated with both the slight reduction in the Rx ferrite volume fraction and the

Table 5
Nanohardness values for ferritic (Rx and non-Rx) and martensitic grains.

Heating rate	CH			UFH		
Soaking time (s)	0.2	1.5	30	0.2	1.5	30
Rx ferrite (GPa)	2.7 ± 0.2	2.6 ± 0.2	2.7 ± 0.2	2.6 ± 0.1	2.6 ± 0.1	2.8 ± 0.2
Non-Rx Ferrite (GPa)				3.2 ± 0.2	3.1 ± 0.2	3.3 ± 0.3
Martensite (GPa)	8.1 ± 1.0	6.7 ± 1.4	7.2 ± 2.0	7.6 ± 2.4	7.4 ± 1.1	6.1 ± 1.0

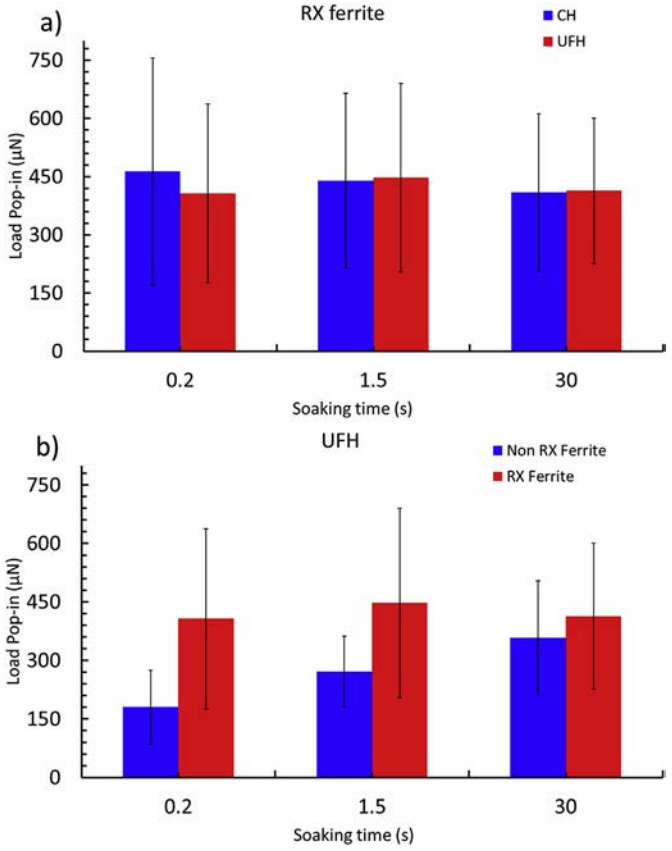

Fig. 4. a) Pop-in load for the Rx ferritic grains after CH (blue) and UFH (red) treatments for different soaking times (0.2, 1.5 and 30 s); b) Variation in pop-in load with soaking time for Rx and non-Rx ferritic grains after UFH treatment. Rx stands for 'recrystallized' (red), Non-Rx stands for 'non-recrystallized' (blue). (For interpretation of the references to color in this figure, the reader is referred to the web version of this article).

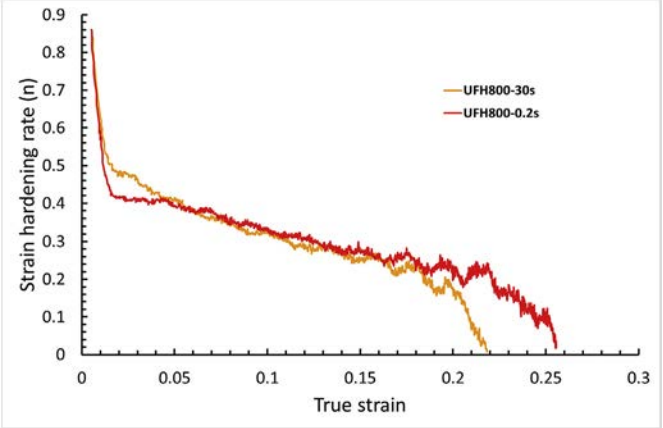

Fig. 5. Representative curve of strain hardening rate vs. true strain for UFH after soaking for 0.2 s (red) and 30 s (orange). (For interpretation of the references to color in this figure, the reader is referred to the web version of this article).

rise in the martensite fraction (Table 2). In the Rx ferritic grains, plastic deformation begins at an earlier stage than in the non-Rx ones due to their lower strength (Table 5). This rise of the yield and ultimate tensile strength occurs at the expense of ductility which is slightly reduced with soaking time. On the other hand, there is no significant effect of soaking time on yield strength for the UFH treated samples, although all cases present higher values compared to their CH counterparts. For short soaking times, the matrix is hardened due to the presence of a high fraction of non–Rx ferrite. The percentage of the non-Rx ferrite decreases with increasing soaking time. However, additional hardening due to the rise of martensite volume fraction compensates softening due to recrystallization [33]. The ultimate tensile strength is mainly dominated by the martensite volume fraction [34]. Nevertheless, the higher volume fraction of martensite does not affect greatly the ductility shown by the UFH treated material, as it is similar to that measured in the CH material. This effect is produced by the coarser microconstituents formed during UFH treatment, and by the lower carbon content present in the martensite, as it is seen from the nanohardness results (Table 5). It is well known that strength of martensite is related to the carbon content [33], and that the plastic deformation accommodated by the individual microconstituents is inversely proportional to their nanohardness [35] resulting in high ductility of the material.

The ductility of the material was also studied in terms of the strain hardening behavior of the UFH material. In order to analyze the work hardening behavior of the UFH samples, the common power-law relationship (1) from Ref. [36].

$$\sigma = k\varepsilon^n \tag{1}$$

was derived to calculate the strain hardening rate (n) using the following equation (2)

$$n = \frac{\ln \frac{\sigma_a}{\sigma_{a-1}}}{\ln \frac{\varepsilon_a}{\varepsilon_{a-1}}} \tag{2}$$

where σ_a and ε_a represents the true stress and true strain in the point *a*, respectively.

Fig. 5 presents the strain hardening behavior with true strain in the UFH samples after soaking for 0.2 s and 30 s. It is seen that at low strains (< 0.05), the UFH800-0.2s sample shows a lower strain hardening rate compared to the UFH800-30s counterpart. This effect can be produced by the higher volume fraction of ferrite formed after soaking for 0.2 s in contrast to soaking for 30 s, which has a higher martensite fraction, requiring a lower stress for the onset of plastic deformation in the ferritic matrix. However, for higher strains, where work hardening is crucial to suppress necking [37], the strain hardening coefficient decreases faster in the sample soaked for 30 s in comparison with that soaked for 0.2 s. This can be caused by the presence of a ferritic matrix mainly composed of Rx ferrite in the UFH800-30s, contrary to the 0.2 s sample, where the non-Rx ferrite dominates in the matrix (Table 2). The non-Rx ferrite presents a substructure, and it is harder than the Rx ferrite, as it is seen from the nanoindentation results (Table 5), thus increasing the strain hardening of the UFH800-2s material. However, the difference between both conditions is somehow reduced due to the presence of martensite in the UFH800-30s. As was reported by Refs. [38,39], martensite islands embedded into the ferritic matrix intensify plastic deformation in the surrounding ferrite, contributing to an increase in the strain hardening of the matrix.

4.2. Effect of the UFH processing on the micro-mechanical response of individual microconstituents

The UFH processing with short soaking time (0.2 s) gives a short time for austenite to nucleate and grow. Therefore, a lower martensite fraction is formed after quenching in comparison to the longer soaking periods (1.5 s and 30 s) (Table 2). As the solubility of carbon in ferrite is very low [40], the martensite present in the UFH800-0.2s samples is enriched in carbon. Thus, the high nanohardness observed in martensite (Table 5) formed in the UFH sample soaked for 0.2 s can be attributed to its high carbon concentration, as martensite hardness strongly depends on the carbon content [41] and dislocation density [42]. The martensite nanohardness tends to decrease with soaking time as a consequence of the homogenization of carbon inside the austenitic grains during intercritical annealing and, thus, in martensitic grains

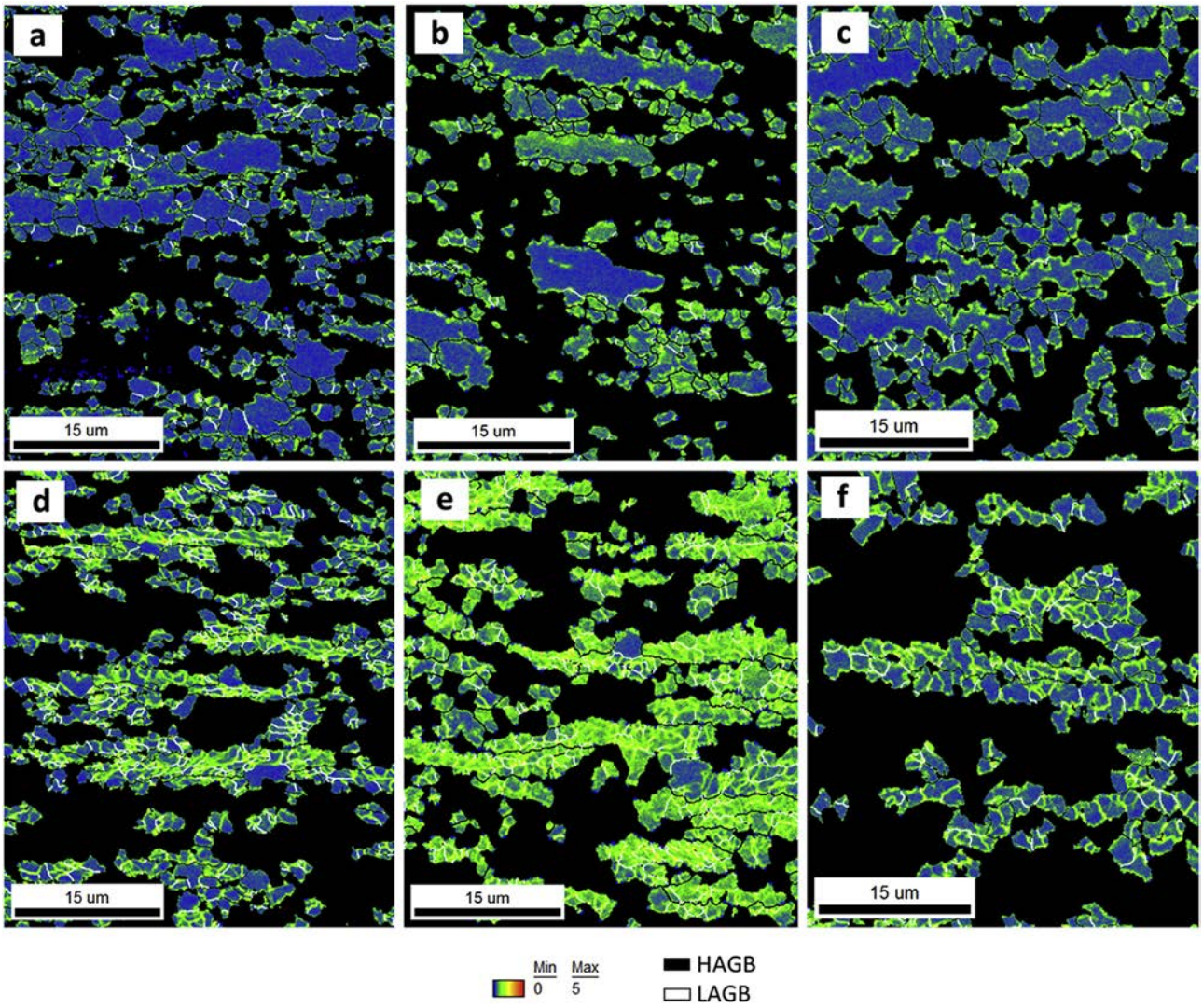

Fig. 6. The KAM maps for the sample after UFH treatment showing the Rx (a, b & c) and non-Rx (d, e & f) ferrite after 0.2 s, 1.5 s and 30 s, respectively. The HAGBs are shown in black and LAGBs in white. (For interpretation of the references to color in this figure, the reader is referred to the web version of this article).

formed therefrom during quenching. Similar results were reported for *Quenching & Partitioning* steels in Ref. [43]. However, the standard deviation of nanohardness in the UFH sample soaked for 0.2 s (± 2.4 GPa) was higher than in the samples soaked for 1.5 s (± 1.1 GPa) or 30 s (± 1.0 GPa). This may be associated with the much shorter time at high temperatures, which shortens the diffusion distance for carbon atoms [19], leading to deviations in the local carbon concentration in different austenitic grains as well as in their interior. The standard deviation tends to decrease from ± 1.1 GPa after soaking for 1.5 s to ± 1.0 GPa after soaking for 30 s. However, this high scatter in the standard deviation of both samples is mainly caused by the growth of some austenitic grains during soaking at peak temperature, which are transformed into martensite during quenching, producing fine martensitic grains enriched with carbon and larger martensitic grains with lower carbon content. In the CH samples, short soaking time (0.2 s) leads to a harder martensite compared to the longer soaking time, which can be attributed to the higher carbon concentration present in fine grains, as in the case of the UFH material. It should be noted that in this case, standard deviation increases with soaking time as a consequence of the intense growth of some austenite grains during soaking, which transform into martensite during the cooling stage, as it was shown in our recent work [13].

Variation of soaking time during UFH treatment also modifies the ferritic matrix and its dislocation structure. The Rx ferrite formed after both CH and UFH treatments presents low orientation gradients within individual grains and, therefore, low strain heterogeneities, as it can be seen from the kernel average misorientation (KAM) maps on Fig. 6. All KAM maps were calculated for the 3rd nearest neighbor, and 5° of upper limit with an accuracy of the used EBSD system better that 0.5°. On the other hand, the non-Rx ferrite presents much higher misorientations (2-3°) compared to its Rx counterparts (0-1°) for any soaking time. The higher misorientations in the non-Rx ferritic grains are associated with the residual strains and geometrically necessary dislocations (GNDs) [44,45] which result in a higher nanohardness compared to the Rx grains (Table 5). The KAM maps of the Rx ferritic grains formed after CH treatment are similar to those for the Rx grains observed for the UFH one, as shown in Fig. 6a–c.

These results confirm the interpretation of the variations in pop-in load with soaking time found in the nanoindentation curves of the ferritic matrix, as presented in section 3.2.2. In agreement with the expectations, the average and the dispersion of pop-in loads show a correlation with the morphology of ferrite. The pop-ins in the Rx ferrite appear at similar loads independently on the heating rate or soaking time, with only a slight reduction in dispersion with soaking time. In contrast, in the non-Rx ferrite, the pop-in loads are substantially smaller, indicative of a higher dislocation density, and increase

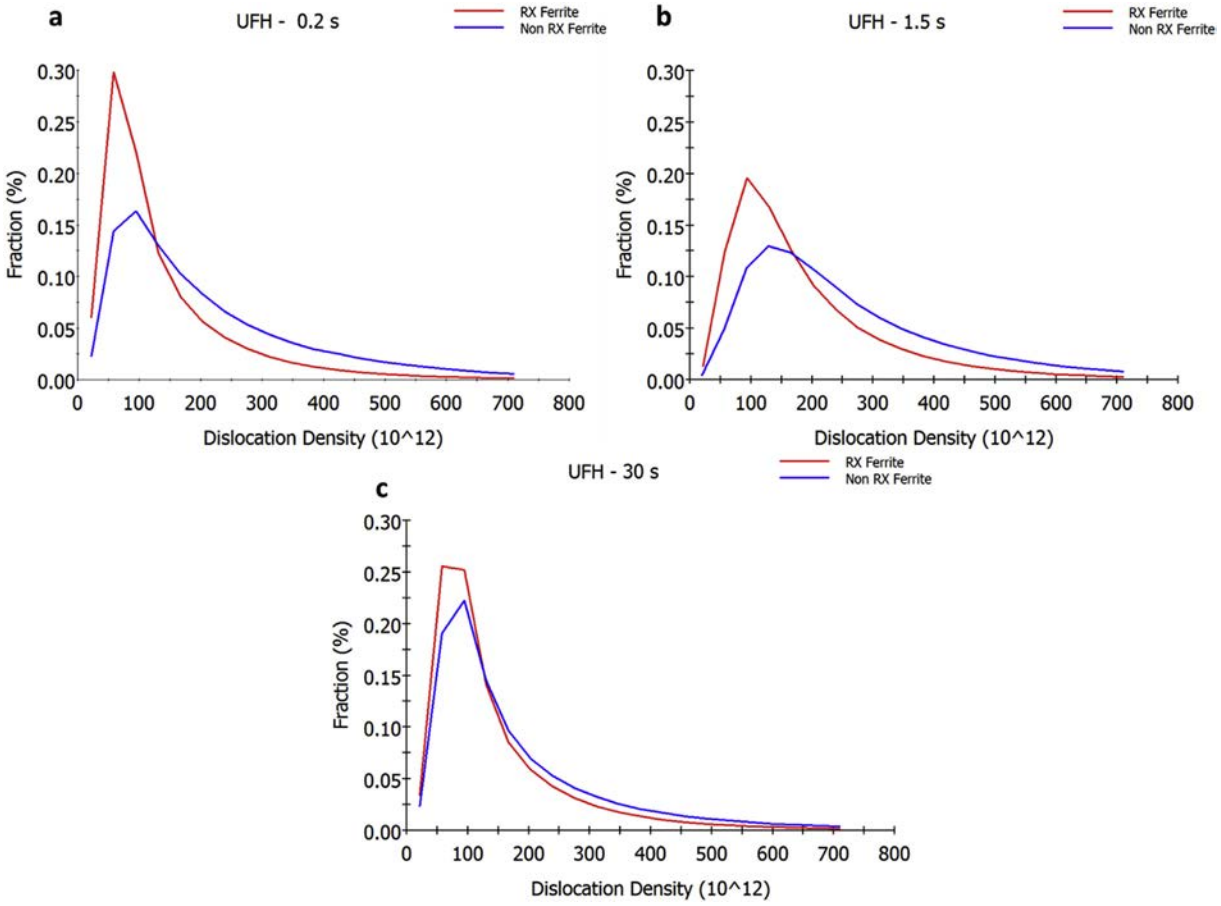

Fig. 7. a, b & c) Evolution of the GND density for Rx (in red) and non-Rx (in blue) ferrite during UFH treatment after soaking for 0.2, 1.5 and 30 s, respectively. (For interpretation of the references to color in this figure, the reader is referred to the web version of this article).

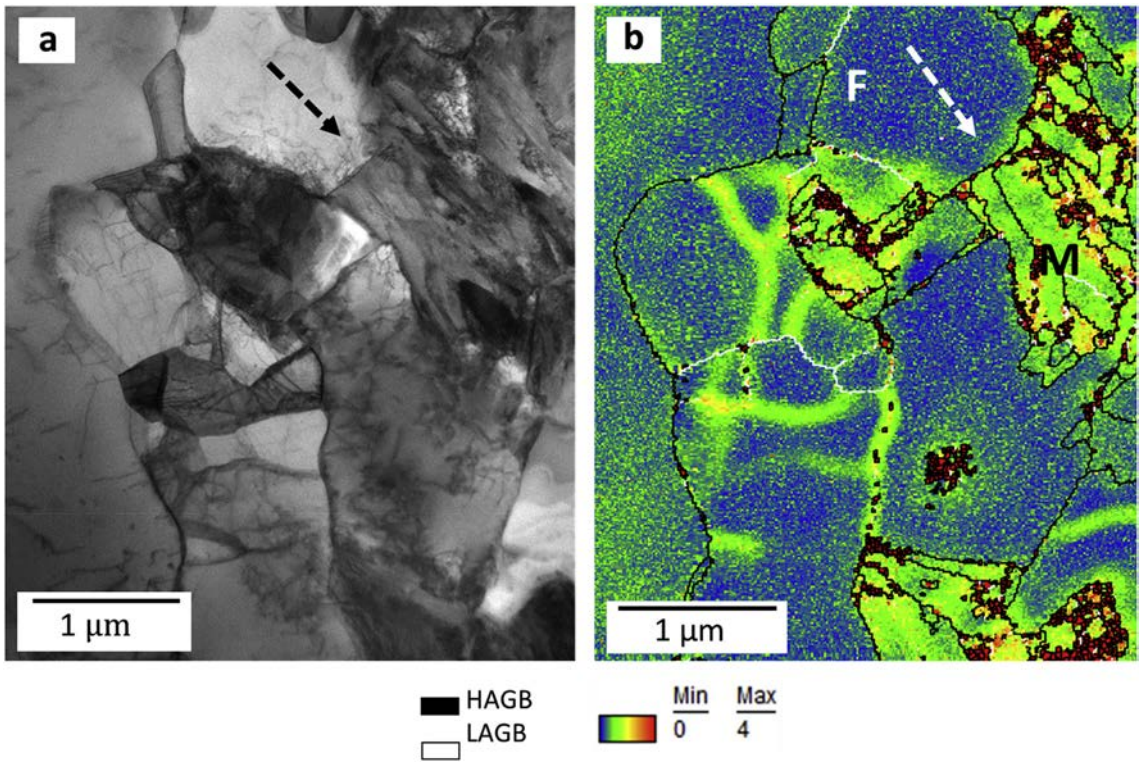

Fig. 8. a) TEM image after UFH treatment for 0.2 s; b) KAM map of the same area obtained from the TKD analysis. The EBSD map gives an idea for the sensitivity of the TKD to determination of the dislocation density. F indicates ferrite, whereas M refers to martensite.

significantly with soaking time (Fig. 4). The value for a 30 s soaking time is similar to that of the Rx grains (Table 5), indicating a reduction in dislocation density during annealing to levels similar to the Rx grains.

The presence of higher dislocation density in the non-Rx ferrite compared to the Rx counterpart is confirmed by the GND density obtained from EBSD analysis (Fig. 7), being $\sim 1.5–3{\cdot}10^{14}\,m^{-2}$ and $\sim 0.5–1{\cdot}10^{14}\,m^{-2}$, respectively. The density of GNDs is calculated from the local misorientations following the method described by Field et al. [26], with an imposed maximum misorientation equal to 5°. The analysis also confirms that the difference in GND density between Rx and non-Rx ferrite decreases with increasing soaking time. After soaking for 30 s, annihilation of dislocations during the recovery stage is almost complete, and the dislocation substructure is formed mainly from subgrains with misorientation between 5 and 15°, which are not detected by KAM mapping, resulting in similar dislocation density in recrystallized and recovered grains.

It should be noted that austenite-martensite phase transformation during quenching can also introduce dislocations into Rx and non-Rx ferrite due to local volume expansion of martensite, which has to be accommodated by the ferritic matrix. This is clearly illustrated in Fig. 8, where dislocations (marked by arrow) are generated in the interior of recrystallized ferritic grain (marked by F in Fig. 8 b) near ferrite/martensite interface due to local micro-deformation induced by austenite-martensite phase transformation (marked by M in Fig. 8b). These dislocations also reduce the dislocation free volume and might affect the nano-mechanical response of the given ferritic grain.

4.3. General recipe for microstructural design in low carbon steels via ultrafast heating

The present work shows that the correct balance of the heat treatment parameters can activate and make all strengthening mechanisms in the steel operate in such a way as to obtain an excellent combination of strength and ductility. The size and distribution of the martensitic phase plays a very important role. At a fixed volume fraction, fine martensite grains are more beneficial for improvement of mechanical strength and ductility retention, than the coarse martensitic grains formed after the CH treatment. First, the small martensite grains have a higher hardness than the coarse ones due to their higher carbon content, as demonstrated by nanoindentation (see Section 3.2.2). Second, they also provide a higher particle strengthening effect [46]. Fine martensite grains can be generated via refining the initial ferritic-pearlitic microstructure in the low carbon steel before ultrafast heating, and using a shorter soaking time (~1 s), which suppresses the growth of austenitic grains at the intercritical temperature. Significant attention should be paid to the ratio of recrystallized/recovered grains in the ferritic matrix. The optimum volume fraction of recrystallized ferrite in the matrix is ~50–60%, due to the following reasons. First, the non-recrystallized ferrite provides additional strengthening effect due to its enhanced mechanical strength arising from its higher dislocation density. Second, it plays a stabilizing role in the strain-hardening process, thus delaying localization of plastic deformation and necking, i.e. improving the overall ductility of the material. In the studied material, such ratios of recrystallized/recovered ferritic grains are also achieved after short soaking time (~1 s), while higher soaking time (> 10 s) dramatically increase the fraction of recrystallized ferrite grains.

5. Conclusions

The effect of heating rate (10 °C/s and 800 °C/s) and soaking time (0.2 s–30 s) on the mechanical behavior of low carbon steel was studied at the macro- and micro-scales and related to the microstructural evolution. The following conclusions can be drawn.

1) The UFH treated steel shows a higher mechanical strength with somewhat lower ductility compared to the CH treated counterparts, independently of the soaking time at the peak temperature. Soaking time does not affect yield strength of the UFH treated material, whereas its ultimate tensile strength increases with soaking time. In the CH treated material, yield and ultimate tensile strength tend to increase with soaking time. This dependence is determined by the evolution of the volume fraction and carbon content of martensite, the ratio of recovered and recrystallized ferrite, and the size of the microconstituents.
2) In all the studied conditions, the martensite grains show the highest nanohardness followed by recovered ferrite and recrystallized ferrite. The nanohardness of the martensite grains depends on the applied heat treatment parameters and appears to be inversely proportional to their volume fraction, as the latter defines the local carbon concentration due to very low solubility of carbon in the ferritic matrix.
3) Two different types of nanomechanical response is shown by the ferritic matrix. The vast majority of recrystallized ferrite grains demonstrated pop-ins on the nanoindentation curves, while recovered ferrite grains are less prone to show such behavior. Correlation with the density of GNDs in ferrite as a function of processing parameters indicate that the pop-in load correlates directly with the dislocation density, i.e., the lower the dislocation density, the bigger the probability of encountering a bigger dislocation free volume under the indenter tip and a higher the pop-in load is required to trigger plasticity. As a result, recrystallized ferrite shows a higher range of pop-in loads in comparison with the non-recrystallized ferrite, with a difference that reduces with soaking time due to recovery of the non-recrystallized ferrite.
4. Recovered ferrite shows higher nanohardness compared to the recrystallized ferrite due to its higher dislocation density. The matrix condition significantly affects the yield strength of the material. A high fraction of harder non-recrystallized ferritic grains increases the yield strength and slightly reduces the work hardening ability of the material.

Data availability

The raw/processed data required to reproduce these findings cannot be shared at this time as the data also forms part of an ongoing study.

Acknowledgements

MAVT acknowledges gratefully the financial support by IMDEA Innovation Award. MAM, JMMA and IS would like to acknowledge MAT4.0-CM project funded by Madrid region under programme S2018/NMT-4381.

Appendix A. Supplementary data

Supplementary data to this article can be found online at https://doi.org/10.1016/j.msea.2019.138276.

References

[1] J. Galán, L. Samek, P. Verleysen, K. Verbeken, Y. Houbaert, Advanced high strength steels for automotive industry, Rev. Metal. (Madr.) 48 (2012) 118–131, https://doi.org/10.3989/revmetalm.1158.
[2] T.E. steel Organization, Eurofer: annual report 2017, http://www.eurofer.org/News&Events/PublicationsLinksList/201705-AnnualReport.pdf, (2017).
[3] T. Lolla, G. Cola, B. Narayanan, B. Alexandrov, S.S. Babu, Development of rapid heating and cooling (flash processing) process to produce advanced high strength steel microstructures, Mater. Sci. Technol. 27 (2011) 863–875, https://doi.org/10.1179/174328409x433813.
[4] R.H. Petrov, J. Sidor, L.A.I. Kestens, Texture formation in high strength low alloy steel reheated with ultrafast heating rates, Mater. Sci. Forum 702–703 (2012) 798–801 https://doi.org/10.4028/www.scientific.net/MSF.702-703.798.
[5] F.M. Castro Cerda, I. Sabirov, C. Goulas, J. Sietsma, A. Monsalve, R.H. Petrov, Austenite formation in 0.2% C and 0.45% C steels under conventional and ultrafast

heating, Mater. Des. 116 (2017) 448–460, https://doi.org/10.1016/j.matdes.2016.12.009.
[6] http://www.flashbainite.com/, (n.d.).
[7] F.M. Castro Cerda, C. Goulas, I. Sabirov, L.A.I. Kestens, R.H. Petrov, The effect of the pre-heating stage on the microstructure and texture of a cold rolled FeCMnAlSi steel under conventional and ultrafast heating, Mater. Char. 130 (2017) 188–197, https://doi.org/10.1016/j.matchar.2017.06.010.
[8] F.M. Castro Cerda, L.A.I. Kestens, A. Monsalve, R.H. Petrov, The effect of ultrafast heating in cold-rolled low carbon Steel : recrystallization and texture evolution, Metals 6 (2016) 288–299, https://doi.org/10.3390/met6110288.
[9] F.M. Castro Cerda, F. Vercruysse, T.N. Minh, L.A.I. Kestens, A. Monsalve, R.H. Petrov, The effect of heating rate on the recrystallization behavior in cold rolled ultra low carbon steel, Steel Res. 87 (2016) 1–9, https://doi.org/10.1002/srin.201600351.
[10] D. De Knijf, A. Puype, C. Föjer, R.H. Petrov, The influence of ultra-fast annealing prior to quenching and partitioning on the microstructure and mechanical properties, Mater. Sci. Eng. A 627 (2015) 182–190, https://doi.org/10.1016/j.msea.2014.12.118.
[11] M. Ferry, D. Muljoni, D.P. Dunne, Recrystallization kinetics of low and ultra low carbon steels during high-rate annealing, ISIJ Int. 41 (2001) 1053–1060, https://doi.org/10.2355/isijinternational.41.1053.
[12] D. Muljono, M. Ferry, D.P. Dunne, Influence of heating rate on anisothermal recrystallization in low and ultra-low carbon steels, Mater. Sci. Eng. A 303 (2001) 90–99, https://doi.org/10.1016/S0921-5093(00)01882-7.
[13] M.A. Valdes-Tabernero, C. Celada-Casero, I. Sabirov, A. Kumar, R.H. Petrov, The effect of heating rate and soaking time on microstructure of an advanced high strength steel, Mater. Char. 155 (2019) 109822, https://doi.org/10.1016/j.matchar.2019.109822.
[14] M.A. Valdes-Tabernero, F. Vercruysse, I. Sabirov, R.H. Petrov, M.A. Monclus, J.M. Molina-Aldareguia, Effect of ultrafast heating on the properties of the microconstituents in a low-carbon steel, Metall. Mater. Trans. A 49 (2018) 3145–3150, https://doi.org/10.1007/s11661-018-4658-4.
[15] F. Vercruysse, Third Generation Advanced High Strength Steel by Ultrafast Annealing, University of Ghent, 2016.
[16] V. Massardier, A. Ngansop, D. Fabrègue, S. Cazottes, J. Merlin, Ultra-rapid intercritical annealing to improve deep drawability of low-carbon, al-killed steels, Metall. Mater. Trans. A 43 (2012) 2225–2236, https://doi.org/10.1007/s11661-012-1096-6.
[17] V. Massardier, A. Ngansop, D. Fabrègue, J. Merlin, J. Capelle, F.V. Cedex, Microstructure and mechanical properties of low carbon Al-killed steels after ultra-rapid annealing cycles, Mater. Sci. Forum 642 (2010) 3368–3373 https://doi.org/10.4028/www.scientific.net/MSF.638-642.3368.
[18] A. Puype, R.H. Petrov, D. De Knijf, J. Sidor, V. Vanroose, Developing of Advanced High Strength Steel via Ultrafast Annealing, University of Ghent, 2014.
[19] F.M. Castro Cerda, C. Goulas, I. Sabirov, S. Papaefthymiou, A. Monsalve, R.H. Petrov, Microstructure, texture and mechanical properties in a low carbon steel after ultrafast heating, Mater. Sci. Eng. A 672 (2016) 108–120, https://doi.org/10.1016/j.msea.2016.06.056.
[20] Q. Meng, J. Li, H. Zheng, High-efficiency fast-heating annealing of a cold-rolled dual-phase steel, Mater. Des. 58 (2014) 194–197, https://doi.org/10.1016/j.matdes.2014.01.055.
[21] N. Fonstein, Advanced High Strength Sheet Steels: Physical Metallurgy, Design, Processing, and Properties, Springer, 2015, https://doi.org/10.1007/978-3-319-19165-2.
[22] S. Shim, H. Bei, E.P. George, G.M. Pharr, A different type of indentation size effect, Scr. Mater. 59 (2008) 1095–1098, https://doi.org/10.1016/j.scriptamat.2008.07.026.
[23] F.M. Castro Cerda, Third Generation High Strength Steels via Ultrafast Heating, Ghent University, 2017.
[24] R.H. Petrov, L.A.I. Kestens, Advanced High-Strength Steels: Electron Backscatter Diffraction (EBSD), Encycl. Iron, Steel, Their Alloy, (2015), pp. 46–69, https://doi.org/10.1081/E-EISA-120050786.
[25] Y. Cao, H. Di, J. Zhang, J. Zhang, T. Ma, R.D.K. Mishra, An electron backscattered diffraction study on the dynamic recrystallization behavior of a nickel – chromium alloy (800H) during hot deformation, Mater. Sci. Eng. A 585 (2013) 71–85, https://doi.org/10.1016/j.msea.2013.07.037.
[26] D.P. Field, P.B. Trivedi, S.I. Wright, M. Kumar, Analysis of local orientation gradients in deformed single crystals, Ultramicroscopy 103 (2005) 33–39, https://doi.org/10.1016/j.ultramic.2004.11.016.
[27] W.C. Oliver, G.M. Pharr, An improved technique for determining hardness and elastic modulus using load and displacement sensing indentation experiments, J. Mater. Res. 7 (1992) 1564–1583, https://doi.org/10.1557/JMR.1992.1564.
[28] A.M. Minor, S.A. Syed Asif, Z. Shan, E.A. Stach, E. Cyrankowski, T.J. Wyrobek, O.L. Warren, A new view of the onset of plasticity during the nanoindentation of aluminium, Nat. Mater. 5 (2006) 697–702, https://doi.org/10.1038/nmat1714.
[29] T. Ohmura, K. Tsuzaki, F. Yin, Nanoindentation-induced deformation behavior in the vicinity of single grain boundary of interstitial-free steel, Mater. Trans. 46 (2005) 2026–2029, https://doi.org/10.2320/matertrans.46.2026.
[30] S.A. Syed Asif, J.B. Pethica, Nanoindentation creep of single- crystal tungsten and gallium arsenide, Philos. Mag. A 76 (1997) 1105–1118, https://doi.org/10.1080/01418619708214217.
[31] T.-H. Ahn, C.S. Oh, K. Lee, E.P. George, H.N. Han, Relationship between yield point phenomena and the nanoindentation pop-in behavior of steel, J. Mater. Res. 27 (2011) 39–44, https://doi.org/10.1557/jmr.2011.208.
[32] R.H. Petrov, J. Sidor, W.J. Kaluba, L.A.I. Kestens, Grain refinement of a cold rolled TRIP assisted steel after ultra short annealing, Mater. Sci. Forum 715–716 (2012) 661–666 https://doi.org/10.4028/www.scientific.net/MSF.715-716.661.
[33] G. Krauss, Martensite in steel : strength and structure, Mater. Sci. Eng. A 273–275 (1999) 40–57, https://doi.org/10.1016/S0921-5093(99)00288-9.
[34] H.-C. Chen, G.-W. Cheng, Effect of martensite strength on the tensile strength of dual phase steels, J. Mat. 24 (1994) 1991–1994, https://doi.org/10.1007/BF02385411.
[35] I. De Diego-Calderón, M.J. Santofimia, J.M. Molina-Aldareguia, M.A. Monclús, I. Sabirov, Deformation behavior of a high strength multiphase steel at macro- and micro-scales, Mater. Sci. Eng. A (2014), https://doi.org/10.1016/j.msea.2014.05.068.
[36] G.E. Dieter, Mechanical Metallurgy.Pdf, second ed., (1988) Ney York.
[37] J. Chiang, B. Lawrence, J.D. Boyd, A.K. Pilkey, Effect of microstructure on retained austenite stability and work hardening of TRIP steels, Mater. Sci. Eng. A 528 (2011) 4516–4521, https://doi.org/10.1016/j.msea.2011.02.032.
[38] I.B. Timokhina, P.D. Hodgson, E.V. Pereloma, Effect of microstructure on the stability of retained austenite in transformation-induced-plasticity steels, Metall. Mater. Trans. A 35 (2004) 2331–2341, https://doi.org/10.1007/s11661-006-0213-9.
[39] N.C. Goel, S. Sangal, K. Tangri, A theoretical model for the flow behavior of commercial dual-phase steels containing metastable retained Austenite : Part I . Derivation of flow curve equations, Metall. Trans. A. 16 (2013) 2013–2021, https://doi.org/10.1007/BF02662402.
[40] H.K.D.H. Bhadeshia, R.W.K. Honeycombe, Steels: Microstructure and Properties, third ed., Elsevier Ltd, Oxford, n.d.
[41] B. Hutchinson, J. Hagström, O. Karlsson, D. Lindell, M. Tornberg, F. Lindberg, M. Thuvander, Microstructures and hardness of as-quenched martensites (0.1–0.5%C), Acta Mater. 59 (2011) 5845–5858, https://doi.org/10.1016/j.actamat.2011.05.061.
[42] Q. Furnemont, M. Kempf, P.J. Jacques, M. Göken, F. Delannay, On the measurement of the nanohardness of the constitutive phases of TRIP-assisted multiphase steels, Mater. Sci. Eng. A 328 (2002) 26–32, https://doi.org/10.1016/S0921-5093(01)01689-6.
[43] J. Hidalgo, K.O. Findley, M.J. Santofimia, Thermal and mechanical stability of retained austenite surrounded by martensite with di ff erent degrees of tempering, Mater. Sci. Eng. A 690 (2017) 337–347, https://doi.org/10.1016/j.msea.2017.03.017.
[44] M. Calcagnotto, D. Ponge, E. Demir, D. Raabe, Orientation gradients and geometrically necessary dislocations in ultrafine grained dual-phase steels studied by 2D and 3D EBSD, Mater. Sci. Eng. A 527 (2010) 2738–2746, https://doi.org/10.1016/j.msea.2010.01.004.
[45] D.A. Hughes, N. Hansen, D.J. Bammann, Geometrically necessary boundaries , incidental dislocation boundaries and geometrically necessary dislocations, Scr. Mater. 48 (2003) 147–153, https://doi.org/10.1016/S1359-6462(02)00358-5.
[46] T.W. Clyne, P.J. Withers, An Introduction to Metal Matrix Composites, first ed., Cambridge University Press, The Pitt Building, Trumpington Street, Cambridge, 1993, https://doi.org/10.1017/CBO9780511623080.

4.4. The sensitivity of the microstructure and properties to the peak temperature in an ultrafast heat treated low carbon-steel

M.A. Valdés-Tabernero*, A. Kumar, R.H. Petrov, M.A. Monclús, J.M. Molina-Aldareguia, I. Sabirov, *Materials Science and Engineering A* 776 (2020) 138999.

DOI: https://doi.org/10.1016/j.msea.2020.138999

Materials Science & Engineering A 776 (2020) 138999

Contents lists available at ScienceDirect

Materials Science & Engineering A

journal homepage: http://www.elsevier.com/locate/msea

The sensitivity of the microstructure and properties to the peak temperature in an ultrafast heat treated low carbon-steel

M.A. Valdes-Tabernero [a,*], A. Kumar [b], R.H. Petrov [b,c], M.A. Monclus [a], J.M. Molina-Aldareguia [a], I. Sabirov [a]

[a] IMDEA Materials Institute, Calle Eric Kandel 2, Getafe, 28906, Madrid, Spain
[b] Department of Materials Science and Engineering, Delft University of Technology, Mekelweg 2, 2628CD, Delft, the Netherlands
[c] Department of Electrical Energy, Metals, Mechanical Constructions & Systems, Ghent University, Technologiepark 46, 9052, Ghent, Belgium

ARTICLE INFO

Keywords:
Metals and alloys
Ultrafast heating
Phase transitions
Scanning electron microscopy
SEM
Nanoindentation

ABSTRACT

In this work, we investigate the sensitivity of the microstructure and mechanical properties of an ultrafast heat treated low carbon-steel to the peak temperature. In all studied cases, the steel was heated within the intercritical temperature range (i.e. between the A_{C1} and A_{C3} temperatures). Both the peak temperature and soaking time were varied, and their effect on the size, the fraction of individual microstructural constituents and their tensile mechanical response were investigated. It is shown that the increasing peak temperature and soaking time promote austenite formation and recrystallization processes in the ferritic matrix. The highest nanohardness is shown by martensitic grains, while recovered ferrite demonstrated slightly higher nanohardness compared to recrystallized ferrite. The applied heat treatment parameters have a strong effect on the nanohardness of martensite, whereas the nanohardness of ferrite microconstituents is not sensitive to variations of peak temperature and soaking time. The non-recrystallized ferrite is harder than its recrystallized counterpart due to the higher dislocation density of the former. Increasing peak temperatures promote strengthening in the material at the expense of its ductility mainly due to increased martensite fraction. The steel demonstrates enhanced strain hardening ability independently of the peak temperature. Analysis of the experimental results showed that the industrial processing window of ±10 °C may lead to some heterogeneity of the local microstructure in the ultrafast heat treated sheets. However, the latter should not have any negative effect on the overall mechanical behavior of the ultrafast heat treated steel sheets on the macro-scale.

1. Introduction

Steel sheets manufacturing is a multistage process, where the steel is subjected to several rolling operations and finally to a heat treatment, which determines its final microstructure and, therefore, its properties. The standard approach for processing advanced high strength steels (AHSS) is based on the homogenization of the microstructure at elevated temperatures followed by cooling with well controlled rates [1]. The typical route used to manufacture components for the automotive industry, where steel is the primarily used material [2], is a relatively long process resulting in very high energy consumption and carbon dioxide emission [3]. A potential solution to decrease the CO_2 emissions produced by vehicles is to reduce the total weight of the car, without compromising passengers' safety. In order to do so, the mechanical properties of the car components should be improved. Therefore, the steel industry is continuously looking for new solutions to fulfill the current societal demands by processing the steel in the most environmentally-friendly manner. Hence, in the last decades, new processing routes were developed, such as the rapid or "flash processing" treatment [4,5]. In literature, this process is also referred to as "ultra-fast heating" (UFH) [6,7] or "ultra-rapid annealing" (URA) [8,9]. It is based on heating the material to intercritical or fully austenitic temperature with heating rates well above 100 °C/s, which is at least one order of magnitude higher than the conventional heating rates (≤10 °C/s), followed by a short soaking at peak temperature and immediate quenching to the room temperature. Thus, the treatment time and the energy consumed for the process are significantly reduced [10].

Complex multiphase microstructure consisting of ferrite and martensite and some retained austenite is typically formed after UFH treatment. The resulting microstructure and properties of the UFH-

* Corresponding author.
E-mail address: miguelvaldestabernero@gmail.com (M.A. Valdes-Tabernero).

https://doi.org/10.1016/j.msea.2020.138999
Received 12 October 2019; Received in revised form 19 January 2020; Accepted 21 January 2020
Available online 24 January 2020

treated material are greatly affected by the initial microstructure as well as the heat treatment parameters, such as heating rate, soaking time and peak temperature [11]. It has been reported that high heating rates increase the austenite start and finish temperatures [12,13]. Moreover, in low carbon steels, recrystallization temperature tends to increase with increasing heating rate and may even exceed the austenite start temperature (A_{C1}) [14,15]. Hence, ferrite to austenite transformation takes place in a non-recrystallized matrix, which leads to the formation of numerous austenite nuclei, while the ferritic matrix undergoes recrystallization and recovery simultaneously. Thus, a complex microstructure with finer grain size is developed [16]. In order to promote grain refinement, the isothermal soaking time is typically kept as short as possible – in the 0.1–0.2 s range [7,11,15,17]. However, such soaking times constitute a challenge for the steel sector due to its difficult implementation in the current industrial lines, impeding the expansion of this processing route. Slightly longer soaking times (1–3 s) can be a feasible solution to maintain the reduced grain size brought about by ultrafast heating [18], but only if the effect of other processing parameters is well understood. One key parameter is the peak temperature, as it influences the mechanism of the austenite formation and growth. At conventional heating rates, the austenite formation kinetics are determined by carbon diffusion, whereas at ultrafast heating rates, formation of austenite starts by carbon diffusion control, which is later overtaken by a massive mechanism [7,9,19]. The martensite formed after quenching gets softer due to higher volume fraction of intercritical austenite and reduced carbon content therein [20]. Additionally, the recrystallized ferrite volume fraction in the heat treated steel tends to increase with increasing peak temperature [21]. Despite the significant effect of peak temperature on the final microstructure of the UFH treated steels, there are no systematic studies focused on the microstructure sensitivity to the peak temperature variations. In addition, it is important to simulate real industrial conditions, as the typical industrial processing temperature window of ±10 °C is about one order of magnitude higher compared to that maintained in a laboratory dilatometry or thermo-mechanical simulator (±1 °C) [7,11]. Therefore, it is essential to understand the effect of peak temperature ranges during UFH on the microstructure and properties in order to select the optimum conditions.

The reported studies on the UFH treatment of steels have mainly focused on microstructure and basic mechanical properties (hardness, tensile strength, ductility). In Refs. [17,22], it was reported that the UFH treatment leads to an improvement on the material strength compared to the conventional heat treatment, without a reduction in ductility. However, although it has been shown in many studies that mechanical behavior of multi-phase materials at the macroscale depends on the morphology, architecture and properties of the individual micro-constituents [1,23,24], there are no such in-depth studies on the UFH treated steels. Hence, understanding the *heat treatment parameters-microstructure-properties* relationship both at macro- and micro-scales, is necessary to develop specific microstructures and properties and to design and optimize precise UFH treatments depending on the requirements and specifications of the final product. Therefore, the objective of this work is to investigate the influence of peak temperature and short soaking times (≤1.5 s) on the microstructure and properties of the individual microstructural constituents, as well as to relate both to the macro-mechanical response of the material.

2. Material and experimental procedures

2.1. Material

The chemical composition of the low carbon steel selected for this investigation was 0.19% C, 1.61% Mn, 1.06% Al, 0.5% Si (in wt. %). The as-received material was a 1 mm thick sheet (50% cold rolled) with a microstructure of 76% of ferrite and 24% of pearlite (Fig. 1). This material was subjected to two kinds of heating experiments: a) dilatometry measurements to determine the formation of austenite at different intercritical temperatures, and b) annealing tests to different intercritical temperatures with varying soaking time followed by quenching. Both types of experiments are described in detail below.

2.2. Dilatometry experiments

Dilatometry measurements were carried out to analyze the austenitization kinetics at different temperatures for the same heating rate. For these experiments, specimens with dimensions of 10x5x1 mm^3 were machined from the as-received material. Tests were carried out in a Bähr DIL805A/D dilatometer (Bähr-Thermoanalyse GmbH, Hüll-Horst, Germany). A *K*-type thermocouple was welded to the midsection of each specimen to control their temperature during the experiment. Specimens were heated from room temperature to different temperatures in the intercritical region (860 °C, 880 °C and 900 °C) at 200 °C/s and soaked for 600 s. Then, specimens were heated to a maximum temperature of 1100 °C at 200 °C/s and soaked for 0.2 s (to ensure full austenitization) followed by quenching to room temperature at −300 °C/s. The volume fraction of the austenite phase formed during isothermal holding was obtained via analysis of the dilatometry data applying the lever rule to the dilatation-time curve [25].

2.3. Intercritical heat treatment

Strips having a length of 100 mm and width of 10 mm were cut along the rolling direction from the cold rolled sheet. A *K*-type thermocouple was spot-welded to the midsection of each strip. A thermo-mechanical simulator Gleeble 3800 was used to perform heat treatments. At the first stage of heat treatments, samples were heated at 10 °C/s to 300 °C and kept at this temperature for 30 s to simulate a preheating in some industrial continuous annealing lines to minimize the thermal stresses during heating. At the second stage, a number of the samples were heated from 300 °C at 800 °C/s (which corresponds to the ultrafast heating rate) to the intercritical peak temperature of 860 °C followed by soaking for 0.2 s or 1.5 s and quenching to room temperature with cooling rate of ~160 °C/s. Hereafter, these specimens will be referred to as UFH860-0.2s and UFH860-1.5s, respectively.

To investigate the influence of peak temperature, additional heat treatments with maximum temperatures equal to 880 °C and 900 °C and same soaking times (0.2 s and 1.5 s) were performed. These conditions are referred to as UFH880-0.2s and UFH880-1.5s for the 880 °C, and UFH900-0.2s and UFH900-1.5s for the 900 °C heat treatment. Microstructural analysis and hardness measurements along the axis of the heat treated strips showed a homogeneously heat treated zone having a length of 10 mm. The specimens processed by the Gleeble thermo-

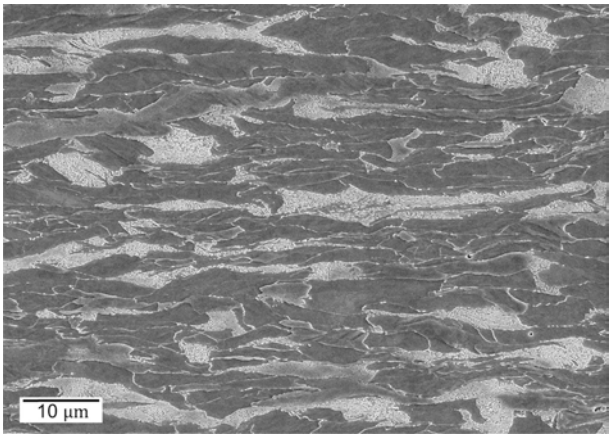

Fig. 1. Initial ferritic-pearlitic microstructure of the material after 50% cold reduction.

mechanical simulator were then subjected to a thorough microstructural and mechanical characterization.

2.4. Microstructural characterization

Scanning electron microscopy (SEM) and electron backscatter diffraction (EBSD) analyses were carried out for a thorough microstructural characterization of the heat treated samples. Specimens were ground and polished to a mirror-like surface applying standard metallographic techniques with final polishing using OP-U (colloidal silica). For SEM characterization, polished specimens were etched with 2 vol% nital solution for ~10 s. The EBSD studies were performed using a FEI Quanta™ Helios NanoLab 600i equipped with a NordlysNano detector controlled by the AZtec Oxford Instruments Nanoanalysis (version 2.4) software. The data were acquired at an accelerating voltage of 18 kV, a working distance of 8 mm, a tilt angle of 70°, and a step size of 65 nm in a hexagonal scan grid. The orientation data were post-processed using HKL Post-processing Oxford Instruments Nanotechnology (version 5.1©) software and TSL Data analysis version 7.3 software. Grains were defined as a minimum of 4 pixels with a misorientation $\geq 5°$. Grain boundaries having a misorientation $\geq 15°$ were defined as high-angle grain boundaries (HAGBs), whereas low-angle grain boundaries (LAGBs) had a misorientation $< 15°$. The volume fractions of transformed/untransformed grains and recrystallized/recovered ferritic grains were determined by a two-step partitioning procedure described in Refs. [17,26]. In this procedure, grains with high (>70°) and low (≤70°) grain average image qualities are separated in a first step, allowing to distinguish between untransformed (ferrite) and transformed (martensite) fractions, respectively. In the second step, recrystallized and non-recrystallized ferritic grains are separated using the grain orientation spread (GOS) criterion: Grains with GOS below 1° are defined as the recrystallized grains, while grains with GOS above 1° are defined as the non-recrystallized ones [27]. Microstructure was observed on the plane perpendicular to the sample transverse direction (the RD–ND plane).

2.5. Mechanical characterization

HysitronTI950 Triboindenter equipped with a Berkovich tip was employed for nanoindentation testing. First, square areas having a size of ~10 × 10 μm^2 were analyzed by EBSD, and individual microstructural constituents were determined. At least ten areas were tested for each material's condition. In order to target specific phases/grains, these square areas were scanned, using the scanning probe microscopy (SPM) mode of the instrument prior to the nanoindentation. In SPM mode, the nanoindenter tip scans the sample surface while in contact with it, using a force of 2 μN, providing the surface topography of the sample. Nanoindentation tests were carried out in displacement control mode at a constant strain rate ($\dot{\varepsilon}=\dot{h}/h$) of 0.07 s^{-1}, where h is the penetration depth and $\dot{h}$ the penetration rate of the indenter. At least 20 indents were performed on each phase at an imposed maximum depth of 150 nm. The nanohardness was determined from the analysis of the load–displacement curves using the Oliver and Pharr method [28].

Vickers hardness tests of all heat treated samples were carried out using Shimadzu HMV hardness tester according to the ASTM E92 – 17 Standard. The RD–ND plane of samples was ground and polished using 1 μm diamond paste at the final stage. A load of 4.9 N was applied for 15 s.

A Kammrath&Weiss module was used for tensile testing of dog bone sub-size samples at room temperature at a constant cross head speed corresponding to an initial strain rate of 10^{-3} s^{-1}. These samples had a gauge length of 4 mm, a gauge width of 1 mm and a thickness of 0.9 mm. They were machined from the homogeneously heat treated zone of the heat treated strips, so their tensile axis was parallel to the RD. All samples were carefully ground and mechanically polished using OP-U (colloidal silica) at the final stage. At least three specimens were tested for each condition, and the results were found to be reproducible.

3. Results

3.1. Microstructural characterization

3.1.1. Dilatometry

Fig. 2 represents the evolution of austenite fraction during isothermal holding at different intercritical temperatures. It is seen that the higher the peak temperature, the higher the initial austenite fraction, as the material is closer to the A_{C3} temperature. For instance, at 860 °C the austenite volume fraction is 19%, and increases to 47% with increasing peak temperature to 900 °C. It is also seen that the peak temperature strongly affects the kinetics of austenite formation and growth. Austenite rapidly grows at the early stages of annealing at 900 °C compared to annealing at lower peak temperatures of 860 °C and 880 °C, which present a similar behavior. Soaking at 900 °C for 600 s is sufficient for full austenitization, which is reached after 522 s. At 880 °C, the austenite fraction achieved at the end of the intercritical holding is 99%, whereas at 860 °C is 94%. Nevertheless, taking into account the positive slope of the curve, it is clear that the material will reach the complete austenitization after soaking for longer time.

3.1.2. SEM analysis

SEM analysis of the Gleeble processed samples was performed to qualitatively characterize the influence of both peak temperature and short soaking times on the microstructure. Fig. 3 displays the microstructure variation at the different peak temperatures studied for holding times of 0.2 s (Fig. 3a–c) and 1.5 s (Fig. 3d–f). The resultant microstructure is heterogeneous after all heat treatments being mainly

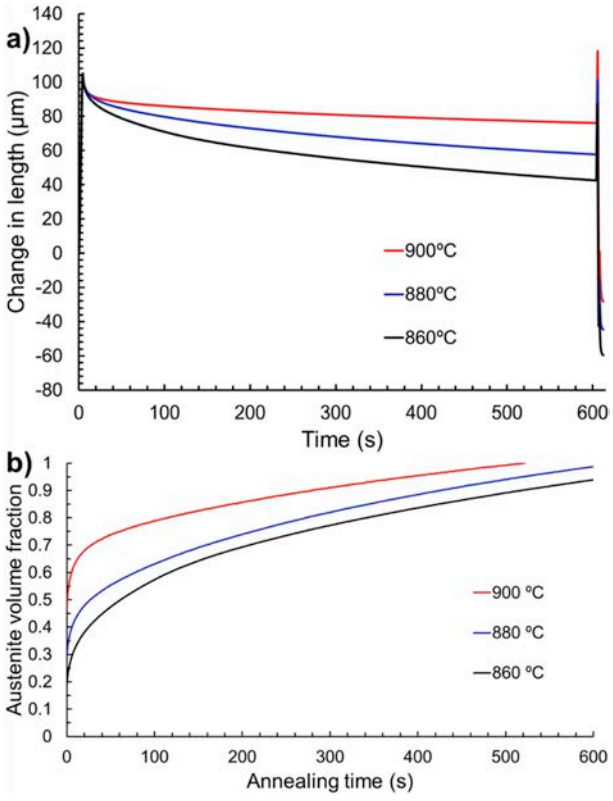

Fig. 2. a) Dilatation-time curves for material heated to 1100 °C at 200 °C/s with soaking for 600 s at different temperatures (860 °C, 880 °C and 900 °C); b) Effect of the peak temperature on the austenite volume fraction during isothermal holding.

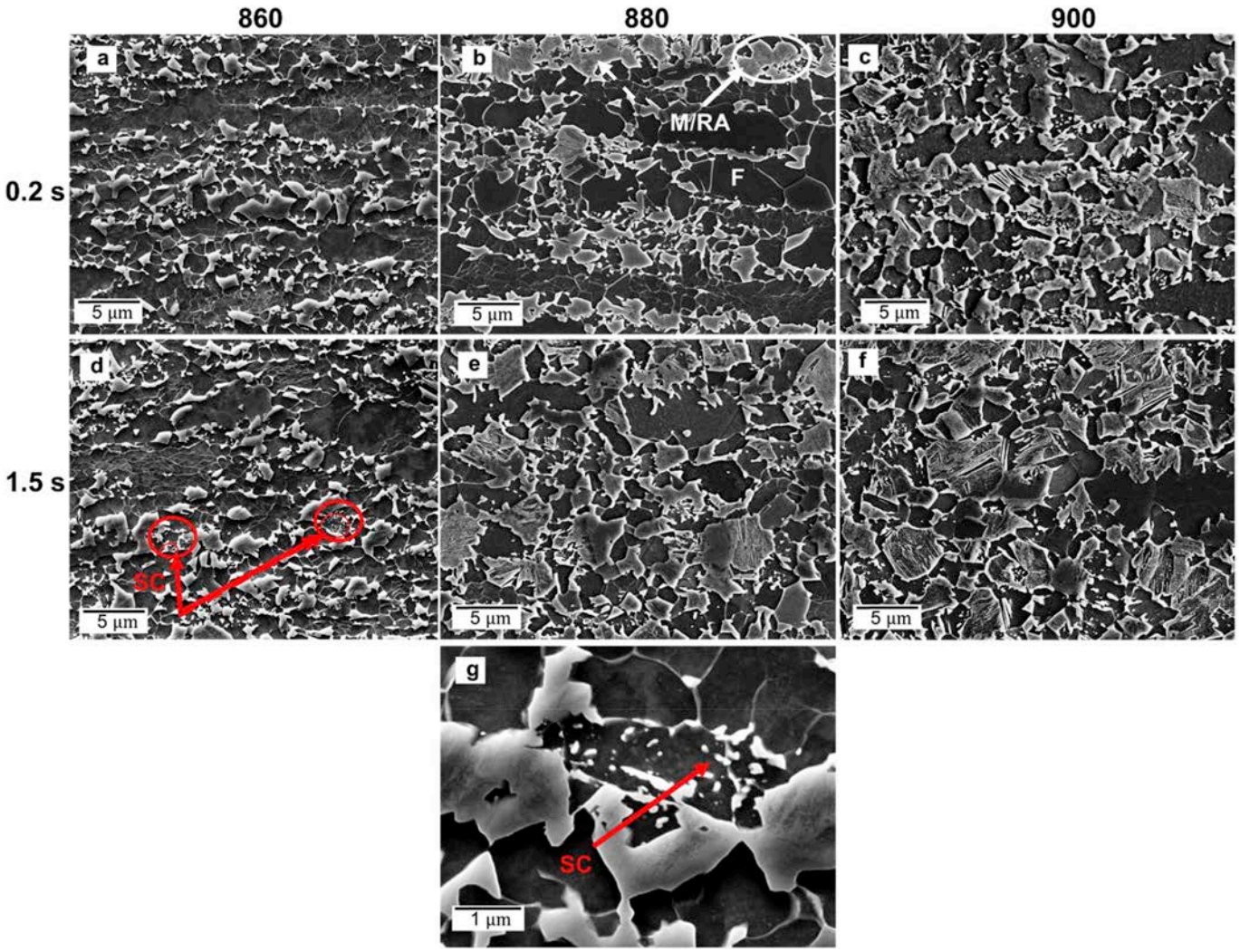

Fig. 3. SEM photos illustrating the influence of peak temperature (860, 880 and 900 °C) and soaking time (0.2 and 1.5 s) on the microstructure: a), b) and c) are for 0.2 s at 860, 880 and 900 °C, respectively; d) & g), e) and f) are for 1.5 s at 860, 880 and 900 °C, respectively. SC: spheroidized cementite; M: martensite; F: ferrite; RA: retained austenite.

formed by ferritic matrix and martensite (marked by a white dashed arrow in Fig. 3b). In turn, the matrix is formed by recrystallized (Rx) and non-recrystallized (non-Rx) ferrite, as it is demonstrated in Section 3.1.3. A qualitative analysis shows that, independently on the heat treatment parameters, all the conditions present a ferritic matrix consisting of coarse and fine grains due to combination of different processes, which take place during UFH (recovery, incomplete recrystallization and grain growth at early stages). Images on Fig. 3a–f demonstrate that the increasing peak temperature leads to grain growth for both microstructural constituents (ferrite and martensite) even after a holding time of 0.2 s. Moreover, it is possible to observe that the martensite fraction substantially grows with increasing soaking time independently of the peak temperature and also with the peak temperature for a specific soaking time. As described in Section 3.1.1, increasing peak temperature and soaking time lead to a higher fraction of intercritical austenite, which is transformed into martensite upon quenching. The higher the intercritical austenite fraction, the lower its carbon content due to the C redistribution in its interior. A small amount of retained austenite grains was also identified by EBSD analysis in all conditions (see Section 3.1.3). In addition, very small amount of spheroidized cementite was observed in the microstructure, which remains in the material from the initial cold rolled state (marked by red arrows on Fig. 3 d). Its presence is related to the short time given for its dissolution, hence, it is more commonly observed in the samples annealed for the shorter soaking time of 0.2 s.

3.1.3. EBSD analysis

EBSD analysis was performed in order to identify and quantitatively characterize the different phases present in the microstructure of the heat treated samples. Fig. 4a illustrates a typical EBSD phase map measured on the UFH860-0.2s sample. Fine retained austenite grains (in white color) and martensite grains (in black color) are embedded into the ferrite matrix composed of recrystallized (Rx) ferrite (in orange color) and non-recrystallized (non-Rx) ferrite (in blue color). LAGBs are seen mainly in the interior of the non-Rx ferrite grains, whereas majority of the Rx ferrite grains are free of LAGBs. The morphology of the microstructure and the individual microconstituents are very similar in all studied conditions, whereas size and volume fraction of individual microconstituents depend on the heat treatment parameters. The results of the quantitative analysis are summarized in Table 1.

Analysis of the effect of soaking time for each temperature shows that at 860 °C, the martensite fraction increases from 6.9% after 0.2 s to 12.6% after 1.5 s. When temperature raises up to 880 °C, the volume fraction of martensite formed after 0.2 s is 11.6%, which increases to 20.2% after 1.5 s. Finally, the 900 °C treatment leads to the highest increment in martensite fraction during soaking, from 16.3% after 0.2 s

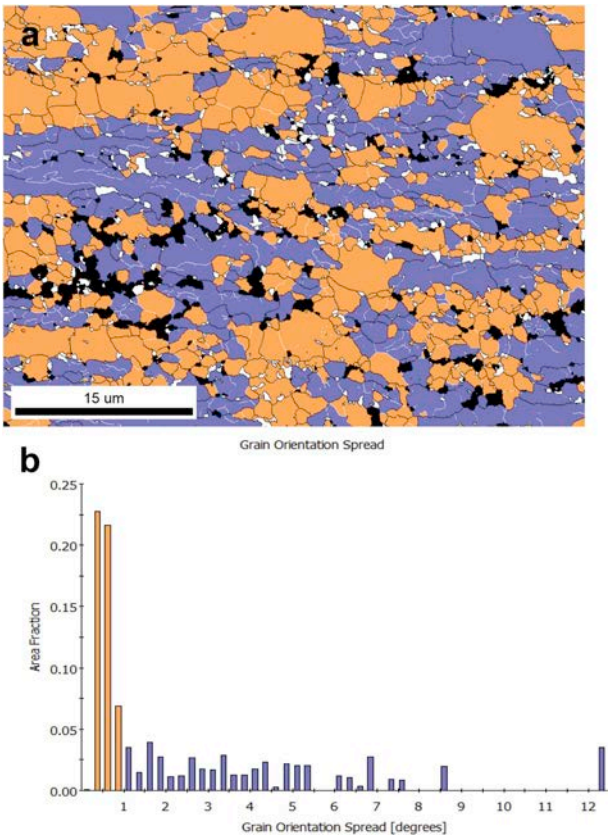

Fig. 4. a) Representative EBSD phase maps for the UFH860-0.2s sample. Rx ferrite is shown in orange; non-Rx ferrite in blue; martensite in black and austenite is shown in white. HAGBs are represented in black and LAGBs in white. b) Histogram of grain orientation spread distribution in the ferrite matrix for the EBSD phase map presented in (a). Rx ferrite grains have GOS<1° (orange bars), whereas non-Rx ferrite grains have GOS>1° (blue bars), as described in Section 2.4. (For interpretation of the references to color in this figure legend, the reader is referred to the Web version of this article.)

Table 1
Data on the volume fraction of microstructural constituents as a function of heat treatment parameters.

Peak temperature (°C)	860		880		900	
Soaking time (s)	**0.2**	**1.5**	**0.2**	**1.5**	**0.2**	**1.5**
Martensite (%)	6.9 ± 3.2	12.6 ± 3.1	11.6 ± 2.1	20.2 ± 2.5	16.3 ± 3.8	27.8 ± 4.6
Retained austenite (%)	2.2 ± 0.4	2.1 ± 0.3	1.2 ± 0.3	2.5 ± 0.7	1.7 ± 0.3	1.7 ± 1.0
Ferrite (%)	90.9 ± 4.0	85.3 ± 2.8	87.2 ± 1.9	77.3 ± 2.6	82.0 ± 3.6	70.5 ± 3.9
Rx ferrite	48.4 ± 9.8	61.8 ± 13.0	67.4 ± 3.8	73.5 ± 3.9	83.3 ± 3.7	80.3 ± 3.6
Non-Rx ferrite	51.6 ± 9.8	38.2 ± 13.0	32.6 ± 3.8	26.5 ± 3.9	16.7 ± 3.7	19.7 ± 3.6

to 27.8% after 1.5 s. For the shortest soaking time, the martensite volume fraction increases by the same amount (~4.7%) when peak temperature is increased from 860 °C to 880 °C and then from 880 °C to 900 °C. Similar dependence can also be noted after soaking for 1.5 s. The ferrite volume fraction presents a reverse trend, as both phases are formed in the intercritical temperature range. The portion of RA is minor in all heat treated conditions, being between 1.2 and 2.5%.

The morphology of the ferritic matrix is greatly affected by both parameters, temperature and soaking time. While at 860 °C for 0.2 s the matrix is to larger extent formed by non-Rx ferrite (~52%), whereas Rx ferrite prevails in the matrix after 1.5 s, reducing the volume fraction of the non-Rx grains to ~ 38% (Fig. 5). With increasing holding time at 880 °C, the non-Rx fraction is reduced to a lesser extent from 33% to 27%. Finally, soaking at 900 °C significantly reduces the volume fraction of non-Rx ferrite: average volume fraction values are in the range of 17–20% and are not affected by soaking time. Therefore, the most pronounced effect of soaking time in the studied temperature-time range occurs at the lower peak temperatures of 860–880 °C, as seen from Fig. 5.

The effect of the holding time (0.2 and 1.5 s) on the Rx and non-Rx ferrite grain size is shown in Fig. 6. The effect of peak temperature after soaking for 0.2 s is shown in Fig. 6a. First, the fraction of grains having size below 1 μm tends to decrease with increasing peak temperature. Second, after UFH to 860 °C, the majority of grains have a size between 1 and 2 μm, although it tends to shift to higher values with peak temperature and reaching the range of 2–3 μm at 900 °C. Third, there are some grains having a size above 6 μm even after heating to the lowest peak temperature of 860 °C and their area fraction increases with peak temperature. The first two observations are even more pronounced when the holding time increases to 1.5 s (Fig. 6b). It is shown that at 860 °C, the fraction of grains below 1 μm has increased with respect to the 0.2 s counterpart, and it is considerably reduced at higher peak temperatures (880 °C and 900 °C). Moreover, the main fraction of grains presents a larger size when temperature is raised, although the fraction of grains larger than 6 μm has decreased for all temperatures at 1.5 s compared to the 0.2 s condition. On the other hand, the average grain size for the non-Rx ferrite at 0.2 s is higher compared to the Rx ferrite at all studied temperatures (Fig. 6c), as the grains retained the initial cold rolled microstructure. In addition, the distribution is narrower compared to the Rx grains, as there are almost no grains below 1 μm. At the lowest temperature the distribution seems to be wider than at higher temperatures (880 and 900 °C), although this is better seen after 1.5 s (Fig. 6d). Coarse grains (>6 μm) are prone to disappear with temperature.

Fig. 7 represents the area fraction for martensite grains plotted versus the equivalent circle diameter (ECD) after soaking for 0.2 s and 1.5 s at the studied peak temperatures. For 860 and 880 °C after 0.2 s (Fig. 7 a), the vast majority of martensite grains present an ultrafine size (below 1 μm). Contrary to the result seen in ferrite, the area fraction of grains <0.5 μm increases when temperature is raised up to 880 °C. However, when temperature further increases to 900 °C, the curve is shifted to the larger grain size values, with the peak above 1 μm and showing a wider size distribution than at 860 or 880 °C. Similar to ferrite, the effects are more pronounced with increasing soaking time to

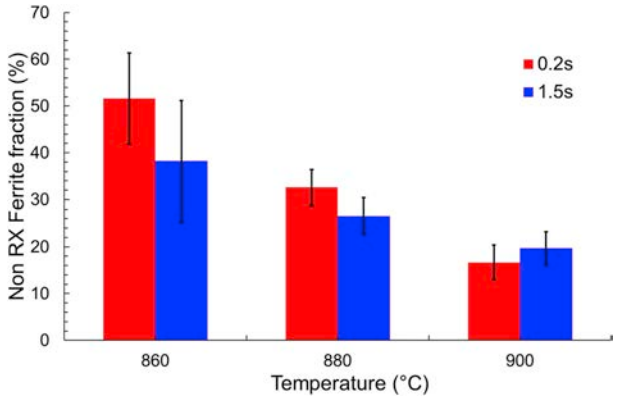

Fig. 5. Volume fraction of non-Rx ferrite obtained from EBSD analysis for different temperatures (860, 880 and 900 °C) and soaking times (0.2 and 1.5 s). In red for 0.2 s and in blue for 1.5 s. (For interpretation of the references to color in this figure legend, the reader is referred to the Web version of this article.)

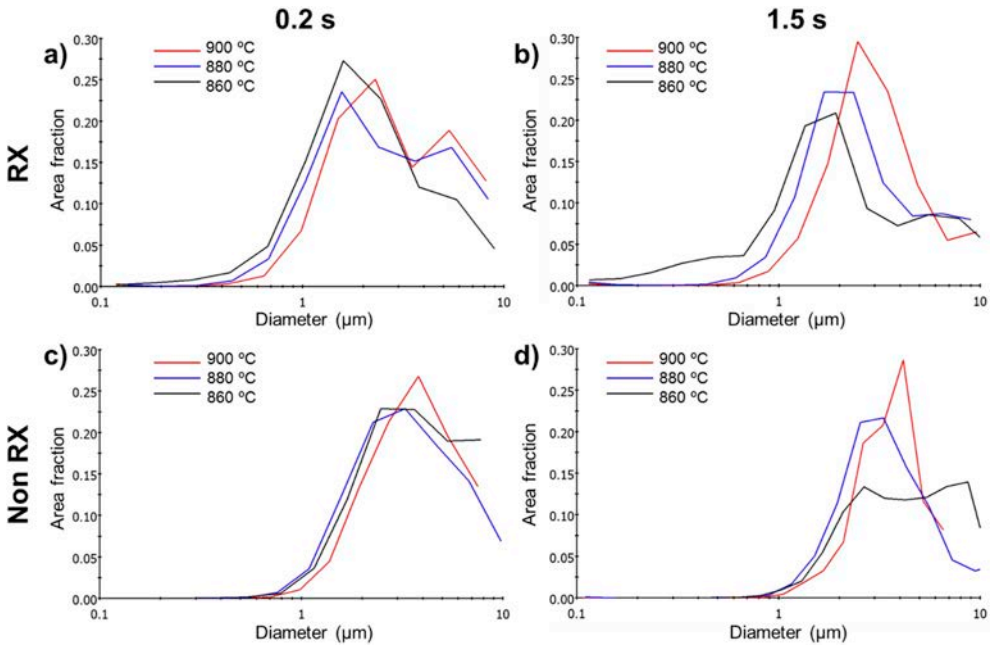

Figure 6. a) & b) representation of the area fraction for recrystallized (RX) ferrite grain size versus the equivalent circle diameter (ECD) after 0.2 and 1.5 s holding time respectively for the different temperatures studied; c) & d) non-recrystallized (non-RX) ferrite grain size after 0.2 and 1.5 s holding time, respectively. Data are obtained from the EBSD measurements.

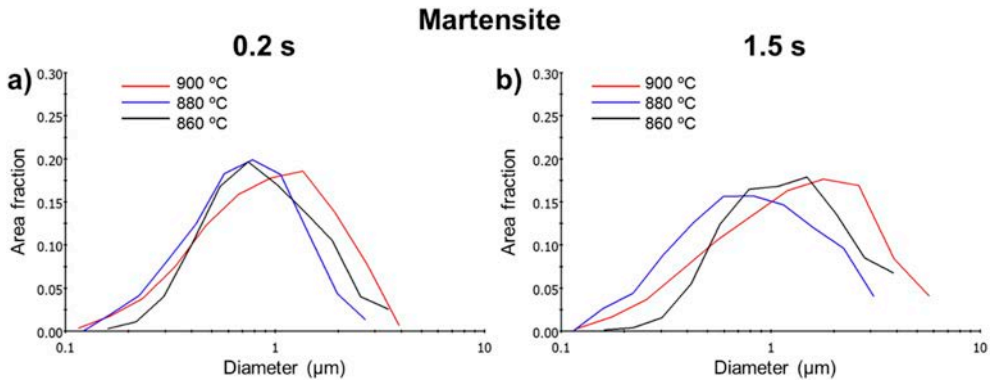

Fig. 7. Martensite area fraction vs ECD after soaking for 0.2 s (a) and 1.5 s (b) at the peak temperatures of 860 °C, 880 °C and 900 °C.

1.5 s. At 860 °C the austenite formed at intercritical temperatures grows, while at 880 °C the fraction of grains below 1 μm increases resulting in a wider size distribution. Finally, at 900 °C the increased intercritical austenite grain size shows a wider distribution than the 880 °C and 860 °C.

3.2. Mechanical characterization

3.2.1. Properties of the individual microconstituents

Nanoindentation tests were performed on selected grains to investigate the influence of maximum temperature and soaking time on the mechanical response of the microstructural constituents. Fig. 8a shows an EBSD map where dark areas correspond to martensite and white areas to ferrite, which were later identified by SPM imaging prior nanoindentation testing (Fig. 8b). An SPM image of the area with the nanoindentation imprints was also recorded immediately after the test as observed in Fig. 8c. Finally, the microstructure was etched with nital 2 vol % to take SEM images (as shown in Fig. 8d) that corroborate the differentiation made by EBSD. Typical load – depth curves for the main two microstructural constituents are shown in Fig. 8e, where the red and blue curves correspond to martensite and Rx ferrite, respectively.

Continuous load-depth curves were obtained from nanoindentation on martensitic grains, while majority of the ferritic grains exhibited pop-in events, particularly the softer Rx-ferrite grains. They are caused by sudden penetration bursts during the loading process. This effect has been related to the transition from an elastic to an elasto-plastic contact. The probability of pop-in events and the pop-in load increase as the dislocation density decreases, as discussed in our previous work [14].

The measured nanohardness values for the main microstructural constituents: Rx ferrite, non-Rx ferrite and martensite are summarized in Table 2 as a function of peak temperature and soaking time. It is clearly seen that neither the soaking time nor the temperature affects the nanohardness of Rx ferrite, which has average values within the range of 2.5–2.6 GPa. Nevertheless, there is a significant difference between Rx and non-Rx ferrite, as the latter presents significantly higher nanohardness values (3.1–3.2 GPa), being also similar for all studied conditions. The martensite phase exhibits the highest nanohardness for all conditions, with the average values showing greater variation for each condition. For instance, after heating to 860 °C and soaking for 0.2 s, the martensite average nanohardness value is 7.6 GPa, which reduces slightly to 7.4 GPa, when soaking increases to 1.5 s, but still within measured standard deviation. The softening effect with soaking time is

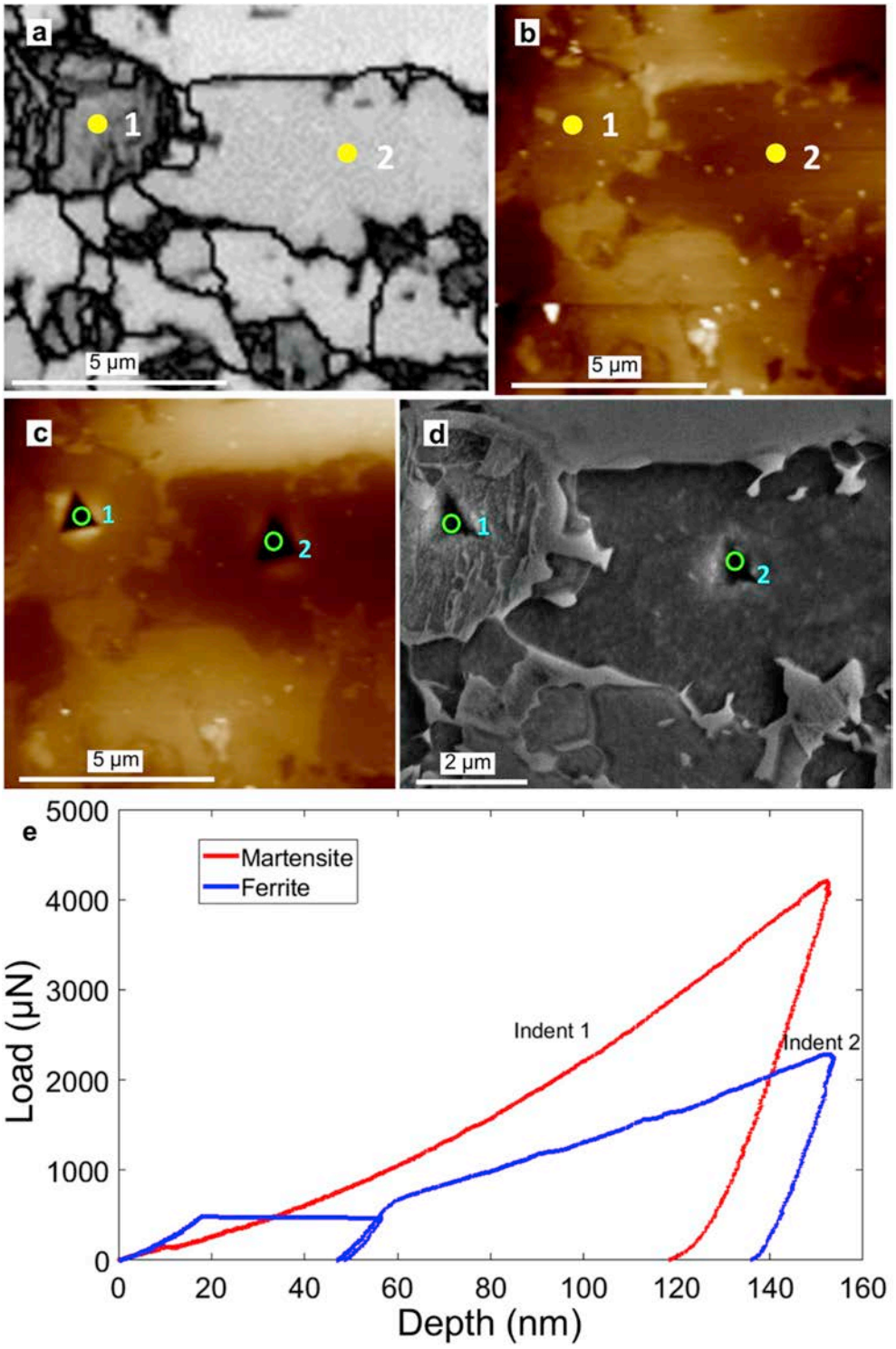

Fig. 8. a) Band slope EBSD map with marked grains where the nanoindentation tests were performed; b) SPM map of the same area without indentation imprints; c) SPM map of the area after indentation; d) SEM image of the area after testing, etched with nital 2 vol%; e) Typical indentation load – penetration depth curves from nanoindentation measurements on martensitic grain (in red color) and ferritic grain (in blue color). (For interpretation of the references to color in this figure legend, the reader is referred to the Web version of this article.)

much more evident at higher peak temperatures: at 880 °C, the nanohardness drops by 10.3%, varying from 6.8 GPa (after 0.2 s) to 6.1 GPa (after 1.5 s), while at 900 °C, the drop is 16.7%, as nanohardness varies from 6.6 GPa to 5.5 GPa for holding times of 0.2 and 1.5 s. Taking into consideration only the raise in temperature from 860 to 900 °C, the average nanohardness drops by 13.1% at 0.2 s (from 7.6 GPa to 6.6 GPa), while a more pronounced drop of 25.7% was observed at 1.5 s (from 7.4 GPa to 5.5 GPa).

3.2.2. *Macro-mechanical characterization*

The effect of peak temperature and short soaking times on the macro-mechanical behavior of the AHSS was studied through hardness testing. The results are presented in Table 3. It is seen that an increment on the peak temperature produces a rise in the hardness values independently of the given soaking time. For 0.2 s, the increase in hardness between 860 °C and 880 °C is insignificant, going from 252 to 255 HV0.5 respectively, while at 900 °C, the hardness increases to 264 HV0.5. The increase in hardness with peak temperature is much more evident for a soaking time of 1.5 s, being 245 HV0.5 at 860 °C, and increasing to 272

Table 2
Data on nanohardness (in GPa) of the individual microconstituents.

Peak temperature (°C)	860		880		900	
Soaking time (s)	0.2	1.5	0.2	1.5	0.2	1.5
Martensite	7.6 ± 2.4	7.4 ± 1.1	6.8 ± 0.8	6.1 ± 0.7	6.6 ± 1.0	5.5 ± 0.6
Recrystallized ferrite	2.6 ± 0.1	2.6 ± 0.1	2.6 ± 0.1	2.5 ± 0.1	2.6 ± 0.2	2.6 ± 0.1
Non-recrystallized ferrite	3.2 ± 0.2	3.1 ± 0.2	3.2 ± 0.2	3.2 ± 0.3	3.1 ± 0.2	3.2 ± 0.2

Table 3
Data on hardness of the heat treated strips.

Peak temperature (°C)	860		880		900	
Soaking time (s)	0.2	1.5	0.2	1.5	0.2	1.5
Hardness (HV0.5)	252 ± 4	245 ± 5	255 ± 5	272 ± 7	264 ± 5	293 ± 8

and 293 HV0.5 at 880 and 900 °C, respectively.

Additionally, tensile testing was carried out for all conditions using miniaturized dog bone samples. Fig. 9 illustrates the typical engineering stress - engineering strain curves. Data on the mechanical properties determined from the curves (0.2% proof strength $\sigma_{0.2}$, ultimate tensile strength σ_{UTS}, uniform elongation ε_u and elongation to failure ε_f) are given in Table 4. One can see that at 860 °C, the yield strength slightly varies with soaking time being 444 MPa and 441 MPa for 0.2 and 1.5 s, respectively. However, for higher peak temperatures and holding times, the yield point is enhanced. For instance, at 880 °C, the $\sigma_{0.2}$ -values increase by more than 20 MPa to 468 and 473 MPa for 0.2 and 1.5 s,

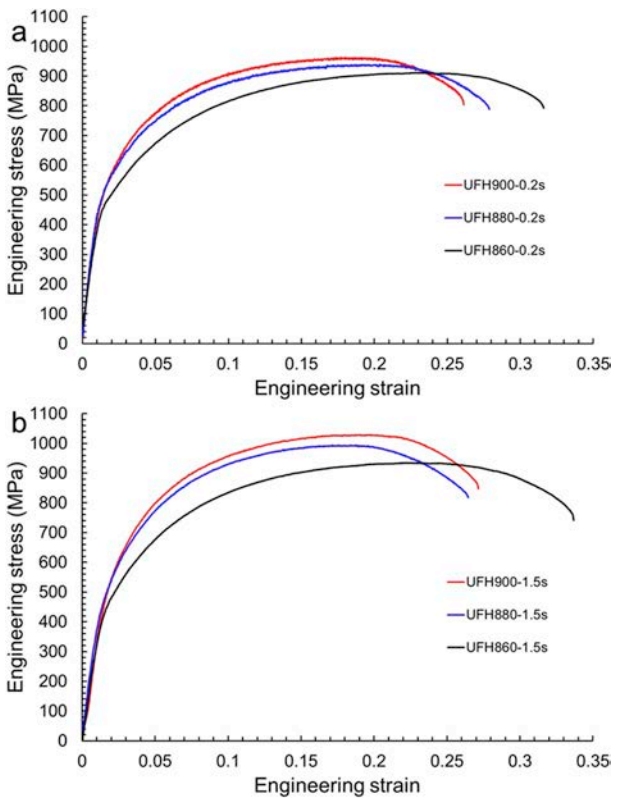

Fig. 9. Typical engineering stress – engineering strain curves from tensile testing of specimens heated to different peak temperatures and soaked for: a) 0.2 s; b) 1.5 s.

Table 4
Basic mechanical properties determined by tensile testing of the heat treated samples.

Peak temperature (°C)	860		880		900	
Soaking time (s)	0.2	1.5	0.2	1.5	0.2	1.5
$\sigma_{0.2}$	444 ± 12	441 ± 8	468 ± 5	473 + 12	479 + 12	492 + 24
σ_{UTS}	926 ± 20	925 ± 10	933 ± 5	1017 ± 28	959 ± 21	1053 ± 42
ε_u (%)	24 ± 1	18 ± 2	18 ± 1	16 ± 2	15 ± 1	15 ± 1
ε_f (%)	33 ± 1	30 ± 2	27 ± 1	24 ± 1	23 ± 1	23 ± 3

respectively. For the maximum peak temperature analyzed (900 °C), the yield strength for both soaking times shows the maximum values, being 479 MPa after 0.2 s and 493 MPa in the 1.5 s UFH treatment. Ultimate tensile strength values show a similar tendency than the yield point. While at 860 °C, the σ_{UTS} is independent of the soaking time, with a value of ~925 MPa, higher peak temperatures and soaking times enhanced the strength of the material. For example, at 880 °C and after 0.2 s, the material presents a σ_{UTS} of 933 MPa which increases up to 959 MPa at 900 °C. The increment in strength is more pronounced after longer soaking times, being 1017 and 1053 MPa for 880 °C and 900 °C respectively. Nevertheless, the uniform elongation shows the opposite trend, being reduced from 24% to 15% when the temperature is increased from 860 to 900 °C after 0.2 s. This reduction in elongation with temperature is less significant after 1.5 s, decreasing from 18% at 860 °C to 15% at 900 °C.

4. Discussion

4.1. Influence of maximum temperature on the microstructure – properties relationship in the UFH steel

Dilatometry tests (Fig. 2) demonstrate that the higher the peak temperature, the higher the initial volume fraction of austenite, as it was reported elsewhere [29,30]. These results are in a good agreement with the outcomes of the EBSD analysis (Table 1), where the austenite/-martensite fraction increases with temperature for the same soaking time. The variations between the initial austenite fraction measured for the studied temperatures through dilatometry and EBSD can be rationalized by the difference in the applied heating rate. While during dilatometry the maximum heating rate employed was 200 °C/s, the samples analyzed by EBSD were processed at 800 °C/s. It is known that high heating rates shift transformations temperatures (A_{C1} and A_{C3}) to higher values [31,32]. Therefore, less amount of austenite is formed for the same peak temperature, when higher heating rates are applied. Moreover, heating at 800 °C/s implies that the entire thermal treatment is faster than heating at 200 °C/s, giving less time for the austenite nucleation process to be accomplished, resulting in the lower initial fraction of austenite observed in the samples heated at 800 °C/s. Furthermore, both characterization techniques, dilatometry and EBSD, confirm that the increase in peak temperature favors the formation of austenite nuclei, as nucleation highly depends on temperature [15,33]. For instance, during the dilatometry test, intercricitical holding at 900 °C results in a faster formation of austenite, and similar observations are made from the EBSD results analyzing the martensite grain size (Fig. 7). In the latter case, the fraction of grains having size below 0.5 μm increases, when temperature is raised from 860 to 880 °C for the shortest soaking time (Fig. 7a). This means that the austenite nucleation is favored at 880 °C, whereas at 860 °C the already formed austenite tends to grow as the area fraction of grains above 1 μm is enlarged, being more evident after soaking for 1.5 s (Fig. 7b). Hence, it is possible to state that at 860 °C, the austenite growth is more significant than nucleation,

whereas at 880 °C, this behavior is inversed. At 900 °C, both effects, nucleation and growth, are promoted, as the area fraction of grains below 0.5 μm and above 1 μm increase with respect to the 860 °C case, due to the high internal energy. The rapid grain growth during ultrafast heating to high peak temperatures has been reported by Massardier et al. [8]. In addition to the grain size, the peak temperature also affects the interior structure of the formed austenite, which transforms into martensite after quenching. While at 860 °C martensitic grains are chemically homogeneous, increasing the temperature and soaking time results in the appearance of non-homogeneous martensite regions, as it is shown in Fig. 3e and f and Fig. 6d which correspond to the UFH900-1.5s sample. Similar observations were reported by Castro et al. [17]. This effect can be rationalized based on the existence of carbon gradients in the grain interior, due to the high fraction of austenite formed, and the lack of time for carbon to diffuse through the grains [34].

Regarding the ferrite phase, it is possible to observe that UFH delays the recrystallization [7,11,14,15,17,35], leading to a matrix formed primarily by non-Rx ferrite, when the material is heated to 860 °C for 0.2 s (Fig. 5). The fraction of non-Rx ferrite significantly decreases with time and peak temperature, although it is not affected by the soaking time at the maximum peak temperature of 900 °C and saturates at 17–20%. The ferrite tends to transform into austenite at high temperatures, thus the driving force for recrystallization is reduced. Moreover, non-Rx grain size decreases with time and temperature (Fig. 6c and d), favored by recrystallization and by the consumption of grains due to austenite formation [32]. Nevertheless, Rx ferritic grains show just the opposite behavior (Fig. 6) growing with temperature and time. In addition, for low temperatures (860 °C), ferrite tends to nucleate whereas, the temperature increment favors the ferrite grain growth, as the first nuclei formed rapidly grows [17]. This is related to the high stored energy from both, deformation induced via cold rolling and heat treatment.

4.2. Influence of the peak temperature on the mechanical behavior of the individual microconstituents

Different microstructural constituents formed during heat treatment show dissimilar response during nanoindentation testing. For instance, Rx ferrite presents a lower nanohardness compared to the non-Rx ferrite independently of the heating rate and soaking time (Table 2). The latter exhibits large orientation gradients, as reported in our previous work [36], mainly associated to the high geometrically necessary dislocations (GND) density and residual stresses [37,38]. Moreover, it should be noted that the austenite to martensite transformation during quenching generates a volume expansion, which needs to be accommodated by the surrounding ferrite, introducing new dislocations in both, Rx ferrite and non-Rx ferrite [39]. The increment of the dislocation density can affect the ferrite mechanical behavior, as reported in Ref. [40]. The nanohardness of any of the ferrite microstructural constituents is not altered by the processing parameters (Table 2). On the other hand, the nanomechanical response of the martensitic grains is greatly affected by the processing parameters. At the lowest peak temperature (860 °C) and shortest holding time (0.2 s), the martensite fraction is low (Table 1) due to the short time given to the austenite nuclei to form and grow. Thus, the carbon concentration within the austenite grains increases, due to the high fraction of ferrite [41]. As a consequence, the martensite grains formed at 860 °C are the hardest (Table 2) in comparison to those formed at higher peak temperatures, as the hardness strongly depends on the carbon content [20,42]. Hence, the martensite strength is reduced with both, peak temperature and soaking time, due to the carbon homogenization in the austenite grains formed during the heat treatment. Similar results on the effect of holding time in DP steels and peak temperature during *Quenching & Partitioning* processing were reported by Mazaheri et al. [43] and Hidalgo et al. [44], respectively. The softening effect of increasing soaking times on the martensitic grains is more pronounced at higher peak temperatures due to the higher austenite fraction (Fig. 2) and the more intensive grain growth (Fig. 7). The latter also increases the diffusion distance of carbon [17] causing its redistribution inside the grains, reflected in the lower standard deviations of the measured nanohardness (Table 2).

4.3. Relation of the peak temperature with the macro-mechanical behavior of the material

The slight decrease in average hardness observed at 860 °C when soaking time is increased from 0.2 s to 1.5 s (Table 3) is due to the higher fraction of Rx ferrite present at 1.5 s (Table 1), as Rx ferrite exhibits lower nanohardness compared to the non-Rx counterpart (Table 2). In addition, the presence of coarser grains at 1.5 s than at 0.2 s also leads to reduction in average hardness, obeying the Hall – Petch law [45]. However, raising the temperature to 880 or 900 °C for 0.2 s leads to higher hardness due to the increased fraction of martensite [46]. On the other hand, holding times of 1.5 s at 880 and 900 °C produce a notable increase in hardness compared to their 0.2 s counterparts, as a consequence of the considerable reduction of the ferrite volume fraction (Table 1). Similar results are observed for both, the yielding point and the ultimate tensile strength during tensile testing. At 860 °C, when holding time is increased from 0.2 to 1.5 s, there is no variation of $\sigma_{0.2}$ or σ_{UTS} (Table 4), although martensite fraction is increased with time (Table 1). This observation can be associated with the reduction of the non-recrystallized ferrite fraction, which presents a higher resistance to deformation compared to its recrystallized counterpart [47]. In addition, the grain size of ferrite also increases with soaking time resulting in a lower strength [45]. Nevertheless, the increment of temperature (880 °C and 900 °C) for a fixed soaking time strengthens the material (yield and ultimate tensile strength), due to a significant increase in the martensite volume fraction [48]. Our observations are consistent with the previous work published elsewhere [49,50]. Nevertheless, the increases in strength with both, temperature and soaking time, results in a significant loss in the ductility of the material. This is associated to the drop in the ferrite fraction, which is softer and more ductile than the martensite [51], which is also confirmed via nanoindentation (Table 2). In addition to the ductility, the strain hardening coefficient was analyzed for the different conditions, following the common power-law relationship in Eq. (1) [52].

$$\sigma = k\varepsilon^{n} \tag{1}$$

The strain hardening rate (n) in Eq. (1) was obtained using the following Eq. (2)

$$n = \frac{\ln \frac{\sigma_a}{\sigma_{a-1}}}{\ln \frac{\varepsilon_a}{\varepsilon_{a-1}}} \tag{2}$$

where σ_a and ε_a represent the true stress and true strain in the point *a*, respectively.

Fig. 10 shows the variation of the strain hardening rate with true strain for 0.2 and 1.5 s samples. For both holding times, at 860 °C the material presents a higher strain hardening rate than its counterparts for any strain, decaying at a lower rate. This effect is associated with the higher fraction of non-Rx ferrite present in the microstructure, as compared to the ferrite formed at higher temperatures. In the non-Rx ferrite, the onset of plastic deformation requires higher stress (Table 2), due to its higher dislocation density. Therefore, when temperature or soaking time are increased, the strain hardening decreases, as a consequence of the reduction in the non-Rx ferrite fraction. When the microstructure shows a high martensite volume fraction, the difference in strain hardening rate is reduced. Several authors have associated this behavior to the martensite islands surrounded by ferrite. The volume expansion caused by the austenite to martensite transformation needs to be accommodated by the surrounding ferrite grains, resulting in strain hardening of the matrix [53,54].

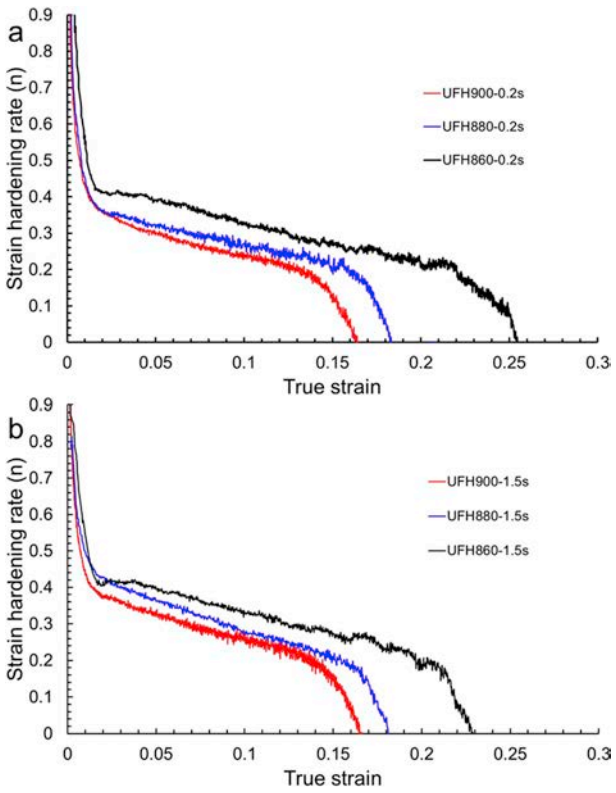

Fig. 10. Representative strain hardening rate - true strain curves determined for samples treated at 860 °C, 880 °C and 900 °C after soaking for 0.2 s (a) and 1.5 s (b).

4.4. Potential microstructural and property gradients in the UFH processed sheets

Analysis of the experimental results from the microstructural (Section 3.1) and mechanical (Section 3.2) characterization shows, that the industrial processing window of 20 °C (i.e. ±10 °C) should lead to some heterogeneity of the microstructure on the meso-scale (i.e. 0.1 … 1 mm). It will show up as some deviations in the size and local volume fraction of individual microstructural constituents (martensite, Rx ferrite and non-Rx ferrite), as well as the hardness of martensite. Nevertheless, such local heterogeneities of the microstructure should not degrade the overall mechanical behavior of the processed sheets on macro-scale. First, there are no significant differences in basic mechanical properties of the UFH processed steel within processing window of 20 °C (Table 4). Second, the UFH processed steel shows high strain hardening ability independently of the peak temperature (see Figs. 9 and 10). The latter should eliminate any minor negative effects from the microstructural heterogeneity in the UFH processed sheets appeared due to the deviation of the local peak temperature within ±10 °C window.

5. Conclusions

We have studied the effect of the UFH parameters, peak temperature (860 °C, 880 °C and 900 °C) and soaking times (0.2 s–1.5), on the microstructure and mechanical response of a Fe-0.19C-1.61Mn-1.06Al-0.5Si steel at different scales. The main conclusions of our study include:

(1) The increase in peak temperature promotes austenite formation. Independently of the peak temperature, mainly nucleation of small austenite grains with their limited growth occurs at the shortest soaking time (0.2 s), whereas both formation of nuclei and their growth proceed after soaking for longer time (1.5 s).

(2) Morphology of the ferritic matrix is significantly altered by both peak temperature and soaking time. The lower peak temperature and shorter soaking time promote nucleation of the recrystallized ferritic grains, while the fraction of the non-recrystallized ferritic matrix undergoing recovery process remains high. With increasing both parameters, the average grain size of the recrystallized ferritic grains and their volume fraction tend to increase. These processes are accompanied by decrease of the ferrite volume fraction due to the increasing volume fraction of the intercritical austenite (i.e. martensite after quenching).

(3) Independently on the applied heat treatment parameters, the highest nanohardness is measured on martensitic grains followed by non-recrystallized ferrite and recrystallized ferrite. Peak temperature and soaking time strongly affect the nanohardness of the martensitic grains. The higher the temperature the larger the grains, reducing the carbon concentration therein. On the contrary, nanohardness of the ferritic microconstituents is affected neither by temperature nor soaking time. The non-recrystallized ferrite is harder than its recrystallized counterpart due to the higher dislocation density of the former.

(4) At the peak temperature of 860 °C, the increase in soaking time within studied range does not produce an improvement in the mechanical properties despite higher martensite volume fraction, due to the decrease of the non-recrystallized ferrite fraction and the grain growth. Nevertheless, increasing peak temperatures to 880 °C and 900 °C favors the strengthening of the material, as the effect of martensite becomes the dominant factor. However, the ductility is considerably reduced with both, temperature and soaking time, due the lower fraction of the ductile ferritic phase.

(5) Analysis of the experimental results from the microstructural and mechanical characterization shows that the industrial processing window of 20 °C may lead to some heterogeneity in the microstructure of the UFH processed sheets. However, the latter should not have any negative effect on their overall mechanical behavior on the macro-scale.

Data availability

The raw/processed data required to reproduce these findings cannot be shared at this time as the data also forms part of an ongoing study.

Declaration of competing interest

The authors declare that they have no known competing financial interests or personal relationships that could have appeared to influence the work reported in this paper.

CRediT authorship contribution statement

M.A. Valdes-Tabernero: Investigation, Formal analysis, Visualization, Funding acquisition, Writing - original draft. **A. Kumar:** Investigation, Writing - review & editing. **R.H. Petrov:** Conceptualization, Methodology, Resources, Writing - review & editing. **M.A. Monclus:** Methodology, Formal analysis, Visualization, Writing - review & editing. **J.M. Molina-Aldareguia:** Methodology, Funding acquisition, Writing - review & editing. **I. Sabirov:** Conceptualization, Supervision, Writing - review & editing.

Acknowledgements

Comunidad de Madrid (Madrid regional government) - Programme S2018/NMT-4381. IMDEA Materials Institute - IMDEA Innovation award. Materials Innovation Institute (M2i) - grant number s16042b.

References

[1] N. Fonstein, Advanced High Strength Sheet Steels: Physical Metallurgy, Design, Processing, and Properties, Springer, 2015, https://doi.org/10.1007/978-3-319-19165-2.

[2] J. Galán, L. Samek, P. Verleysen, K. Verbeken, Y. Houbaert, Advanced high strength steels for automotive industry, Rev. Metal. (Madr.) 48 (2012) 118–131, https://doi.org/10.3989/revmetalm.1158.

[3] T.E. steel Organization, Eurofer: annual report. http://www.eurofer.org/News&Events/PublicationsLinksList/201705-AnnualReport.pdf, 2017.

[4] R.H. Petrov, L.A.I. Kestens, W.J. Kaluba, Y. Houbaert, Recrystallization and austenite formation in a cold rolled TRIP steel during ultra fast heating, Steel Grips 1 (2003) 289–293.

[5] T. Lolla, G. Cola, B. Narayanan, B. Alexandrov, S.S. Babu, Development of rapid heating and cooling (flash processing) process to produce advanced high strength steel microstructures, Mater. Sci. Technol. 27 (2011) 863–875, https://doi.org/10.1179/174328409x433813.

[6] R.H. Petrov, J. Sidor, L.A.I. Kestens, Texture formation in high strength low alloy steel reheated with ultrafast heating rates, Mater. Sci. Forum 702–703 (2012) 798–801. https://doi.org/10.4028/www.scientific.net/MSF.702-703.798.

[7] F.M. Castro Cerda, I. Sabirov, C. Goulas, J. Sietsma, A. Monsalve, R.H. Petrov, Austenite formation in 0.2% C and 0.45% C steels under conventional and ultrafast heating, Mater. Des. 116 (2017) 448–460, https://doi.org/10.1016/j.matdes.2016.12.009.

[8] V. Massardier, A. Ngansop, D. Fabrègue, J. Merlin, Identification of the parameters controlling the grain refinement of ultra-rapidly annealed low carbon Al-killed steels, Mater. Sci. Eng. A 527 (2010) 5654–5663, https://doi.org/10.1016/j.msea.2010.05.024.

[9] V. Massardier, A. Ngansop, D. Fabrègue, S. Cazottes, J. Merlin, Ultra-rapid intercritical annealing to improve deep drawability of low-carbon, al-killed steels, Metall. Mater. Trans. A 43 (2012) 2225–2236, https://doi.org/10.1007/s11661-012-1096-6.

[10] http://www.flashbainite.com/, 2011.

[11] F.M. Castro Cerda, C. Goulas, I. Sabirov, L.A.I. Kestens, R.H. Petrov, The effect of the pre-heating stage on the microstructure and texture of a cold rolled FeCMnAlSi steel under conventional and ultrafast heating, Mater. Char. 130 (2017) 188–197, https://doi.org/10.1016/j.matchar.2017.06.010.

[12] H. Li, K. Gai, L. He, C. Zhang, H. Cui, M. Li, Non-isothermal phase-transformation kinetics model for evaluating the austenization of 55CrMo steel based on Johnson – Mehl – Avrami equation, Mater. Des. 92 (2016) 731–741, https://doi.org/10.1016/j.matdes.2015.12.110.

[13] N. Li, J. Lin, D.S. Balint, T.A. Dean, Experimental characterisation of the effects of thermal conditions on austenite formation for hot stamping of boron steel, J. Mater. Process. Technol. 231 (2016) 254–264, https://doi.org/10.1016/j.jmatprotec.2015.12.008.

[14] M.A. Valdes-Tabernero, F. Vercruysse, I. Sabirov, R.H. Petrov, M.A. Monclús, J. M. Molina-Aldareguia, Effect of ultrafast heating on the properties of the microconstituents in a low-carbon steel, Metall. Mater. Trans. A 49 (2018) 3145–3150, https://doi.org/10.1007/s11661-018-4658-4.

[15] M. Ferry, D. Muljoni, D.P. Dunne, Recrystallization kinetics of low and ultra low carbon steels during high-rate annealing, ISIJ Int. 41 (2001) 1053–1060, https://doi.org/10.2355/isijinternational.41.1053.

[16] D. Muljono, M. Ferry, D.P. Dunne, Influence of heating rate on anisothermal recrystallization in low and ultra-low carbon steels, Mater. Sci. Eng. A 303 (2001) 90–99, https://doi.org/10.1016/S0921-5093(00)01882-7.

[17] F.M. Castro Cerda, C. Goulas, I. Sabirov, S. Papaefthymiou, A. Monsalve, R. H. Petrov, Microstructure, texture and mechanical properties in a low carbon steel after ultrafast heating, Mater. Sci. Eng. A 672 (2016) 108–120, https://doi.org/10.1016/j.msea.2016.06.056.

[18] A. Puype, Developing of Advanced High Strength Steel via Ultrafast Annealing, Master thesis, University of Ghent, 2014.

[19] M. Yonemura, H. Nishibata, T. Nishiura, N. Ooura, Y. Yoshimoto, K. Fujiwara, K. Kawano, T. Terai, Y. Inubushi, I. Inoue, K. Tono, M. Yabashi, Fine microstructure formation in steel under ultrafast heating, Sci. Rep. 9 (2019) 11241, https://doi.org/10.1038/s41598-019-47668-6.

[20] B. Hutchinson, J. Hagström, O. Karlsson, D. Lindell, M. Tornberg, F. Lindberg, M. Thuvander, Microstructures and hardness of as-quenched martensites (0.1–0.5%C), Acta Mater. 59 (2011) 5845–5858, https://doi.org/10.1016/j.actamat.2011.05.061.

[21] F. Vercruysse, Third Generation Advanced High Strength Steel by Ultrafast Annealing, Master Thesis, University of Ghent, 2016.

[22] Q. Meng, J. Li, H. Zheng, High-efficiency fast-heating annealing of a cold-rolled dual-phase steel, Mater. Des. 58 (2014) 194–197, https://doi.org/10.1016/j.matdes.2014.01.055.

[23] A. Kumar, S.K. Makineni, A. Dutta, C. Goulas, M. Steenbergen, R.H. Petrov, J. Sietsma, Design of high-strength and damage-resistant carbide-free fine bainitic steels for railway crossing applications, Mater. Sci. Eng. A 759 (2019) 210–223, https://doi.org/10.1016/j.msea.2019.05.043.

[24] A. Kumar, A. Dutta, S.K. Makineni, M. Herbig, R.H. Petrov, J. Sietsma, In-situ observation of strain partitioning and damage development in continuously cooled carbide-free bainitic steels using micro digital image correlation, Mater. Sci. Eng. A 757 (2019) 107–116, https://doi.org/10.1016/j.msea.2019.04.098.

[25] D. Quidort, Y.J.M. Brechet, A model of isothermal and non isothermal transformation kinetics of bainite in 0.5 % C steels, ISIJ Int. 42 (2002) 1010–1017, https://doi.org/10.2355/isijinternational.42.1010.

[26] R.H. Petrov, L.A.I. Kestens, Advanced high-strength steels: electron backscatter diffraction (EBSD), Encycl. Iron, Steel, Their Alloy (2015) 46–69, https://doi.org/10.1081/E-EISA-120050786.

[27] Y. Cao, H. Di, J. Zhang, J. Zhang, T. Ma, R.D.K. Mishra, An electron backscattered diffraction study on the dynamic recrystallization behavior of a nickel – chromium alloy (800H) during hot deformation, Mater. Sci. Eng. A 585 (2013) 71–85, https://doi.org/10.1016/j.msea.2013.07.037.

[28] W.C. Oliver, G.M. Pharr, An improved technique for determining hardness and elastic modulus using load and displacement sensing indentation experiments, J. Mater. Res. 7 (1992) 1564–1583, https://doi.org/10.1557/JMR.1992.1564.

[29] J. Huang, W.J. Poole, M. Militzer, Austenite formation during intercritical annealing, Metall. Mater. Trans. A 35 (2004) 3363–3375, https://doi.org/10.1007/s11661-004-0173-x.

[30] R.R. Mohanty, O.A. Girina, N.M. Fonstein, Effect of heating rate on the austenite formation in low-carbon high-strength steels annealed in the intercritical region, Metall. Mater. Trans. A 42 (2011) 3680–3690, https://doi.org/10.1007/s11661-011-0753-5.

[31] H. Azizi-Alizamini, M. Militzer, W.J. Poole, Austenite formation in plain low-carbon steels, Metall. Mater. Trans. A 42 (2011) 1544–1557, https://doi.org/10.1007/s11661-010-0551-5.

[32] P. Li, J. Li, Q. Meng, W. Hu, D. Xu, Effect of heating rate on ferrite recrystallization and austenite formation of cold-roll dual phase steel, J. Alloys Compd. 578 (2013) 320–327, https://doi.org/10.1016/j.jallcom.2013.05.226.

[33] D. Muljono, M. Ferry, D.P. Dunne, Influence of heating rate on anisothermal recrystallization in low and ultra-low carbon steels, Mater. Sci. Eng. A 303 (2001) 90–99, https://doi.org/10.1016/S0921-5093(00)01882-7.

[34] P. Li, J. Li, Q. Meng, W. Hu, D. Xu, Effect of heating rate on nucleation and growth of austenite in cold rolled dual phase steel, Ironmak. Steelmak. 42 (2014) 81–87, https://doi.org/10.1179/1743281214y.0000000228.

[35] F.M. Castro Cerda, F. Vercruysse, T.N. Minh, L.A.I. Kestens, A. Monsalve, R. H. Petrov, The effect of heating rate on the recrystallization behavior in cold rolled ultra low carbon steel, Steel Res. 87 (2016) 1–9, https://doi.org/10.1002/srin.201600351.

[36] M.A. Valdes-Tabernero, R.H. Petrov, M.A. Monclús, J.M. Molina-Aldareguia, I. Sabirov, The effect of soaking time after ultrafast heating on the microstructure and mechanical behavior of a low carbon steel, Mater. Sci. Eng. A 765 (2019) 138276, https://doi.org/10.1016/j.msea.2019.138276.

[37] M. Calcagnotto, D. Ponge, E. Demir, D. Raabe, Orientation gradients and geometrically necessary dislocations in ultrafine grained dual-phase steels studied by 2D and 3D EBSD, Mater. Sci. Eng. A 527 (2010) 2738–2746, https://doi.org/10.1016/j.msea.2010.01.004.

[38] D.A. Hughes, N. Hansen, D.J. Bammann, Geometrically necessary boundaries , incidental dislocation boundaries and geometrically necessary dislocations, Scripta Mater. 48 (2003) 147–153, https://doi.org/10.1016/S1359-6462(02)00358-5.

[39] Y. Deng, H. Di, J. Zhang, R.D.K. Misra, Stretching the mechanical properties in a 590 MPa ferrite-martensite dual-phase steel through rapid heating, Metall. Res. Technol. 114 (2017) 503, https://doi.org/10.1051/metal/2017038.

[40] M.D. Taylor, K.S. Choi, X. Sun, D.K. Matlock, C.E. Packard, L. Xu, F. Barlat, Correlations between nanoindentation hardness and macroscopic mechanical properties in DP980 steels, Mater. Sci. Eng. A 597 (2014) 431–439, https://doi.org/10.1016/j.msea.2013.12.084.

[41] H.K.D.H. Bhadeshia, R.W.K. Honeycombe, Steels: Microstructure and Properties, third ed., Elsevier Ltd, Oxford, 2006 (n.d).

[42] Q. Furnemont, M. Kempf, P.J. Jacques, M. Göken, F. Delannay, On the measurement of the nanohardness of the constitutive phases of TRIP-assisted multiphase steels, Mater. Sci. Eng. A 328 (2002) 26–32, https://doi.org/10.1016/S0921-5093(01)01689-6.

[43] Y. Mazaheri, A. Kermanpur, A. Najafizadeh, Nanoindentation study of ferrite-martensite dual phase steels developed by a new thermomechanical processing, Mater. Sci. Eng. A 639 (2015) 8–14, https://doi.org/10.1016/j.msea.2015.04.098.

[44] J. Hidalgo, K.O. Findley, M.J. Santofimia, Thermal and mechanical stability of retained austenite surrounded by martensite with different degrees of tempering, Mater. Sci. Eng. A 690 (2017) 337–347, https://doi.org/10.1016/j.msea.2017.03.017.

[45] P.H. Chang, A.G. Preban, The effect of ferrite grain size and martensite volume fraction on the tensile properties of dual phase steel, Acta Metall. 33 (1985) 897–903, https://doi.org/10.1016/0001-6160(85)90114-2.

[46] M. Mazinani, W.J. Poole, Effect of martensite plasticity on the deformation behavior of a low-carbon dual-phase steel, Metall. Mater. Trans. A 38 (2007) 328–339, https://doi.org/10.1007/s11661-006-9023-3.

[47] G. Krauss, Martensite in steel: strength and structure, Mater. Sci. Eng. A 273–275 (1999) 40–57, https://doi.org/10.1016/S0921-5093(99)00288-9.

[48] H.-C. Chen, G.-W. Cheng, Effect of martensite strength on the tensile strength of dual phase steels, J. Mat. 24 (1994) 1991–1994, https://doi.org/10.1007/BF02385411.

[49] M. Asadi, B.C. De Cooman, H. Palkowski, Influence of martensite volume fraction and cooling rate on the properties of thermomechanically processed dual phase steel, Mater. Sci. Eng. A 538 (2012) 42–52, https://doi.org/10.1016/j.msea.2012.01.010.

[50] A.R. Marder, Effect of heat treatment on the properties and structure of molybdenum and vanadium dual-phase Steels, Metall. Trans. A. 12 (1981) 1569–1579, https://doi.org/10.1007/BF02643562.

[51] R.G. Davies, Influence of martensite composition and content on the properties of dual phase steels, Metall. Trans. A. 9 (1978) 671–679, https://doi.org/10.1007/BF02659924.

[52] G.E. Dieter, Mechanical Metallurgy., Third ed., McGraw-Hill Education, New York, 1986.
[53] I.B. Timokhina, P.D. Hodgson, E.V. Pereloma, Effect of microstructure on the stability of retained austenite in transformation-induced-plasticity steels, Metall. Mater. Trans. A 35 (2004) 2331–2341, https://doi.org/10.1007/s11661-006-0213-9.
[54] N.C. Goel, S. Sangal, K. Tangri, A theoretical model for the flow behavior of commercial dual-phase steels containing metastable retained austenite: Part I. derivation of flow curve equations, Metall. Trans. A. 16 (1985) 2013–2021, https://doi.org/10.1007/BF02662402.

5. CONCLUSIONS

5. Conclusions

The following main conclusions can be drawn from the outcomes of this PhD thesis:

1- Ultrafast heating process applied to a low carbon steel (Fe-0-19C-1.61Mn-1.06Al-0.5Si) leads to the formation of a complex, hierarchic microstructure, where martensite and retained austenite are embedded into ferritic matrix. In turn, the ferritic matrix consists of recrystallized and non-recrystallized ferritic grains. The volume fraction of retained austenite is very low (≤ 2.5 %) compared to that of other microstructural constituents.

2- The processing parameters, such as heating rate, peak temperature and soaking time at peak temperature greatly affect the grain size, morphology, distribution and volume fraction of the different microconstituents (recrystallized and non-recrystallized ferrite, martensite and retained austenite). The effect of soaking time on microstructure is more pronounced in the UFH samples in comparison with the samples heated at conventional heating rate. The increase in both the peak temperature and soaking time during UFH process promote austenite formation and growth, i.e. the increase in the volume fraction of martensite. The average grain size of the recrystallized ferritic grains and their volume fraction also tend to increase with both peak temperature and soaking time during UFH processing.

3- The nanomechanical response of the ferritic matrix is governed by the internal structure of the microconstituents independently on the applied processing parameters. The non-recrystallized ferrite shows higher nanohardness than its recrystallized counterpart due to the higher dislocation density of the former. On the other hand, martensite response is highly influenced by the heat treatment parameters, which affect the size and fraction of martensite and, therefore, its final carbon content.

4- The ultrafast heating rates enhance the tensile mechanical properties of the material compared to conventional ones without a significant reduction in ductility. The final mechanical properties are dictated by the microstructure: volume fraction and grain size of martensite, non-recrystallized ferrite and recrystallized ferrite. Increasing peak temperatures favours the strengthening of the material due to enhanced fraction of martensite. However, the ductility is considerably reduced with both temperature and soaking time due the lower fraction of the ductile ferritic phase.
5- The application of the ultrafast heating rate and short soaking times (< 3 s) results in the best combination of strength and ductility. An industrial processing window of ± 10 ºC may lead to some heterogeneity of the microstructure in the processed sheets without reduction in the overall macro-mechanical performance of the steel.

6. FUTURE WORK

6. Future work

As a future work, the following studies can be proposed:

- In order to fully understand and later on optimize the UFH processing, the effect of other processing parameters (such as the cooling rate) on microstructure and mechanical properties should be thoroughly investigated. Such studies are necessary for commercialization of UFH process.

- As it has been observed in AHSS, the Mn content can significantly affect the grain size of the different microconstituents due to the strong solute drag effect observed. Therefore, varying content of the alloying elements, specially Mn, appears as another tool for intelligent microstructural design in steels via ultra-fast processing.

- The vast majority of studies of the UFH process are focused on the microstructure and basic mechanical properties. However, AHSS are widely employed in the automotive industry, where components operate under cyclic loading. Therefore, it may be interesting to focus next studies on the relation between the microstructure formed and the fatigue behavior of the material.

No reports about formability/impact resistance, which simulates industrial production environment, are available in the current literature. Hence, deeper investigations of these properties would be beneficial for the development and implementation of the UFH process by industrial actors.

7. REFERENCES

7. References

[1] N. Fonstein, Advanced High Strength Sheet Steels: Physical Metallurgy, Design, Processing, and Properties, Springer, 2015. doi:10.1007/978-3-319-19165-2.

[2] N. Fonstein, Dual-phase steels, Automot. Steels Des. Metall. Process. Appl. (2016) 169–216. doi:10.1016/B978-0-08-100638-2.00007-9.

[3] B. Engl, L. Keßler, F.-J. Lenze, T.W. Schaumann, Recent Experience with the Application of TRIP and Other Advanced Multiphase Steels, SAE Tech. Pap. Ser. 1 (2010). doi:10.4271/982408.

[4] P.K. Mallick, Materials, design and manufacturing for lightweight vehicles, 1st ed., Woodhead Publishing, Boca Raton Boston New York Washington, DC, 2010. doi:10.1533/9781845697822.

[5] E. De Moor, P.J. Gibbs, J.G. Speer, D.K. Matlock, J.G. Schroth, Strategies for third-generation advanced high-strength steel development, in: Iron Steel Technol., 2010: pp. 133–144.

[6] T.E. steel Organization, Eurofer: Annual Report, (2017). http://www.eurofer.org/News&Events/PublicationsLinksList/201705-AnnualReport.pdf.

[7] Transport emissions, (n.d.). https://ec.europa.eu/clima/policies/transport_en.

[8] Reducing CO2 emissions from passenger cars, (n.d.). https://ec.europa.eu/clima/policies/transport/vehicles/cars_en.

[9] J. Galán, L. Samek, P. Verleysen, K. Verbeken, Y. Houbaert, Advanced high strength steels for automotive industry, Rev. Metal. 48 (2012) 118–131.

doi:10.3989/revmetalm.1158.

[10] J.G. Speer, D.K. Matlock, B.C. De Cooman, J.G. Schroth, Carbon partitioning into austenite after martensite transformation, Acta Mater. 51 (2003) 2611–2622. doi:10.1016/S1359-6454(03)00059-4.

[11] J.G. Speer, E. De Moor, A.J. Clarke, Critical Assessment 7: Quenching and partitioning, Mater. Sci. Technol. 31 (2015) 3–9. doi:10.1179/1743284714Y.0000000628.

[12] D.K. Matlock, J.G. Speer, E. De Moor, P.J. Gibbs, Recent developments in advanced high strength sheet steels for automotive applications: an overview, JESTECH. 15 (2012) 1–12.

[13] D. De Knijf, R.H. Petrov, C. Föjer, L.A.I. Kestens, Effect of fresh martensite on the stability of retained austenite in quenching and partitioning steel, Mater. Sci. Eng. A. 615 (2014) 107–115. doi:10.1016/j.msea.2014.07.054.

[14] I. De Diego-Calderón, M.J. Santofimia, J.M. Molina-Aldareguia, M.A. Monclús, I. Sabirov, Deformation behavior of a high strength multiphase steel at macro- and micro-scales, Mater. Sci. Eng. A. 611 (2014) 201–2011. doi:10.1016/j.msea.2014.05.068.

[15] W.L. Haworth, J.G. Parr, The effect of rapid heating on the alpha-gamma transformation of iron, Trans AMS. 58 (1965) 476–488.

[16] R.A. Grange, The Rapid Heat Treatment of Steel, Metall. Trans. 2 (1971) 65–78. doi:10.1007/BF02662639.

[17] V.N. Gridnev, S.P. Oshkaderov, Use of fast heat-treatment for improving the structural strength of steels, Met. Sci. Heat Treat. 29 (1986) 823–825. doi:10.1007/BF00707749.

[18] T. Lolla, G. Cola, B. Narayanan, B. Alexandrov, S.S. Babu, Development of rapid heating and cooling (flash processing) process to produce advanced high strength steel microstructures, Mater. Sci. Technol. 27 (2011) 863–875. doi:10.1179/174328409x433813.

[19] R.H. Petrov, J. Sidor, W.J. Kaluba, L.A.I. Kestens, Grain refinement of a cold Rolled

TRIP assisted steel after ultra short annealing, Mater. Sci. Forum. 715–716 (2012) 661–666. doi:10.4028/www.scientific.net/MSF.715-716.661.

[20] R.H. Petrov, J. Sidor, L.A.I. Kestens, Texture formation in high strength low alloy steel reheated with ultrafast heating rates, Mater. Sci. Forum. 702–703 (2012) 798–801. doi:10.4028/www.scientific.net/MSF.702-703.798.

[21] F.M. Castro Cerda, C. Goulas, I. Sabirov, S. Papaefthymiou, A. Monsalve, R.H. Petrov, Microstructure, texture and mechanical properties in a low carbon steel after ultrafast heating, Mater. Sci. Eng. A. 672 (2016) 108–120. doi:10.1016/j.msea.2016.06.056.

[22] F.M. Castro Cerda, F. Vercruysse, T.N. Minh, L.A.I. Kestens, A. Monsalve, R.H. Petrov, The effect of heating rate on the recrystallization behavior in cold rolled ultra low carbon steel, Steel Res. 87 (2016) 1–9. doi:10.1002/srin.201600351.

[23] F.M. Castro Cerda, I. Sabirov, C. Goulas, J. Sietsma, A. Monsalve, R.H. Petrov, Austenite formation in 0.2% C and 0.45% C steels under conventional and ultrafast heating, Mater. Des. 116 (2017) 448–460. doi:10.1016/j.matdes.2016.12.009.

[24] http://www.flashbainite.com/, (2011).

[25] J. Huang, W.J. Poole, M. Militzer, Austenite formation during intercritical annealing, Metall. Mater. Trans. A. 35 (2004) 3363–3375. doi:10.1007/s11661-004-0173-x.

[26] C. Lesch, P. Álvarez, W. Bleck, J. Gil Sevillano, Rapid transformation annealing: A novel method for grain refinement of cold-rolled low-carbon steels, Metall. Mater. Trans. A. 38 (2007) 1882–1890. doi:10.1007/s11661-006-9052-y.

[27] M. Militzer, H. Azizi-Alizamini, V.C. Sangem, Ultra-Fine Grained Dual-Phase Steels, J. Ultrafine Grained Nanostructured Mater. 45 (2012) 1–6. doi:10.7508/jufgnsm.2012.01.001.

[28] H. Guo, M. Enomoto, Effects of substitutional solute accumulation at α/γ boundaries on the growth of ferrite in low carbon steels, Metall. Mater. Trans. A. 38 (2007) 1152–1161. doi:10.1007/s11661-007-9139-0.

[29] M. Thompson, M. Ferry, P.A. Manohar, Simulation of Hot-band Microstructure of

C-Mn Steels during High Speed Cooling., ISIJ Int. 41 (2001) 891–899. doi:10.2355/isijinternational.41.891.

[30] N. Yoshinaga, K. Ushioda, A. Itami, O. Akisue, α+γ and γ Phases Annealing In UItra Low-carbon Sheet Steels, 34 (1994) 33–42. doi:10.2355/isijinternational.34.33.

[31] C. Goulas, Developing novel heat treatments for automotive spring steels: Phase transformations, microstructure and performance., PhD Thesis, Delft University of Technology, 2018. doi:10.4233/uuid:ce01998a-0830-494e-a403-9f0696aa0dce.

[32] C.P. Scott, B. Shalchi Amirkhiz, I. Pushkareva, F. Fazeli, S.Y.P. Allain, H. Azizi-Alizamini, New insights into martensite strength and the damage behaviour of dual phase steels, Acta Mater. 159 (2018) 112–122. doi:10.1016/j.actamat.2018.08.010.

[33] M. Ferry, D. Muljoni, D.P. Dunne, Recrystallization kinetics of low and ultra low carbon steels during high-rate annealing, ISIJ Int. 41 (2001) 1053–1060. doi:10.2355/isijinternational.41.1053.

[34] D. Muljono, M. Ferry, D.P. Dunne, Influence of heating rate on anisothermal recrystallization in low and ultra-low carbon steels, Mater. Sci. Eng. A. 303 (2001) 90–99. doi:10.1016/S0921-5093(00)01882-7.

[35] V. Massardier, A. Ngansop, D. Fabrègue, J. Merlin, Identification of the parameters controlling the grain refinement of ultra-rapidly annealed low carbon Al-killed steels, Mater. Sci. Eng. A. 527 (2010) 5654–5663. doi:10.1016/j.msea.2010.05.024.

[36] B. Bandi, J. van Krevel, N. Aslam, P. Srirangam, A Model and Experimental Validation to Predict Heating Rates for Overlap Between Ferrite Recrystallization and Austenite Transformation in Dual Phase Steel Manufacture, JOM. 71 (2019) 1386–1395. doi:10.1007/s11837-019-03358-2.

[37] D. Xu, J. Li, Q. Meng, Y. Liu, P. Li, Effect of heating rate on microstructure and mechanical properties of TRIP-aided multiphase steel, J. Alloys Compd. 614 (2014) 94–101. doi:10.1016/j.jallcom.2014.06.075.

[38] G. Liu, J. Li, S. Zhang, J. Wang, Q. Meng, Dilatometric study on the recrystallization and austenization behavior of cold-rolled steel with different heating rates, J. Alloys Compd. 666 (2016) 309–316. doi:10.1016/j.jallcom.2016.01.137.

[39] P. Li, J. Li, Q. Meng, W. Hu, D. Xu, Effect of heating rate on ferrite recrystallization and austenite formation of cold-roll dual phase steel, J. Alloys Compd. 578 (2013) 320–327. doi:10.1016/j.jallcom.2013.05.226.

[40] H. Azizi-Alizamini, M. Militzer, W.J. Poole, Austenite formation in plain low-carbon steels, Metall. Mater. Trans. A. 42 (2011) 1544–1557. doi:10.1007/s11661-010-0551-5.

[41] L.S. Thomas, D.K. Matlock, Formation of Banded Microstructures with Rapid Intercritical Annealing of Cold-Rolled Sheet Steel, Metall. Mater. Trans. A. 49 (2018) 4456–4473. doi:10.1007/s11661-018-4742-9.

[42] A. Karmakar, M. Mandal, A. Mandal, M. Basiruddin Sk, S. Mukherjee, D. Chakrabarti, Effect of Starting Microstructure on the Grain Refinement in Cold-Rolled Low-Carbon Steel During Annealing at Two Different Heating Rates, Metall. Mater. Trans. A. 47 (2016) 268–281. doi:10.1007/s11661-015-3248-y.

[43] J.P. Pedraza, R. Landa-Mejia, O. Garcia-Rincon, C.I. Garcia, The Effect of Rapid Heating and Fast Cooling on the Transformation Behavior and Mechanical Properties of an Advanced High Strength Steel (AHSS), Metals (Basel). 9 (2019) 545. doi:10.3390/met9050545.

[44] H. Azizi-Alizamini, M. Militzer, W.J. Poole, Formation of ultrafine grained dual phase steels through rapid heating, ISIJ Int. 51 (2011) 958–964. doi:10.2355/isijinternational.51.958.

[45] G. Liu, S. Zhang, J. Li, J. Wang, Q. Meng, Fast-heating for intercritical annealing of cold-rolled quenching and partitioning steel, Mater. Sci. Eng. A. 669 (2016) 387–395. doi:10.1016/j.msea.2016.05.106.

[46] P. Li, J. Li, Q. Meng, W. Hu, D. Xu, Effect of heating rate on nucleation and growth of austenite in cold rolled dual phase steel, Ironmak. Steelmak. 42 (2014) 81–87. doi:10.1179/1743281214y.0000000228.

[47] G. Liu, S. Zhang, Q. Meng, J. Wang, J. Li, Effect of heating rate on microstructural evolution and mechanical properties of cold-rolled quenching and partitioning steel, Ironmak. Steelmak. 44 (2017) 202–209. doi:10.1080/03019233.2016.1209887.

[48] X.C. Xiong, B. Chen, M.X. Huang, J.F. Wang, L. Wang, The effect of morphology on the stability of retained austenite in a quenched and partitioned steel, Scr. Mater. 68 (2013) 321–324. doi:10.1016/j.scriptamat.2012.11.003.

[49] M. Kulakov, W.J. Poole, M. Militzer, The effect of the initial microstructure on recrystallization and austenite formation in a DP600 steel, Metall. Mater. Trans. A. 44 (2013) 3564–3576. doi:10.1007/s11661-013-1721-z.

[50] V. Andrade-Carozzo, P.J. Jacques, Interactions between Recrystallisation and Phase Transformations during Annealing of Cold Rolled Nb-Added TRIP-Aided Steels, Mater. Sci. Forum. 539–543 (2007) 4649–4654. doi:10.4028/www.scientific.net/msf.539-543.4649.

[51] A.C.C. Reis, L. Bracke, R.H. Petrov, W.J. Kaluba, L.A.I. Kestens, Grain refinement and texture change in interstitial free steels after severe rolling and ultra-short annealing, ISIJ Int. 43 (2003) 1260–1267. doi:10.40210.2355/isijinternational.43.1260.

[52] L.A.I. Kestens, A.C.D. Reis, W.J. Kaluba, Y. Houbaert, Grain Refinement and Texture Change in Interstitial Free Steels after Severe Rolling and Ultra-Short Annealing, Mater. Sci. Forum. 467–470 (2004) 287–292. doi:10.4028/www.scientific.net/MSF.467-470.287.

[53] F.M. Castro Cerda, L.A.I. Kestens, R.H. Petrov, “ Flash ” Annealing in a Cold-Rolled Low Carbon Steel Alloyed with Cr , Mn , Mo , and Nb : Part II — Anisothermal Recrystallization and Transformation Textures, Steel Res. Int. 90 (2019) 1–13. doi:10.1002/srin.201800277.

[54] F.M. Castro Cerda, C. Goulas, I. Sabirov, L.A.I. Kestens, R.H. Petrov, The effect of the pre-heating stage on the microstructure and texture of a cold rolled FeCMnAlSi steel under conventional and ultrafast heating, Mater. Charact. 130 (2017) 188–197. doi:10.1016/j.matchar.2017.06.010.

[55] F.M. Castro Cerda, L.A.I. Kestens, A. Monsalve, R.H. Petrov, The Effect of Ultrafast Heating in Cold-Rolled Low Carbon Steel : Recrystallization and Texture Evolution, Metals (Basel). 6 (2016) 288–299. doi:10.3390/met6110288.

[56] T. Senuma, K. Kawasaki, Y. Takemoto, Recrystallization Behavior and Texture

Formation of Rapidly Annealed Cold-Rolled Extralow Carbon Steel Sheets, Mater. Trans. 47 (2006) 1769–1775. doi:10.2320/matertrans.47.1769.

[57] R.H. Petrov, F. Hajyakbari, F.R. Saz, J. Sidor, M.J. Santofimia, J. Sietsma, L.A.I. Kestens, Microstructure and Properties of Ultrafast Annealed High Strength Steel, Mater. Sci. Forum. 753 (2013) 554–558. doi:10.4028/www.scientific.net/MSF.753.554.

[58] D. De Knijf, A. Puype, C. Föjer, R.H. Petrov, The influence of ultra-fast annealing prior to quenching and partitioning on the microstructure and mechanical properties, Mater. Sci. Eng. A. 627 (2015) 182–190. doi:10.1016/j.msea.2014.12.118.

[59] I. Samajdar, B. Verlinden, P. Van Houtte, D. Vanderschueren, γ -Fibre recrystallization texture in IF-steel : an investigation on the recrystallization mechanisms, Mater. Sci. Eng. A. 238 (1997) 343–350. doi:10.1016/S0921-5093(97)00455-3.

[60] J. Kang, B. Bacroix, H. Réglé, K.H. Oh, H. Lee, Effect of deformation mode and grain orientation on misorientation development in a body-centered cubic steel, Acta Mater. 55 (2007) 4935–4946. doi:10.1016/j.actamat.2007.05.014.

[61] R.H. Petrov, L.A.I. Kestens, Y. Houbaert, Recrystallization of a Cold Rolled Trip-assisted Steel during Reheating for Intercritical Annealling., Isij. 41 (2001) 883–890. doi:10.2355/isijinternational.41.883.

[62] M.J. Holzweissig, J. Lackmann, S. Konrad, M. Schaper, T. Niendorf, Influence of Short Austenitization Treatments on the Mechanical Properties of Low-Alloy Steels for Hot Forming Applications, Metall. Mater. Trans. A. 46 (2015) 3199–3207. doi:10.1007/s11661-015-2907-3.

[63] Y. Deng, H. Di, J. Zhang, R.D.K. Misra, Stretching the mechanical properties in a 590 MPa ferrite-martensite dual-phase steel through rapid heating, Metall. Res. Technol. 114 (2017) 503. doi:10.1051/metal/2017038.

[64] Q. Meng, J. Li, H. Zheng, High-efficiency fast-heating annealing of a cold-rolled dual-phase steel, Mater. Des. 58 (2014) 194–197. doi:10.1016/j.matdes.2014.01.055.

[65] S. Shim, H. Bei, E.P. George, G.M. Pharr, A different type of indentation size effect, Scr. Mater. 59 (2008) 1095–1098. doi:10.1016/j.scriptamat.2008.07.026.

[66] T. Ohmura, K. Tsuzaki, S. Matsuoka, Evaluation of the matrix strength of Fe-0.4 wt% C tempered martensite using nanoindentation techniques, Philos. Mag. 82 (2002) 1903–1910. doi:10.1080/01418610208235702.

[67] T. Ohmura, T. Hara, K. Tsuzaki, Evaluation of temper softening behavior of Fe–C binary martensitic steels by nanoindentation, Scr. Mater. 49 (2003) 1157–1162. doi:10.1016/j.scriptamat.2003.08.025.

[68] Y. Mazaheri, A. Kermanpur, A. Najafizadeh, Nanoindentation study of ferrite-martensite dual phase steels developed by a new thermomechanical processing, Mater. Sci. Eng. A. 639 (2015) 8–14. doi:10.1016/j.msea.2015.04.098.

[69] G. Rosenberg, I. Sinaiová, Ľ. Juhar, Effect of microstructure on mechanical properties of dual phase steels in the presence of stress concentrators, Mater. Sci. Eng. A. 582 (2013) 347–358. doi:10.1016/j.msea.2013.06.035.

[70] M.D. Taylor, K.S. Choi, X. Sun, D.K. Matlock, C.E. Packard, L. Xu, F. Barlat, Correlations between nanoindentation hardness and macroscopic mechanical properties in DP980 steels, Mater. Sci. Eng. A. (2014). doi:10.1016/j.msea.2013.12.084.

[71] Q. Furnemont, M. Kempf, P.J. Jacques, M. Göken, F. Delannay, On the measurement of the nanohardness of the constitutive phases of TRIP-assisted multiphase steels, Mater. Sci. Eng. A. 328 (2002) 26–32. doi:10.1016/S0921-5093(01)01689-6.

[72] B. Hutchinson, J. Hagström, O. Karlsson, D. Lindell, M. Tornberg, F. Lindberg, M. Thuvander, Microstructures and hardness of as-quenched martensites (0.1–0.5%C), Acta Mater. 59 (2011) 5845–5858. doi:10.1016/j.actamat.2011.05.061.

[73] B.B. He, M.X. Huang, Z.Y. Liang, A.H.W. Ngan, H.W. Luo, J. Shi, W.Q. Cao, H. Dong, Nanoindentation investigation on the mechanical stability of individual austenite grains in a medium-Mn transformation-induced plasticity steel, Scr. Mater. 69 (2013) 215–218. doi:10.1016/j.scriptamat.2013.03.030.

[74] N. Nakada, Y. Arakawa, K.S. Park, T. Tsuchiyama, S. Takaki, Dual phase structure formed by partial reversion of cold-deformed martensite, Mater. Sci. Eng. A. 553 (2012) 128–133. doi:10.1016/j.msea.2012.06.001.

[75] R.H. Petrov, F. HajyAkbary, J. Sidor, M.J. Santofimia, J. Sietsma, L.A.I. Kestens, Ultra-fast annealing of high strength steel, Int. Virtual J. Mach. Technol. Mater. 8 (2012) 68–71.

[76] A.C.D. Reis, L. Bracke, R.H. Petrov, W.J. Kaluba, L.A.I. Kestens, Grain refinement and texture change in interstitial free steels after severe rolling and ultra-short annealing, ISIJ Int. 43 (2003) 1260–1267. doi:10.4028/www.scientific.net/MSF.467-470.287.

[77] A. Puype, Developing of advanced high strength steel via ultrafast annealing, Master thesis, University of Ghent, 2014.

[78] R.R. Mohanty, O.A. Girina, N.M. Fonstein, Effect of heating rate on the austenite formation in low-carbon high-strength steels annealed in the intercritical region, Metall. Mater. Trans. A. 42 (2011) 3680–3690. doi:10.1007/s11661-011-0753-5.

[79] J. Stockemer, P. Vanden Brande, Recrystallization of a cold-rolled low-carbon steel by cold-plasma-discharge rapid annealin, Metall. Mater. Trans. A. 34 (2003) 1341. doi:10.1007/s11661-003-0245-3.

[80] F. Vercruysse, Third generation advanced high strength steel by ultrafast annealing, Master thesis, University of Ghent, 2016.

[81] L. Barbé, K. Verbeken, E. Wettinck, Effect of the Addition of P on the Mechanical Properties of Low Alloyed TRIP Steels, ISIJ Int. 46 (2006) 1251–1257. doi:10.2355/isijinternational.46.1251.

[82] E.M. Bellhouse, J.R. McDermid, Effect of continuous galvanizing heat treatments on the microstructure and mechanical properties of high Al-low Si transformation induced plasticity steels, Metall. Mater. Trans. A. 41 (2010) 1460–1473. doi:10.1007/s11661-010-0185-7.

[83] B.C. De Cooman, Structure-properties relationship in TRIP steels containing carbide-free bainite, Curr. Opin. Solid State Mater. Sci. 8 (2004) 285–303.

doi:10.1016/j.cossms.2004.10.002.

[84] G. Krauss, Steels: Processing, Structure, and Performance, 2nd ed., ASM International, Materials Park, Ohio 44073-0002, 2015.

[85] D. Quidort, Y.J.M. Brechet, A model of isothermal and non isothermal transformation kinetics of bainite in 0.5 % C steels, ISIJ Int. 42 (2002) 1010–1017. doi:10.2355/isijinternational.42.1010.

[86] V. Randle, Tutorial review Electron backscatter diffraction : Strategies for reliable data acquisition and processing, Mater. Charact. 60 (2009) 913–922. doi:10.1016/j.matchar.2009.05.011.

[87] R.H. Petrov, L.A.I. Kestens, Advanced high-strength steels: electron backscatter diffraction (EBSD), Encycl. Iron, Steel, Their Alloy. (2015) 46–69. doi:10.1081/E-EISA-120050786.

[88] Y. Cao, H. Di, J. Zhang, J. Zhang, T. Ma, R.D.K. Mishra, An electron backscattered diffraction study on the dynamic recrystallization behavior of a nickel – chromium alloy (800H) during hot deformation, Mater. Sci. Eng. A. 585 (2013) 71–85. doi:10.1016/j.msea.2013.07.037.

[89] D.P. Field, P.B. Trivedi, S.I. Wright, M. Kumar, Analysis of local orientation gradients in deformed single crystals, Ultramicroscopy. 103 (2005) 33–39. doi:10.1016/j.ultramic.2004.11.016.

[90] O. Engler, V. Randle, Introduction to texture analysis: macrostructure, microstructure and orientation mapping, 2nd ed., CRC Press, Boca Raton, 2009.

[91] C.F. Jatczak, Retained Austenite and Its Measurement by X-Ray Diffraction, SAE Tech. Pap. (1980). doi:10.4271/800426.

[92] N.H. van Dijk, A.M. Butt, L. Zhao, J. Sietsma, S.E. Offerman, J.P. Wright, S. van der Zwaag, Thermal stability of retained austenite in TRIP steels studied by synchrotron X-ray diffraction during cooling, Acta Mater. 53 (2005) 5439–5447. doi:10.1016/j.actamat.2005.08.017.

[93] R.Z. Valiev, I. Sabirov, A.P. Zhilyaev, T.G. Langdon, Bulk Nanostructured Metals for Innovative Applications, JOM. 64 (2012) 1134–1142. doi:10.1007/s11837-012-

0427-9.

[94] R.R. Keller, R.H. Geiss, Transmission EBSD from 10 nm domains in a scanning, J. Microsc. 245 (2012) 245–251. doi:10.1111/j.1365-2818.2011.03566.x.

[95] S. Suzuki, Features of Transmission EBSD and its Application, JOM. 65 (2013) 1254–1263. doi:10.1007/s11837-013-0700-6.

[96] P.W. Trimby, Orientation mapping of nanostructured materials using transmission Kikuchi diffraction in the scanning electron microscope, Ultramicroscopy. 120 (2012) 16–24. doi:10.1016/j.ultramic.2012.06.004.

[97] P.W. Trimby, Y. Cao, Z. Chen, S. Han, K.J. Hemker, J. Lian, X. Liao, P. Rottmann, S. Samudrala, J. Sun, J.T. Wang, J. Wheeler, J.M. Cariney, Characterizing deformed ultrafine-grained and nanocrystalline materials using transmission Kikuchi diffraction in a scanning electron microscope, Acta Mater. 62 (2014) 69–80. doi:10.1016/j.actamat.2013.09.026.

[98] N. Mortazavi, C. Geers, M. Esmaily, V. Babic, M. Sattari, K. Lindgren, P. Malmberg, B. Jönsson, M. Halvarsson, J.E. Svensson, I. Panas, L.G. Johansson, Interplay of water and reactive elements in oxidation of alumina-forming alloys, Nat. Mater. 17 (2018) 610–617. doi:10.1038/s41563-018-0105-6.

[99] N. Mortazavi, M. Esmaily, M. Halvarsson, The capability of Transmission Kikuchi Diffraction technique for characterizing nano-grained oxide scales formed on a FeCrAl stainless steel, Mater. Lett. (2015). doi:10.1016/j.matlet.2015.02.008.

[100] D. Wang, H. Kahn, F. Ernst, A.H. Heuer, “Colossal” interstitial supersaturation in delta ferrite in stainless steels: (II) low-temperature nitridation of the 17-7 PH alloy, Acta Mater. 124 (2017) 237–246. doi:10.1016/j.actamat.2016.11.004.

[101] C. Hofer, V. Bliznuk, A. Verdiere, R.H. Petrov, F. Winkelhofer, H. Clemens, S. Primig, High-resolution characterization of the martensite-austenite constituent in a carbide-free bainitic steel, Mater. Charact. 144 (2018) 182–190. doi:10.1016/j.matchar.2018.07.011.

[102] K. Tugcu, G. Sha, X.Z. Liao, P.W. Trimby, J.H. Xia, M.Y. Murashkin, Y. Xie, R.Z. Valiev, S.P. Ringer, Enhanced grain refinement of an Al – Mg – Si alloy by high-

pressure torsion processing at 100 ◦ C, Mater. Sci. Eng. A. 552 (2012) 415–418. doi:10.1016/j.msea.2012.05.063.

[103] G. Sha, K. Tugcu, X. Liao, P.W. Trimby, M.Y. Murashkin, R.Z. Valiev, S.P. Ringer, Strength, grain refinement and solute nanostructures of an Al–Mg–Si alloy (AA6060) processed by high-pressure torsion, Acta Mater. 63 (2014) 169–179. doi:10.1016/j.actamat.2013.10.022.

[104] J.L. Sun, P.W. Trimby, X. Si, X.Z. Liao, N.R. Tao, J.T. Wang, Nano twins in ultrafine-grained Ti processed by dynamic plastic deformation, Scr. Mater. 68 (2013) 475–478. doi:10.1016/j.scriptamat.2012.11.025.

[105] J. Kacher, P. Elizaga, S.D. House, K. Hattar, M. Nowell, I.M. Robertson, A Thermal stability of Ni / NiO multilayers, Mater. Sci. Eng. A. 568 (2013) 49–60. doi:10.1016/j.msea.2013.01.033.

[106] W.C. Oliver, G.M. Pharr, An improved technique for determining hardness and elastic modulus using load and displacement sensing indentation experiments, J. Mater. Res. 7 (1992) 1564–1583. doi:10.1557/JMR.1992.1564.

ANNEX I

List of publications

- M.A. Valdes-Tabernero, F. Vercruysse, I. Sabirov, R.H. Petrov, M.A. Monclus, J.M. Molina-Aldareguia. "Effect of Ultrafast Heating on the Properties of the Microconstituents in a Low-Carbon Steel", Metallurgical and Materials Transactions A 49 (2018) 3145-3150, https://doi.org/10.1007/s11661-018-4658-4

  Article published in highly ranked (Q1) international journal in the area of metallurgy and metallurgical engineering.

  Impact Factor: 1.985

  My contribution to this manuscript: Investigation, Formal analysis, Visualization, Funding acquisition, Writing - original draft.

- M.A. Valdes-Tabernero, C. Celada-Casero, I. Sabirov, A. Kumar, R.H. Petrov. "The effect of heating rate and soaking time on microstructure of an advanced high strength steel", Materials Characterization 155 (2019) 109822, https://doi.org/10.1016/j.matchar.2019.109822

  Article published in highly ranked (Q1) international journal in the area of materials science.

  Impact Factor: 3.22

  My contribution to this manuscript: Investigation, Formal analysis, Visualization, Funding acquisition, Writing - original draft.

- M.A. Valdes-Tabernero, R.H. Petrov, M.A. Monclus, J.M. Molina-Aldareguia, I. Sabirov, “The effect of soaking time after ultrafast heating on the microstructure and mechanical behavior of a low carbon steel”, Materials Science and Engineering A 765 (2019) 138276, https://doi.org/10.1016/j.msea.2019.138276
  Article published in highly ranked (Q1) international journal in the area of materials science.
  Impact Factor: 4.081
  My contribution to this manuscript: Investigation, Formal analysis, Visualization, Funding acquisition, Writing - original draft.

- M.A. Valdes-Tabernero, A. Kumar, R.H. Petrov, M.A. Monclus, J.M. Molina-Aldareguia, I. Sabirov. “The sensitivity of the microstructure and properties to the peak temperature in an ultrafast heat treated low carbon-steel”, Materials Science and Engineering A 776 (2020) 138999, https://doi.org/10.1016/j.msea.2020.138999
  Article published in highly ranked (Q1) international journal in the area of materials science.
  Impact Factor: 4.081
  My contribution to this manuscript: Investigation, Formal analysis, Visualization, Funding acquisition, Writing - original draft.